Durham E-Theses

The role of the R-SNARE VAMP714 in Arabidopsis under salt stress

SUN, JIALEI

The role of the R-SNARE VAMP714 in *Arabidopsis* under salt stress

Jialei Sun

This thesis is submitted for the degree of

Doctor of Philosophy

Department of Biosciences

Durham University

October 2025

Table of Contents

List of Abbreviations

2,4-D	2,4-dichlorophenoxyacetic acid
4-Cl-IAA	4-chloroindole-3-acetic acid
ABA	Abscisic acid
ABCB	ATP Binding Cassette subfamily B
Ag	Silver
AKT1	*Arabidopsis thaliana* K$^+$ transporter 1
ARF	Auxin response factor
AUX1/LAX	Auxin-resistant1/like aux1
Be	Beryllium
BP	Biological process
CaCl$_2$	Calcium chloride
CAT	Catalase
CK	Cytokinin
Col-0	Columbia ecotype
CTL1	Choline transporter-like 1
DAB	3,3'-Diaminobenzidine
DEG	Differentially expressed gene
DMF	N-N-dimethylformamide
DMSO	Dimethyl sulfoxide
DN	Dominant-negative
dpg	Days post-germination
ER	Endoplasmic reticulum
FPKM	Fragments Per Kilobase of transcript sequence per Millions base pairs sequenced
GA	Gibberellic acid
GFP	Green fluorescent protein
GI	GIGANTEA

GO	Gene Ontology
GUS	β-glucuronidase
HCl	Hydrochloric acid
HKT	High-affinity potassium transporter
HSP	Heat-shock protein
IAA	Indole-3-acetic acid
IAM	Indole-3-acetamide
IAOx	Indole-3-acetaldoxime
IBA	Indole-3-butyric acid
ICP-MS	Inductively coupled plasma-mass spectrometry
In	Indium
IPyA	Indole-3-pyruvic acid
KEGG	Kyoto Encyclopedia of Genes and Genomes
MAPK	Mitogen-activated protein kinase
MEGA	Molecular Evolutionary Genetics Analysis
MS	Murashige and Skoog
Na_2HPO_4	Sodium phosphate dibasic
NaCl	Sodium chloride
NBT	Nitro blue tetrazolium chloride
NCBI	National Center for Biotechnology Information
NPA	N-1-naphthylphthalamic acid
NSCC	Nonselective cation channel
PAA	Phenylacetic acid
PCA	Principal component analysis
PIN	PIN-FORMED
PLT	PLETHORA
PPBo	4-Phenoxyphenylboronic acid
PPI	Protein–protein interaction
QC	Quiescent centre

RAM	Root apical meristem
RNA-seq	RNA Sequencing
ROS	Reactive oxygen species
RT	Room temperature
RT-qPCR	Quantitative real time PCR
SBS	Sequencing-by-synthesis
SCR	SCARECROW
SHR	SHORT-ROOT
SNARE	Soluble N-ethylmaleimide-sensitive factor attachment protein receptor
SOS	Salt overly sensitive
TAM	Tryptamine
t-SNARE	Target cell-associated SNARE
UPGMA	Unweighted pair group method with arithmetic mean
VAMP7	Vesicle-associated membrane protein 7
v-SNARE	Vesicle-associated SNARE
WT	Wild-type

Declaration

The material contained within this thesis has not previously been submitted for a degree at Durham University or any other university. The research reported within this thesis has been conducted by the author unless indicated otherwise.

Statement of Copyright

The copyright of this thesis (including any appendices or supplementary materials to this thesis) rests with the author, unless otherwise stated.

Jialei Sun

October 2025

Acknowledgments

I have told everyone again and again how happy, lucky, and proud I am to be **Professor Keith Lindsey's** Ph.D. student. Keith is my Ph.D. supervisor, my friend, and my family in the United Kingdom. As **supervisor Keith**, he always makes sure I have the tools and materials for experiments and supports me in attending conferences. I have been blessed to have a professional and knowledgeable supervisor who is passionate and kind. This thesis exists because of his tireless help. As **friend Keith**, he is my first friend in the UK. I will never forget him greeting me at Newcastle airport three years ago, during the pandemic. As **family Keith**, he always cares for me when I struggle or feel unsettled. Every year, the lab members gather to share food and laughter to celebrate Christmas, and those moments make me feel at home. Once again, I appreciate everything that **Supervisor Keith**, **Friend Keith**, and **Family Keith** do. I will carry your generosity and your lessons with me always.

I would like to express my gratitude to my co-supervisor, **Professor Jennifer F. Topping**. She guides and helps me greatly. I am very grateful to **Dr. Julien Agneessens**. He is like a big brother to me. He always has time to answer my questions and gives me fresh ideas, which makes my Ph.D. days smooth. I would like to express my gratitude to **Dr. Xiaoyan Gu**, the predecessor in the lab. She always explains every experimental detail with patience and care. Once again, I appreciate everything that you do.

I am grateful to my current lab family, **Alice**, **Cian**, **Ola**, and **Phoebe**. You make long days at the bench feel full of light. I am grateful to members from many corners of the world: **Alexandre**, **Archie**, **Ashish**, **Haozhan**, **Helen**, **Joanna**, **Maria**, **Merci**, **Michael**, **Qing**, **Shraboni**, **Sumera**, and **Yuqi**. Each of you brings laughter and support to my life here. I am grateful to **Tim** and **Joanne** in

bioimaging, for guiding me through tricky microscopy and sharing your expertise. I am grateful to **Gavin**, **Caroline**, **Lucy**, **Gail**, and **Abigail** in purchasing, for making sure we never run out of supplies. I am grateful to **Dr. Emma**, for doing the ICP-MS analyses that underpin so much of my work. I am grateful to **Emma**, from the support staff, for all the little things you do every day. I am grateful to my friends **Jiayi** and **Peng**. Your company makes me feel warm. You all make this journey possible, and I carry your kindness with me, always.

I am grateful to **China Scholarship Council** and **Durham University** for funding to support my studies at Durham University.

To my dad Shouli and mom Min who gave me my life and strength, to people who loved and accompanied me through the last 29 years.

Durham, United Kingdom, 2025

Abstract

PIN-FORMED (PIN) proteins mediate the polar transport of auxin and require vesicle trafficking for their localisation and abundance at the plasma membrane. The work described in this thesis investigates the hypothesised role of the PIN trafficking component VAMP714, an R-SNARE, in these processes under salt stress, a stress with known auxin-mediated effects on root development.

Salt stress induced *VAMP714* transcription and altered its protein localisation from membrane-associated vesicles to diffuse cytosolic pools. At the same time, auxin responses became restricted to the root cap and PIN polarity was progressively lost. Native-promoter overexpression of *VAMP714* maintained root elongation and restricted lateral root proliferation under salinity, whereas constitutive overexpression and knockout lines did not, indicating dosage sensitivity. Tolerance depended on polar auxin transport.

Protein–protein interaction assays identified CTL1 as a partner of VAMP714 at *trans*-Golgi and early endosomal compartments. CTL1 was required for VAMP714 distribution and for PIN1, but not for PIN2, polarity. Salt stress induced *CTL1* expression in roots, and exogenous choline modified a root-specific CTL1–VAMP714 regulatory loop, suggesting a lipid–SNARE module controlling auxin-carrier trafficking.

Transcriptome analysis of *vamp714* mutants revealed early changes in redox and vesicle trafficking genes, with CYP96A12 emerging as a candidate regulator. Protein interaction networks highlighted AP-3, SNAP29, SYP23, and MEMB11 as dynamic partners. ROS assays showed enhanced H_2O_2 accumulation in mutants, with compensatory catalase activity, indicating a role for VAMP714 in ROS compartmentalisation. Additionally, VAMP714 may be

involved in, or associated with, the SOS-mediated response to salt stress under the conditions examined in this study.

Ionomic analysis showed that salt increased Na^+ concentrations and destabilised K^+ and Ca^{2+} homeostasis in both wild type and mutants. Auxin treatments did not restore ionic balance but elevated Ca^{2+} independently of VAMP714. Inhibition of YUCCA-mediated auxin biosynthesis impaired ionic regulation in a VAMP714-dependent manner, while exogenous Ca^{2+} partially rescued growth through a parallel pathway.

Together, these findings establish VAMP714 as a stress-inducible trafficking regulator that safeguards PIN polarity, shapes redox dynamics, and connects auxin signalling with SOS-dependent ion homeostasis during early salt adaptation.

Chapter 1: Introduction

1.1 Climate change and agriculture: salt stress as a preeminent abiotic threat

Climate change is one of the most critical global challenges of our time, affecting every sector of human life (Schmidhuber and Tubiello, 2007; Wheeler and Von Braun, 2013; Zhao et al., 2017). This rapid progression over recent decades is unprecedented compared to historical natural fluctuations (Diffenbaugh et al., 2017; Howden et al., 2007; Jentsch et al., 2007; Millar and Woolfenden, 1999). There is broad agreement among scientists that human activities, such as greenhouse gas emissions, are one of the primary causes accelerating the rate of climate change (Arto and Dietzenbacher, 2014; Asseng et al., 2015; Hegerl et al., 2019; Lamb et al., 2021; Malik et al., 2016; Raupach et al., 2007; Wheeler and Von Braun, 2013). The economic, social, and environmental consequences of climate change are far-reaching, influencing infrastructure, ecosystems, and global markets (Moser and Hart, 2015; Raihan, 2023; Upadhyay, 2020).

Agriculture, as one of the most fundamental sectors, is particularly vulnerable to climate change (Challinor et al., 2014; Howden et al., 2007; Zhao et al., 2017). For example, climate change disrupts crop growth cycles through altering precipitation patterns (Rosenzweig et al., 2002), increasing temperatures (Asseng et al., 2015; Ben Mariem et al., 2021; Challinor et al., 2014), and extreme weather events (Rosenzweig et al., 2001). In worldwide, it threatens food production while reducing the quality of agricultural products (Curtin, 2009; Gregory et al., 2005; Smith and Gregory, 2013). Two billion people (accounting for 25.9% the total global population) suffer starvation or cannot obtain adequate nutritious food due to the effects of climate change on crop yield (World Health Organization, 2020).

Plants are the basis of most food chains and are experiencing a multitude of abiotic stresses as a direct consequence of climate change (Ferguson, 2019; Parmesan and Hanley, 2015; Vaughan et al., 2018). These stresses include extreme temperatures, drought, flooding, and increased soil salinity, all of which compromise plant growth and productivity (Ratnakumar et al., 2016; Raza et al., 2019; Rivero et al., 2022). Among these, salt stress has emerged as one of the most severe challenges for plants, particularly in arid regions (Ladeiro, 2012; Naorem et al., 2023; Yadav et al., 2011). Specifically, high salt concentrations harm plant development in many ways, such as strongly inhibiting germination (Ikeya et al., 2020; Jin et al., 2021; Safdar et al., 2019), stimulating oxidative stress (Leshem et al., 2007), causing ion imbalance (Ma et al., 2012), and even triggering drought stress (Mahajan and Tuteja, 2005). Therefore, understanding plant responses to salt stress is essential for a targeted breeding program of crop improvement (Isayenkov and Maathuis, 2019; Wang et al., 2003).

1.2 Multifaceted physiological disruptions induced by salt stress

Salt stress imposes a multifaceted assault on plant systems, initiating a cascade of interrelated physiological and biochemical challenges.

At the cellular level, the rapid accumulation of Na^+ disrupts ionic homeostasis by forcing K^+ efflux and hindering the uptake of other essential macronutrients (Qi and Spalding, 2004). This not only compromises membrane potential but also impedes protein synthesis (Dubey, 1999). Meanwhile, elevated salinity perturbs intracellular signal transduction pathways, including calcium signalling and hormonal cascades, resulting in widespread metabolic dysregulation (Mahajan et al., 2008). Additionally, enzymatic activities are inhibited, leading to the accumulation of toxic intermediates and disruption of energy production in chloroplasts (Hameed et al., 2021; Møller, 2001).

In parallel, the accumulation of Na$^+$ in the rhizosphere alters soil biophysics fundamentally. In detail, high salt concentrations destabilize soil aggregates, collapse pore architecture, and reduce both porosity and aggregate stability (Li et al., 2014b; Rengasamy et al., 2003; Zia-ur-Rehman et al., 2016). These structural changes limit gas exchange and water infiltration, leading to zones of localized hypoxia in the root zone and further constraining water uptake (Li et al., 2014b; Rengasamy et al., 2003).

Beyond direct ionic toxicity, salt stress induces secondary osmotic and drought pressures. The elevated osmotic potential in the soil matrix withdraws water from root cells, inducing cellular dehydration, turgor loss, and subsequent wilting, which hampers nutrient translocation and disrupts carbon assimilation pathways (Munns and Tester, 2008; Zhu, 2001). The ensuing water deficit, which is similar with drought stress, further impairs stomatal regulation and photosynthetic efficiency, compounding growth inhibition (Farooq et al., 2012).

Moreover, the saline environment catalyzes an overproduction of reactive oxygen species (ROS) within cellular compartments (Ahmad et al., 2010; Hayat et al., 2012; Luo et al., 2021; Saed-Moucheshi et al., 2014). This oxidative burst inflicts damage on proteins through carbonylation, peroxidation of membrane lipids, inactivation of critical enzymes, degradation of chlorophyll molecules, and fragmentation of nucleic acids (Hasanuzzaman et al., 2021).

1.3 Physiological and molecular strategies of plant salt tolerance

To counteract high salt damage, plants have developed a series of physiological and biochemical mechanisms, such as synthesizing osmotic regulating substances, absorbing and transporting ions selectively, removing ROS, regulating hormones, and controlling the expression of salt-tolerant genes

(Liang et al., 2018; Zhou et al., 2024) (Fig. 1.1).
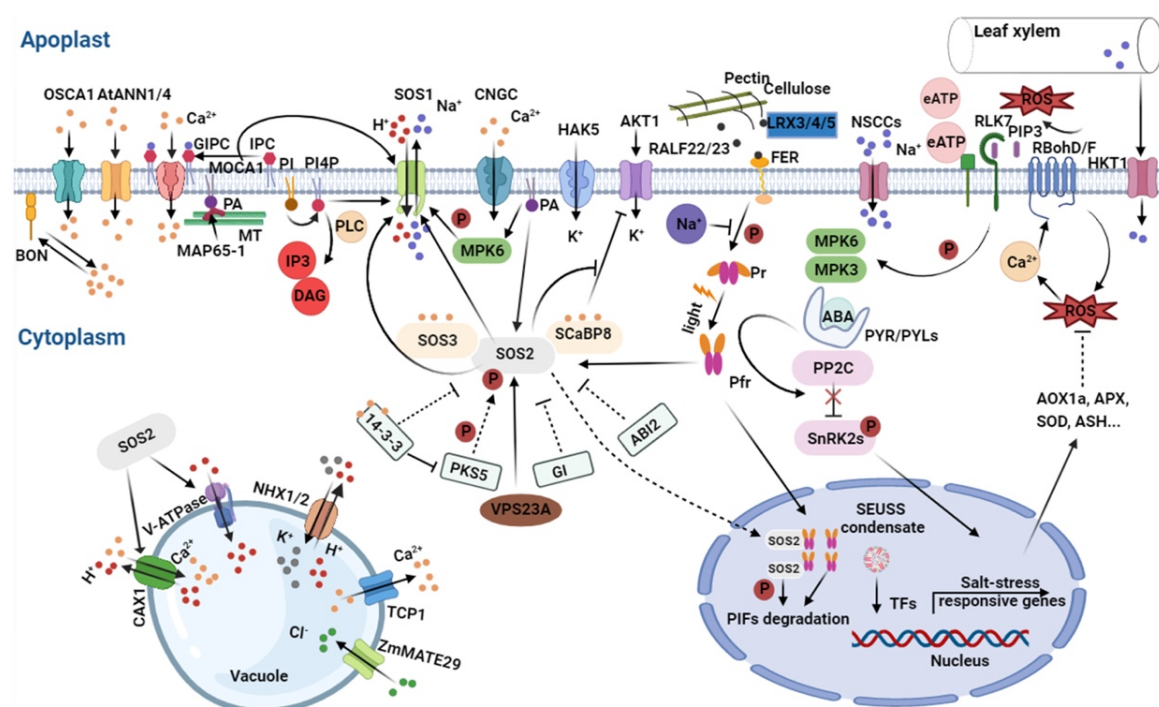
Fig. 1.1 Salt response signalling in plants (Zhou et al., 2024).

Plants sense osmotic stress or directly detect Na^+/Cl^-. Cell wall changes and phospholipid derivatives may contribute to salt perception. GIPC sphingolipids bind Na^+ for extracellular sensing. Tissue-specific Ca^{2+} signals, decoded by sensors like SCaBP8, guide precise responses. ROS levels and water status are tightly regulated under salinity. The SOS pathway maintains ionic homeostasis and interacts with other networks. Na^+ sequestration into organelles and increased K^+ uptake help restore Na^+/K^+ balance and enhance salt tolerance. CWI, cell wall integrity; GIPC, glycosyl inositol phosphorylceramide; ROS, reactive oxygen species; SOS, salt overly sensitive. The vacuolar TCP1 indicated in the diagram should be TPC1, TWO Pore Channel 1.

Firstly, plants synthesize small molecular weight osmolytes to counter osmotic stress. For example, proline is a free amino acid in plants, which has a low molecular weight, high water solubility, and no charge under normal physiological pH (Liang et al., 2018). Moreover, glycinebetaine is another vital osmotic regulator, which is highly water-soluble and non-toxic even at high

concentrations (Chen and Murata, 2008). In addition, it stabilizes the structure and activity of enzymes and protein complexes and maintains the integrity of cell membranes (Li et al., 2011). It also enhances the accumulation of heat-shock proteins (HSPs) and mediates calcium signalling pathways under salt stress (Li et al., 2014b).

Secondly, plants employ ion-specific transport mechanisms to counteract ionic toxicity. For instance, plants could increase Na^+ efflux and transport Na^+ into the vacuole to minimize toxicity under salt stress (Hasegawa et al., 2000; Tester and Davenport, 2003; Yamaguchi et al., 2001). Na^+ mainly enters plants by using ion channels that are shared with K^+, including high-affinity potassium transporters (HKTs) (Haro et al., 2005), nonselective cation channels (NSCCs) (Demidchik and Tester, 2002), and the *Arabidopsis thaliana* K^+ transporter 1 (AKT1) (Hirsch et al., 1998). Under salt stress, plants can regulate these pathways to achieve minimal toxicity. The Salt Overly Sensitive (SOS) pathway is the classical mechanism for Na^+ efflux, which comprises SOS1, SOS2, and SOS3 along with related proteins (Ji et al., 2013).

Moreover, plants synthesize antioxidants to counter oxidative stress. They respond to salt stress by overexpressing ROS-scavenging enzymes (Das and Roychoudhury, 2014). Plants also rely on the expression of salt stress-responsive genes and the synthesis of related hormones, such as abscisic acid (ABA), auxin, gibberellic acid (GA), and salicylic acid (SA) to resist salt stress (Yu et al., 2020). In addition to the SOS pathway, mitogen-activated protein kinase (MAPK) cascade signalling genes are expressed in response to salt stress (Zhang and Klessig, 2001). MYB family transcription factors (Zhao et al., 2019), WRKY family transcription factors (Jiang and Deyholos, 2009), and NAC family transcription factors (Xu et al., 2015) are also involved in the salt response.

1.4 ROS signalling under salt stress

As noted above, the disruption of ROS homeostasis is a key mechanism by which salt stress damages plants. Millions of years ago, oxygen-producing photosynthetic organisms released molecular oxygen into the early atmosphere of Earth, leading to the formation of ROS as undesirable side products (Halliwell, 2006). ROS mainly comprises $O_2^{\cdot-}$, H_2O_2, $OH^{\cdot}$, and $^1O_2$, and excessive levels cause extensive damage to proteins, DNA and lipids, thereby affecting normal cellular functioning (Apel and Hirt, 2004; Foyer and Noctor, 2005; Mittler, 2017).

Salt stress can trigger the overproduction of ROS in plants, which serve as both harmful oxidants and essential signalling molecules (Apel and Hirt, 2004; Miller et al., 2008; Mittler, 2002). Controlled ROS levels function as signals to activate stress-responsive pathways and reprogram cellular metabolism (Miller et al., 2008; Mittler, 2002). For example, ROS can be perceived by various cellular targets, which then activate downstream transcription factors and defence responses (Mittler et al., 2004). NADPH oxidases on the plasma membrane are rapidly activated under salt stress, contributing to the initial ROS burst (Liu et al., 2020a). This ROS signal is further amplified by feedback loops that integrate environmental cues and internal metabolic states (Sasidharan et al., 2021). Subsequently, ROS modulates gene expression by altering the redox state of key regulatory proteins (Foyer and Noctor, 2005). For instance, one study has clarified that specific transcription factors are activated upon ROS signalling, thereby inducing the expression of antioxidant enzymes (Limón-Pacheco and Gonsebatt, 2009). These enzymes, such as superoxide dismutase, catalase (CAT), and various peroxidases, serve to scavenge excess ROS and restore redox homeostasis (Limón-Pacheco and Gonsebatt, 2009). Beyond that, ROS signalling is tightly interconnected with hormonal pathways, such as ethylene (Peng et al., 2014), which further regulates salt stress responses.

Redox regulation also involves the reversible oxidation of cysteine residues in proteins, which serves as a molecular switch to modulate enzyme activities and protein–protein interactions (Spadaro et al., 2010). Additionally, ROS can activate MAPK cascades that further propagate the stress signal and coordinate diverse cellular responses (Pitzschke and Hirt, 2009; Raja et al., 2017). Collectively, these studies highlight that ROS are not merely toxic byproducts but also crucial mediators to salt-induced stress.

1.5 SOS signalling under salt stress

In addition to ROS signalling, the SOS signalling pathway also plays a central role in mediating cellular responses and maintaining ion homeostasis under salt stress (Ji et al., 2013). Under natural conditions, Na^+ absorption is mediated by dedicated ion transporters of the HKT family, which sustain essential life activities (Platten et al., 2006). Moreover, it is speculated that Na^+ enters the plant via plasma-membrane NSCCs and may also passively infiltrate through anatomical "leaks" in the root endodermis (Demidchik and Tester, 2002; Hasegawa et al., 2000; Munns and Tester, 2008). Simultaneously, the Na^+/H^+ antiporter SOS1 facilitates the export of Na^+ from the cell (Shi et al., 2000), and the NHX1 antiporter sequesters Na^+ into the vacuole for storage (Apse et al., 2003). All of these mechanisms enable plants to maintain a steady state of Na^+ uptake, efflux, and compartmentalization.

In addition to Na^+ and K^+, Ca^{2+} is intimately linked to the transduction of the SOS signalling pathway (Liu and Zhu, 1998). Under high Na^+ stress, a transient spike in cytosolic Ca^{2+} is generated in plant root cells, and this Ca^{2+} signal activates the SOS signalling cascade to protect cells from ion toxicity (Chinnusamy et al., 2005). As mentioned above, the main members of the SOS signalling pathway are the three components SOS1-3 (Ali et al., 2023) (Fig. 1.2). The *SOS3* gene encodes a myristoylated calcium-binding protein that functions

as a primary sensor of the increased cytosolic Ca^{2+} induced by excess Na^+ (Ishitani et al., 2000; Liu and Zhu, 1998). Upon binding Ca^{2+}, SOS3 interacts with and activates the serine/threonine protein kinase SOS2 (Halfter et al., 2000; Liu and Zhu, 1998; Liu et al., 2000). The interaction between SOS3 and SOS2 in roots, or alternatively between SCaBP8 and SOS2 in shoots, (Halfter et al., 2000; Liu and Zhu, 1998; Liu et al., 2000), results in the activation of the downstream target SOS1, which then facilitates the efflux of Na^+ from the cell (Shi et al., 2000).

In recent years, additional components of the SOS signalling pathway have been progressively identified. For example, GIGANTEA (GI), a flowering time regulator, has been shown to interact with SOS2 to regulate the salt response (Ke et al., 2017; Kim et al., 2013). Furthermore, the calcium-permeable transporter ANN4 interacts with SCaBP8 and SOS2, establishing it as an indispensable component of this signalling cascade (Ma et al., 2019). Similarly, BIN2 has been identified as a negative regulator of SOS2 kinase activity, acting as a molecular switch under the salt stress response (Li et al., 2020). Linker histone variant HIS1-3 and WRKY1 regulate the expression of *SOS* genes (Wu et al., 2022). Additionally, the nuclear calcium-sensing pathway RSA1-RITF1 fine-tunes *SOS1* expression (Guan et al., 2013), while the UBC1/UBC2-MYB42/MPK4 module positively regulates *SOS2* transcription (Sun et al., 2020). PLATZ2 functions as a transcriptional repressor of *SOS3* and *SCaBP8* genes (Liu et al., 2020b).
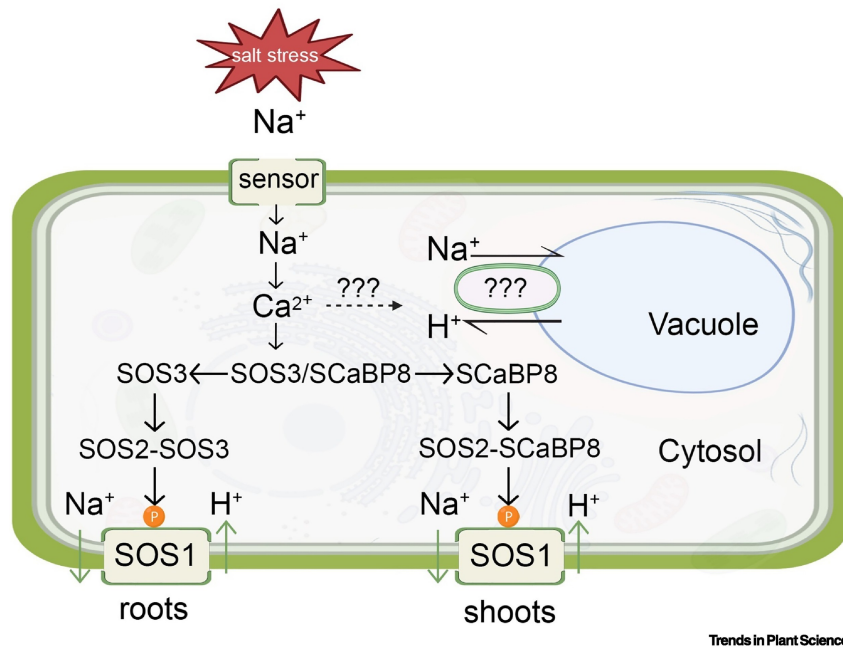
Fig. 1.2 Core SOS pathway in roots and shoots of plants under salt stress (Ali et al., 2023).

1.6 Plant hormones regulation of salt stress adaptation

In addition to ROS and SOS signalling, plant hormones are compounds synthesized via specific biosynthetic pathways and are essential for mediating growth and developmental responses under environmental stress conditions (Peleg and Blumwald, 2011). The classical plant hormones include ABA, auxin, cytokinin (CK), ethylene, GA, and SA, all of which regulate numerous physiological and biochemical processes (Yu et al., 2020) (Fig. 1.3). For example, ABA increases the relative water content, meanwhile reducing cell membrane injury and the Na^+/K^+ ratio under salt stress, in rice (Wei et al., 2015). Moreover, NAC2 is a transcription factor in *Arabidopsis thaliana* that functions downstream of both ethylene and auxin signalling, playing key roles in the response to salt stress as well as in the regulation of lateral root formation (He et al., 2005). In *Arabidopsis thaliana*, CK is generally considered to be a negative regulator of plant salt resistance, but it plays different roles in the salt stress response among different species (Yu et al., 2022). The expression of the ethylene receptor ETR1 is suppressed by salt exposure in *Arabidopsis*

thaliana (Zhao and Schaller, 2004). The ethylene receptor NTHK1 affects ion accumulation and related gene expression to regulate salt stress response in tobacco (Cao et al., 2006; Zhang et al., 2001; Zhou et al., 2006). In addition, salt stress-mediated stabilization of EIN3/EIL1 enhances salinity tolerance by preventing excessive ROS accumulation in *Arabidopsis thaliana* (Peng et al., 2014). Salt stress also negatively regulates GA biosynthesis while positively regulating ABA biosynthesis, which in turn inhibits seed germination in soybean (Shu et al., 2017). Furthermore, GA2ox5, a gibberellin metabolic enzyme, participates in plant growth, root gravitropism, and the salt stress response in rice (Shan et al., 2014). SA treatment negatively affects the response to salt stress, associated with an imbalance in antioxidant metabolism in pea (Barba-Espín et al., 2011).
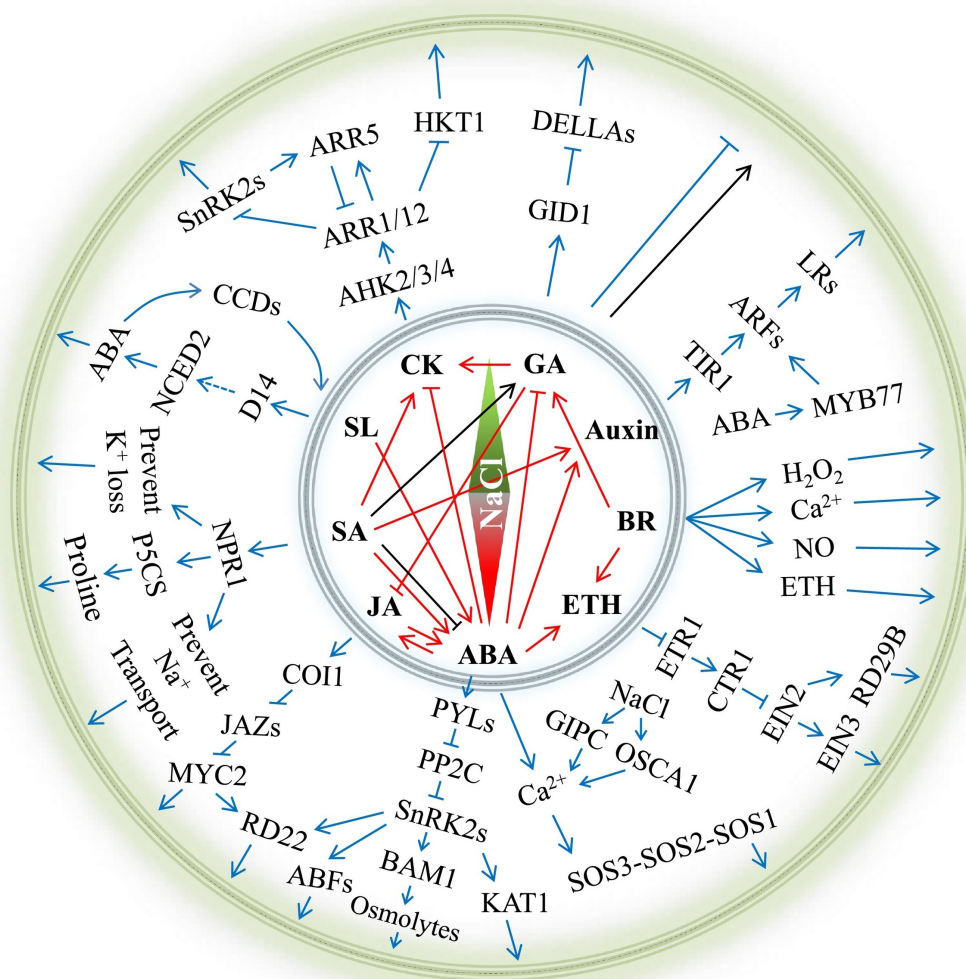
Salt stress adaptation and plant growth

— Black line represents the germination stage
— Red line represents the regulatory relationship between hormones
— Blue line represents the hormone signaling in salt resistance

Trends in Plant Science

Fig. 1.3 Hormone-mediated salt tolerance in plants (Yu et al., 2020).

1.7 Auxin signalling pathway in *Arabidopsis thaliana*

As a model plant, *Arabidopsis thaliana* is a genetically self-fertilising germplasm (Krämer, 2015; Weigel, 2012), with advantages of being diploid (facilitating mutant analysis), a short reproductive cycle, a small genome and distinct morphological characteristics (Arabidopsis Genome Initiative genome analysis, 2000). Furthermore, discoveries in *Arabidopsis thaliana* are being translated to

crop genetic improvement (Parry et al., 2020). Many *Arabidopsis thaliana* papers have been referenced by papers researching crops (Provart et al., 2016). Therefore, the work described in this thesis uses *Arabidopsis thaliana* as the research organism to carry out new research.

1.7.1 Auxin biosynthesis

Auxins are ubiquitously present in plants. They are a class of low-molecular-weight compounds that induce growth, participating in numerous biological processes, such as cell signalling, cell cycle regulation, endocytosis, embryogenesis, organogenesis, and overall growth modulation (Gomes and Scortecci, 2021; Perrot-Rechenmann and Napier, 2005).

Classical auxins can be divided into two main groups. The first group consists of endogenous auxins naturally synthesized within plants, including indole-3-acetic acid (IAA), indole-3-butyric acid (IBA), phenylacetic acid (PAA), and 4-chloroindole-3-acetic acid (4-Cl-IAA) (Koepfli et al., 1938; Porter and Thimann, 1965; Simon and Petrášek, 2011; Zimmerman and Wilcoxon, 1935). Among these, IAA is the most prevalent and abundant in plant tissues (Bartel, 1997; Guo et al., 2019). In addition, synthetic auxins, such as 2,4-dichlorophenoxyacetic acid (2,4-D) and naphthalene-1-acetic acid (NAA), are widely used experimentally (Simon and Petrášek, 2011).

The predominant biosynthetic route for IAA is the tryptophan-dependent pathway, which comprises four alternative branches, namely the indole-3-acetaldoxime (IAOx), indole-3-acetamide (IAM), indole-3-pyruvic acid (IPyA), and tryptamine (TAM) pathways, mediated by transamination and decarboxylation reactions (Cao et al., 2019; Di et al., 2016). Among them, only the IPyA pathway has been fully characterised, and whereby tryptophan is initially converted into IPyA by the TAA family of aminotransferases, and subsequently, IPyA is transformed into IAA by the YUC family of flavin mono-

oxygenases, which are typically associated with the endoplasmic reticulum (ER) membrane (Cao et al., 2019) (Fig. 1.4).

Fig. 1.4 The auxin biosynthesis pathways identified in plants (Cao et al., 2019).

Solid arrows indicate pathways in which the enzymes, genes, or intermediates are known, and dashed arrows indicate pathways that are not well defined.
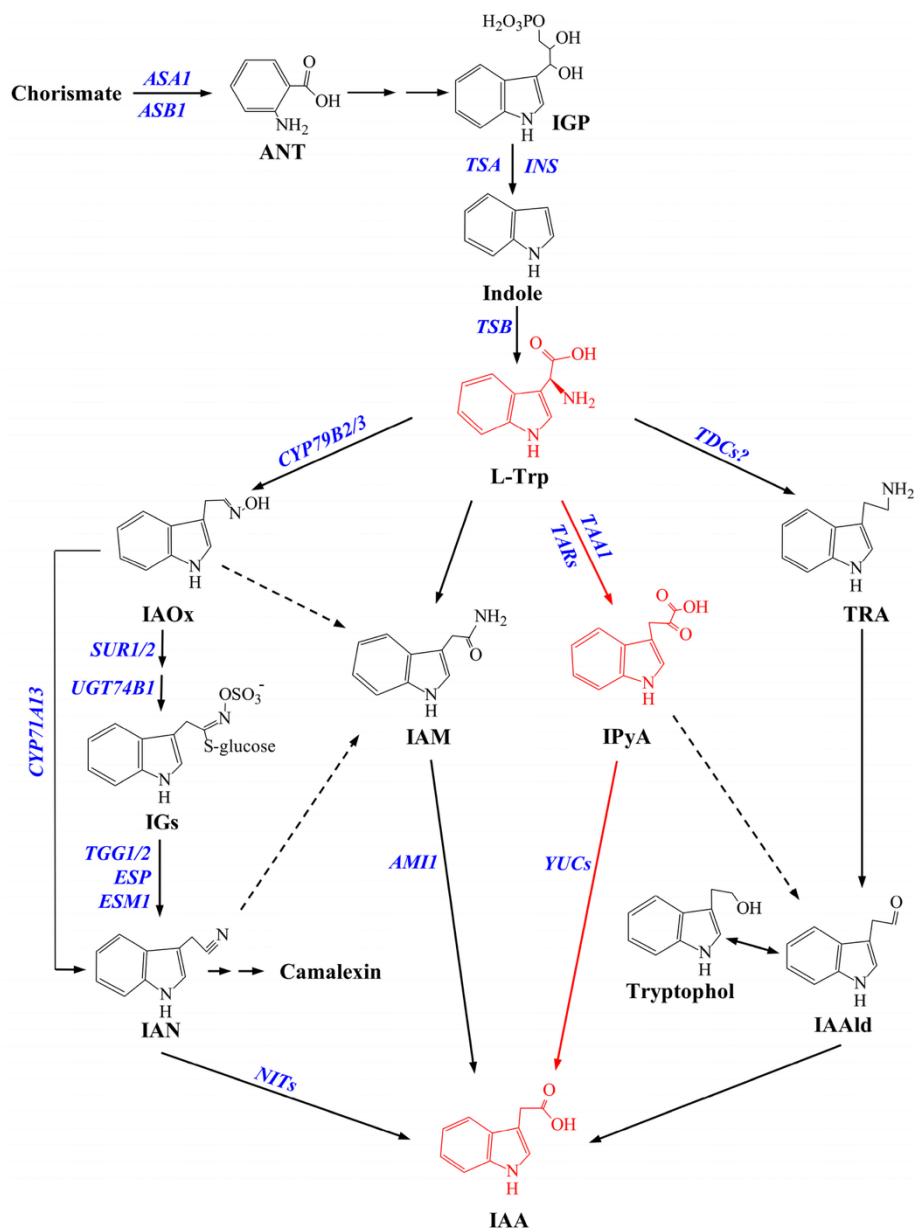
1.7.2 Regulatory networks and auxin dynamics in quiescent centre (QC) maintenance

The QC is located at the centre of the stem cell niche and is composed of typically slowly-dividing cells surrounded by rapidly dividing initial cells (Clowes, 1953, 1954, 1958; Dubrovsky and Barlow, 2015; Dubrovsky and Ivanov, 2021). The QC is part of root apical meristem (RAM) stem cell niche, and the initials undergo rounds of division followed by expansion and differentiation to produce nearly all tissues required for root function (Strotmann and Stahl, 2021).

The spatiotemporal regulatory network of the QC is complex (Strotmann and Stahl, 2021) (Fig. 1.5). One well-studied molecular factor that inhibits QC divisions while preserving the stem cell identity of surrounding initials is the homeodomain transcription factor WOX5 (Pi et al., 2015; Sarkar et al., 2007). Moreover, the *PLETHORA* (*PLT*) genes are highly expressed in root stem cell niches (Aida et al., 2004), and play a central role in regulating root formation and development (Galinha et al., 2007). In addition, a network based on SCARECROW (SCR) and SHORT-ROOT (SHR), members of the GRAS transcription factor family, is crucial for proper QC positioning (Nakajima et al., 2001; Sabatini et al., 2003). *SHR* is also expressed in the stele and its protein moves to adjacent cell layers, including the QC and endodermis (Nakajima et al., 2001). SHR and its downstream target SCR jointly regulate QC dynamics (Koizumi et al., 2012; Sozzani et al., 2010), and the SHR-SCR complex also suppresses infrequent QC divisions (Clark et al., 2020). Furthermore, in the root apex, an IAA gradient exists with a prominent maximum in the QC (Petersson et al., 2009). The root apex is a major source of IAA, and all cell types show high synthetic capacity, indicating that local biosynthesis significantly contributes to auxin homeostasis (Petersson et al., 2009). *WOX5* transcription is repressed by auxin treatment and confined to the QC (Ding and Friml, 2010). Moreover, auxin induces the expression of *PLT* genes (Aida et al., 2004), which form instructive protein gradients that balance stem cell differentiation and

replenishment within the RAM (Galinha et al., 2007).
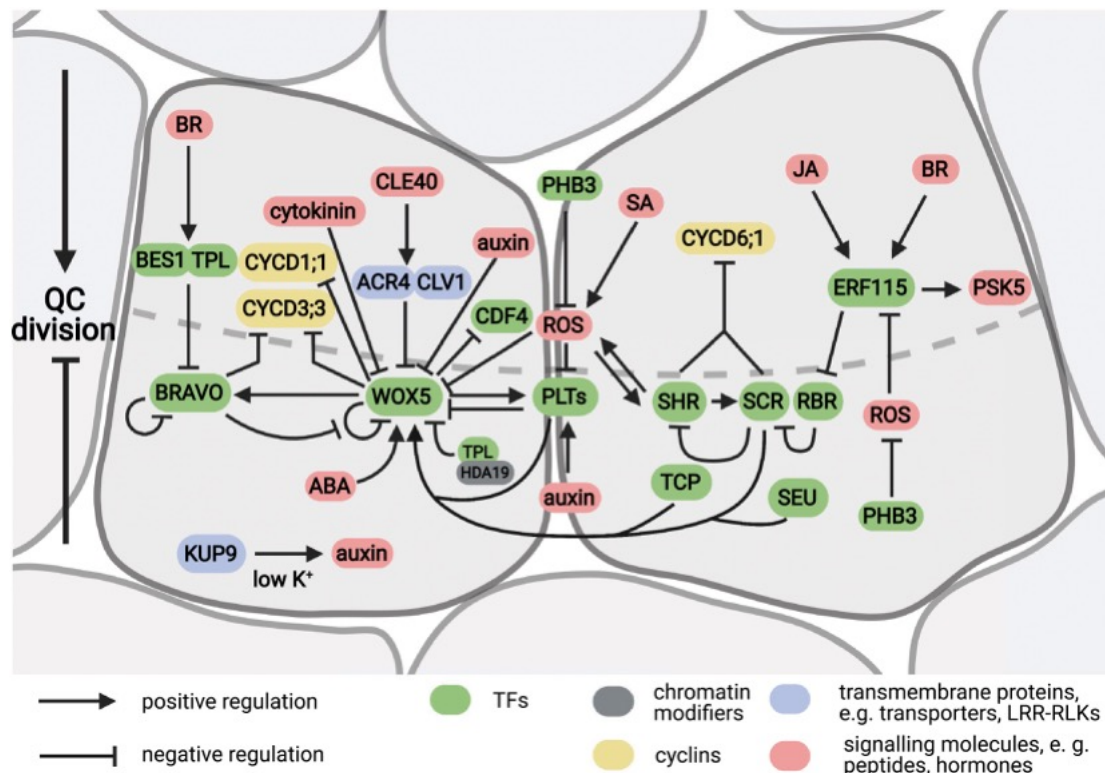
Fig. 1.5 A model of the intricate regulatory network of molecular factors involved in QC division control, in *Arabidopsis thaliana* (Strotmann and Stahl, 2021).

1.7.3 Auxin distribution, transportation, and signal transduction

The differential distribution of auxin, characterized by local auxin maxima and gradients, is determined primarily by directional intercellular transport, in addition to local biosynthesis and activation from inactive precursors (Petrášek and Friml, 2009) (Fig. 1.6).

Auxin is synthesized primarily in young, developing tissues (such as the shoot apex, young leaves, and root tip) and redistributed throughout the plant (Michniewicz et al., 2007). These asymmetric auxin distributions orchestrate organogenesis and tropic responses by concentrating auxin at maxima to specify tissue patterning and redirect growth in response to environmental cues such as gravity and light.

For auxin transportation, current evidence indicates that auxin undergoes two distinct transport routes within the plant. One route is a rapid, non-polar transport via the phloem, while the other is a slower, carrier-mediated polar auxin transport between various tissues (Goldsmith, 1977; Michniewicz et al., 2007). To be specific, non-polar auxin transport is extensively redistributed from source tissues to other regions through bulk flow within mature phloem. In contrast, polar auxin transport is characterized by its slower, controlled, and directional movement, mediated by carrier proteins, through the vascular cambium and between other cells in the root tip. Polar auxin transport can be further categorized into long-distance movement (through the entire plant) and short-distance movement (within specific tissues) (Michniewicz et al., 2007).

Polar auxin transport within the root tip involves movement toward the root apex from the vascular cambium through the meristem, followed by upward and inward transport that creates a concentration maximum in the stem cell niche and columella (Michniewicz et al., 2007; Rashotte et al., 2000). This directional movement is coordinated by AUXIN-RESISTANT1/LIKE AUX1 (AUX1/LAX) influx permeases, ATP Binding Cassette subfamily B (ABCB) transporters, and PIN-FORMED (PIN) efflux carriers, all driven by chemiosmotic gradients (Band et al., 2014; Peer et al., 2011; Petrášek and Friml, 2009) (Fig. 1.6). In detail, IAA enters the cell via lipophilic diffusion and anion uptake, processes facilitated by the proton-coupled AUX1/LAX transporters (Bennett et al., 1996; Swarup et al., 2005; Yang and Murphy, 2009; Yang et al., 2006). When auxin levels fluctuate, some ABCB family members modulate cellular auxin loading (Cho and Cho, 2013). In *Arabidopsis thaliana*, the *AUX1/LAX* gene family comprises *AUX1*, *LAX1*, *LAX2*, and *LAX3*, which encode polytopic transmembrane proteins similar to amino acid transporters (Péret et al., 2012). Mutations in *AUX1/LAX* genes lead to auxin-related developmental abnormalities and affect key processes such as primary root and lateral root development, root gravitropism, root hair formation, vascular patterning, seed germination, apical

hook formation, leaf morphogenesis, phyllotactic patterning, female gametophyte development, and embryogenesis (Swarup and Bhosale, 2019). Intracellular IAA exists as a membrane-impermable anion and requires facilitators or transporter proteins for cellular efflux (Morris, 2000; Raven, 1975). Full-length PIN carriers mediate tissue-specific, directional auxin efflux, and a subset of ABCB transporters works in conjunction with PIN proteins to extrude auxin through the plasma membrane (Zažímalová et al., 2010).

For auxin signal transduction, auxin is perceived by the TIR1/AFB F-box proteins, then recruiting and ubiquitinating Aux/IAA repressors for proteasomal degradation, thereby rapidly de-repressing downstream transcription (Quint and Gray, 2006). Freed Auxin response factors (ARFs) then bind AuxRE motifs in target gene promoters to activate or repress transcriptional programs that govern development and physiology (Quint and Gray, 2006). In parallel, auxin also triggers fast, non-transcriptional responses, such as changes in ion flux and endocytosis, via pathways independent of TIR1/AFB, to fine-tune growth and environmental adaptation (Quint and Gray, 2006).
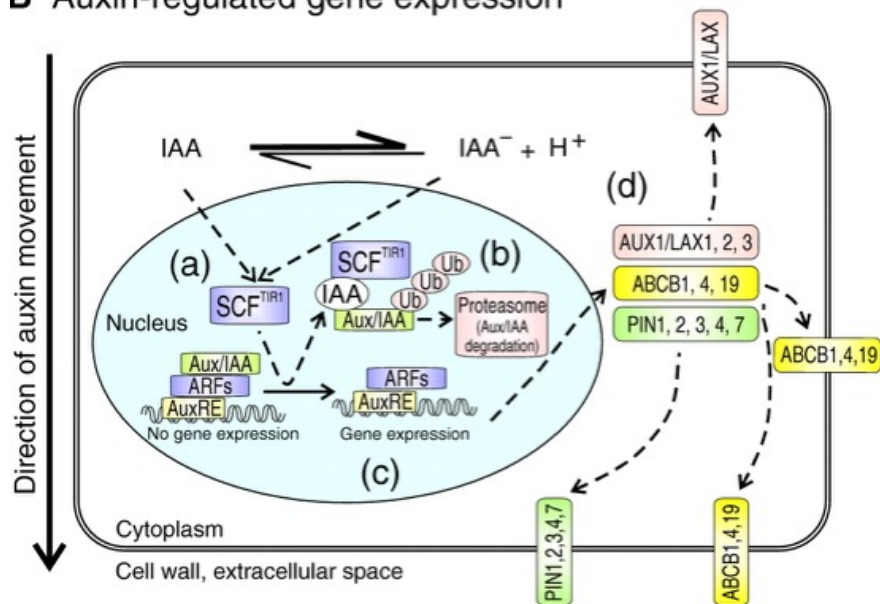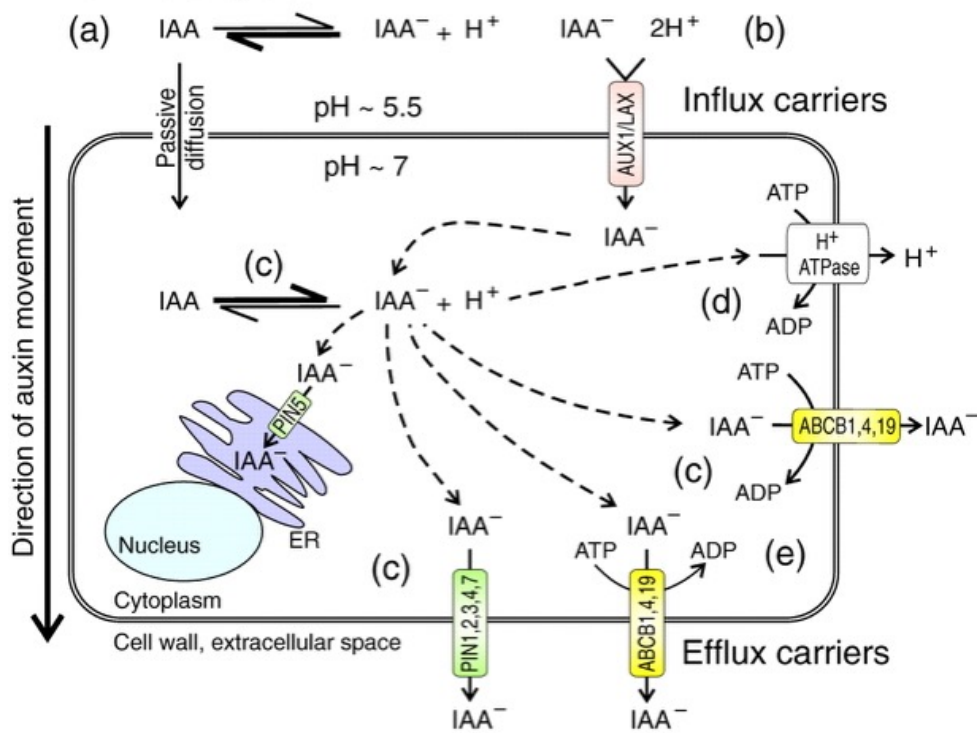
Fig. 1.6 Auxin transport across the plasma membrane and auxin-regulated gene expression (Petrášek and Friml, 2009).

1.7.4 Polar auxin transportation mediated by PIN proteins

PIN proteins represent a plant-specific family of transmembrane proteins that mediate directional auxin flux within tissues, thereby establishing auxin maxima and gradients critical for development (Petrášek and Friml, 2009; Vieten et al., 2007).

In *Arabidopsis thaliana*, eight *PIN* genes have been identified, which are generally classified into two major subfamilies (Křeček et al., 2009). The larger subfamily comprises PIN1–PIN4 and PIN6–PIN7, characterized by a unique central hydrophilic loop that separates two hydrophobic domains, each containing approximately five transmembrane regions (Křeček et al., 2009). In contrast, PIN5 and PIN8, which lack the central hydrophilic loop, constitute a distinct subfamily (Ding et al., 2012; Mravec et al., 2009).

PIN5, PIN6, and PIN8 are localized to the endoplasmic reticulum, where they mediate the exchange of auxin between the cytosol and the ER lumen (Ding et al., 2012; Mravec et al., 2009; Simon et al., 2016). PIN1 is polarly localized to the basal plasma membrane of auxin-transporting vascular (and precursor) cells, accumulating on the side facing the root tip, to function as a directional efflux carrier (Galweiler et al., 1998; Steinmann et al., 1999). Meanwhile, PIN2 localizes to the plasma membranes of cortical and epidermal cells within the meristematic and elongation zones of roots, exhibiting a distinct polar distribution (Müller et al., 1998). PIN3 predominantly localizes to the lateral plasma membrane of gravity-sensing columella and pericycle cells and rapidly relocalizes toward the lower side upon gravistimulation, thereby directing lateral auxin efflux (Friml et al., 2002b). PIN4 is predominantly localized at the basal plasma membrane of quiescent centre cells and their surrounding provascular and endodermal initials in both developing and mature root meristems, where it establishes an auxin sink beneath the QC (Friml et al., 2002a). PIN7 is localized predominantly to the lateral and basal plasma membranes of

provascular cells in both the root meristem and elongation zones, and overlaps with PIN3 distribution in the columella (Blilou et al., 2005).

PIN proteins regulate intercellular auxin distribution via a dynamic cycle of vesicle transport to the plasma membrane, endocytosis and recycling, which for PIN1 is an actin-dependent process (Geldner et al., 2001). Analogously, the endocytosis of PIN2 primarily relies on clathrin-mediated mechanisms (Dhonukshe et al., 2007), while PIN1 and PIN2 recycling from the plasma membrane depends on ARF, GEF, and GNOM (Friml, 2010; Kleine-Vehn et al., 2008, 2010) (Fig. 1.7). Notably, auxin itself inhibits this recycling, leading to the accumulation of PIN proteins at the plasma membrane and thereby promoting auxin efflux (Paciorek et al., 2005).
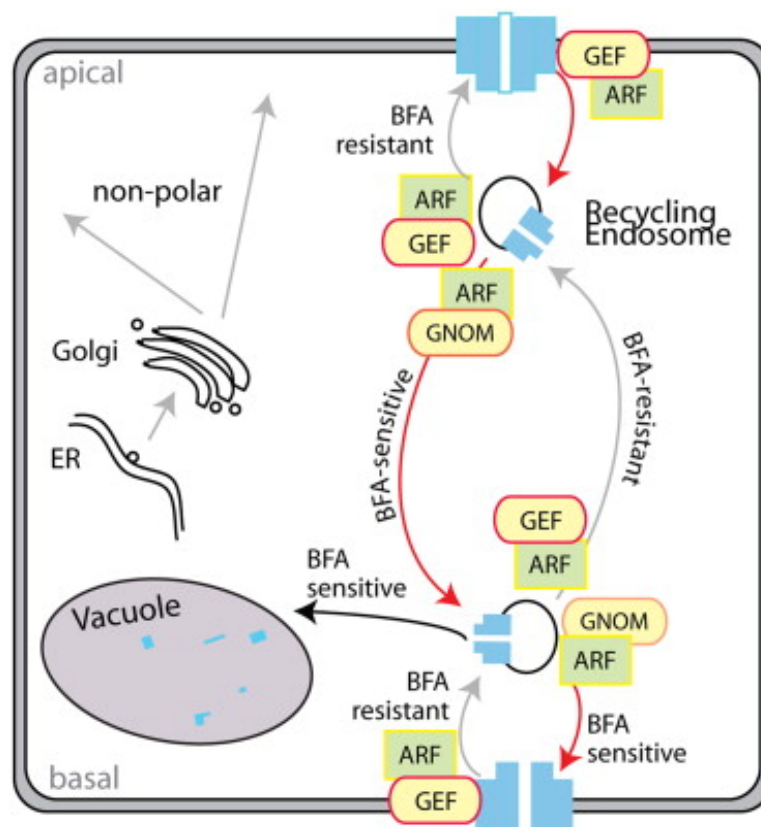
Fig. 1.7 Subcellular trafficking of PIN auxin transporters (Friml, 2010).

1.7.5 PIN-mediated auxin redistribution underlies diverse tropic responses

PIN proteins establish auxin gradients and local maxima necessary to guide plant growth, and are critical for several tropic responses, including phototropism, gravitropism, obstacle avoidance, and hydrotropism (Han et al., 2021; Petrášek and Friml, 2009; Vieten et al., 2007) (Fig. 1.8).

In terms of phototropism, PIN3 repolarizes toward the shaded side, redirecting auxin to that side of the hypocotyl, under unilateral blue light (Ding et al., 2011). Although the precise kinetics of PIN3 polarization remain under investigation, these dynamic relocalization events are central to the establishment of lateral auxin gradients required for phototropic responses (Ding et al., 2011).

In terms of gravitropism, PIN2 is differentially regulated, via gravity-induced, auxin-controlled vacuolar trafficking and degradation, to establish and fine-tune the asymmetric auxin distribution that drives bending (Baster et al., 2013). Similarly, PIN3 becomes polarized to the lower side of hypocotyl endodermal cells, redirecting auxin flow to create the asymmetric distribution necessary for gravitropic bending (Kleine-Vehn et al., 2010; Rakusová et al., 2011).

In terms of obstacle avoidance, PIN-mediated auxin transport is reoriented, generating an asymmetric auxin distribution between the concave and convex sides of the deformed root, which triggers a bending response that allows roots to bypass obstacles (Lee et al., 2020). The overall role of PIN-dependent auxin redistribution is clear in enabling roots to navigate complex soil environments (Zhang and Friml, 2019).

Hydrotropism appears to be less dependent on polar auxin transport in *Arabidopsis thaliana* (Kaneyasu et al., 2007). Here, auxin response rather than polar auxin transport is essential. Nevertheless, a study in cucumber roots

demonstrates the PIN5 becomes asymmetrically expressed, accumulating on the concave, high-humidity side, which directs differential auxin dynamics essential for hydrotropic bending (Morohashi et al., 2017).
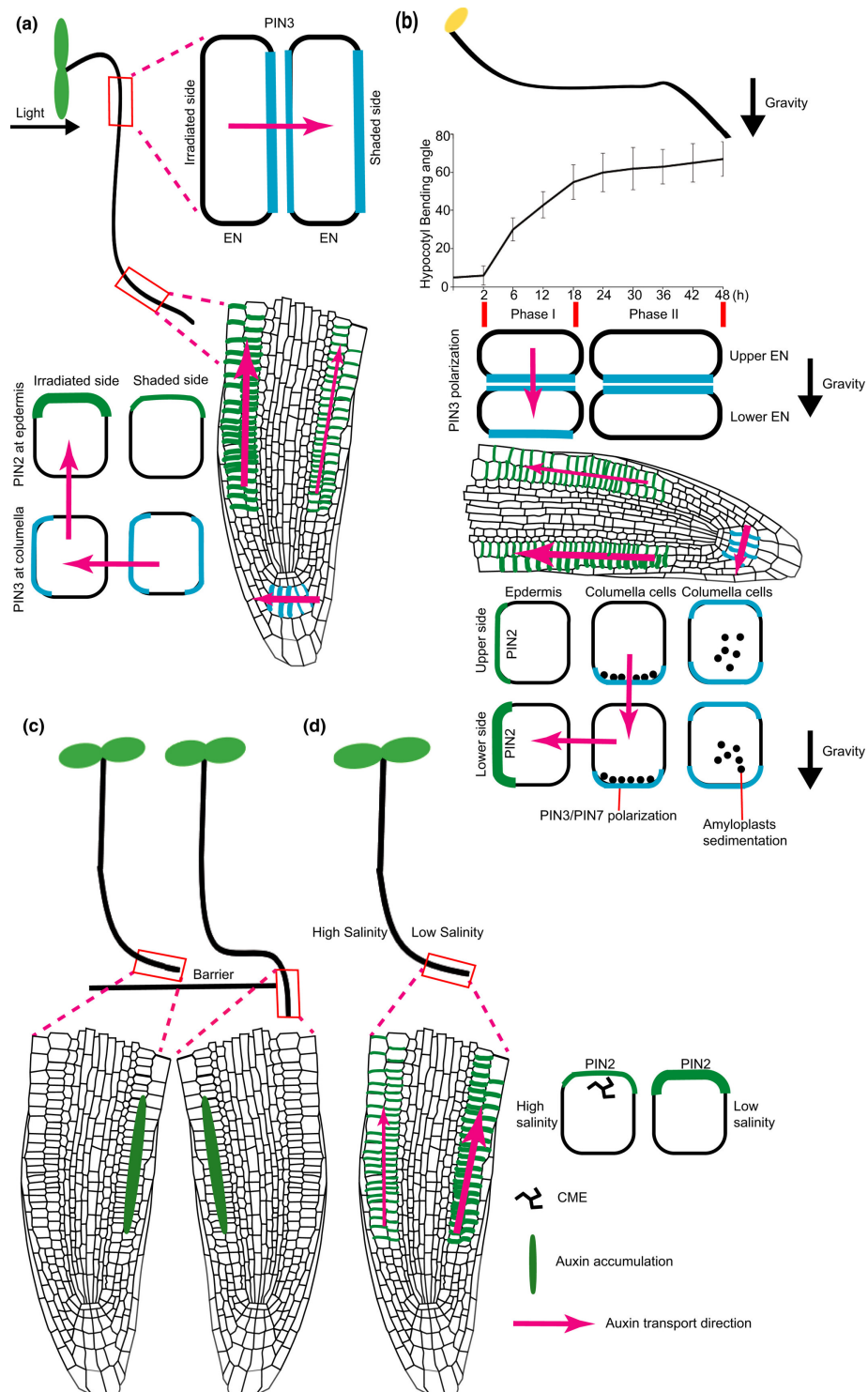
Fig. 1.8 PIN polarization-dependent polar auxin fluxes during tropisms (Han et al., 2021).

1.7.6 Hormonal crosstalk converging on PIN-mediated auxin transport

Plant hormone regulation of physiology and development is frequently characterized by complex feedback mechanisms and extensive crosstalk among signalling pathways (Vanstraelen and Benková, 2012). A quintessential example is, under osmotic stress, enhanced ABA signalling predominates to downregulate PIN1 abundance (overriding any ethylene influence) while CK responses are modestly reduced and ethylene signalling is dispensable, yet auxin could restore PIN localization and root growth. This exemplifies a tissue-specific crosstalk between ABA, CK, ethylene and auxin that converges on PIN-mediated auxin transport (Rowe et al., 2016). ABA also reduces shootward auxin transport by downregulating *PIN2* expression and reducing PIN2 abundance at the plasma membrane, thereby altering auxin distribution in the root (Xie et al., 2021). Glucose induces expression of the ABA-responsive transcription factor ABI5, which suppresses PIN1 accumulation and thus lowers auxin levels to inhibit root meristem growth (Yuan, et al., 2014).

Furthermore, CK disrupts *PIN* gene expression in lateral root founder cells, thereby blocking the establishment of the auxin gradient necessary for proper lateral root primordium patterning (Laplaze et al., 2007). CK rapidly downregulates PIN1 by diverting it from endocytic recycling toward vacuolar lytic degradation, thereby modulating auxin distribution without altering transcription (Marhavý et al., 2011). Also, CK modulates polar auxin transport by differentially regulating *PIN* expression, repressing *PIN1*, *PIN3*, and *PIN4* while promoting *PIN7* transcription, thereby reshaping auxin distribution to control root meristem activity (Růžička et al., 2009).

Additionally, ethylene suppresses lateral root formation while enhancing IAA transport and upregulating the PIN3 and PIN7 (Lewis et al., 2011). Analogously, GA-driven root elongation depends on PIN1-mediated polar auxin transport, since loss of PIN1 function delays GA-induced DELLA protein degradation and

impairs the GA-promoted auxin response (Fu and Harberd, 2003). Meanwhile, SA modulates root auxin distribution in a concentration-dependent manner by regulating PIN carriers: at low SA levels it activates PIN1 while repressing PIN2 and PIN7 to promote auxin accumulation and meristem enlargement, whereas at high SA levels it represses PIN1, PIN2, and PIN7 to deplete auxin from the stem cell niche and inhibit meristematic division (Pasternak et al., 2019).

1.8 Salt stress-mediated perturbation of auxin homeostasis disrupts normal root development in *Arabidopsis thaliana*

Last century, people knew salinity is a critical abiotic stress that severely inhibits plant growth and development, with high salt levels markedly reducing root and shoot growth in many species (Gueta-Dahan et al., 1997; Hootsmans and Wiegman, 1998; Lin and Kao, 1996; Rodriguez et al., 1997; Zhong and Läuchli, 1993), including *Arabidopsis thaliana* (Wu et al., 1996). Auxin biosynthesis, transport, and feedback produce localized gradients that integrate development with environmental cues, including abiotic stresses such as drought and salinity (Marzi et al., 2024).

The root system is necessary for plants to absorb water and nutrients to support the growth and development of above-ground organs (Wang et al., 2006). The root system is the first organ to be stressed (Dinneny, 2019), with salt stress rapidly impairing cell division and expansion (Gong et al., 2020). Not only this, auxin distribution and levels may be disrupted, and the expression of auxin-related genes (including transporters) is altered, linking auxin signalling to the inhibition of root growth observed in saline conditions (Ribba et al., 2020). For example, salt stress inhibits root meristem growth by elevating nitric oxide levels, which stabilize AXR3/IAA17 and repress *PIN* gene expression, thereby lowering auxin levels and signalling to constrain root elongation (Liu et al., 2015). Salt stress rapidly reduces IAA levels and disrupts PIN2-mediated auxin

transport, shifting auxin out of the QC into elongation-zone epidermal and cortical cells, which impairs meristem activity and alters root architecture (Smolko et al., 2021). Moreover, salt stress impairs root development by altering auxin homeostasis, modulating YUC-, GH3-, and UGT-mediated IAA biosynthesis and conjugation while rapidly suppressing PIN2-driven auxin transport to redistribute auxin from the QC to epidermal and cortical cells, thereby reducing meristem activity and inhibiting root growth (Cackett et al., 2022). Salt stress disrupts root meristem maintenance by flattening redox gradients, particularly oxidizing the root cap initials and quiescent centre, which coincides with diffuse mislocalization of AUX1 and PIN1/2, leading to loss of the auxin maximum and impaired root development (Jiang et al., 2016). Collectively, these findings highlight that salt stress impairs the auxin transport network, fundamentally affecting root development.

1.9 Core steps of vesicular transport in plant cells

The membrane transport system in plant cells encompasses biosynthetic secretion, endocytosis, and vesicular transport pathways (Bonifacino and Glick, 2004; Uemura and Ueda, 2014). The vesicle transport system comprises four fundamental steps (Bonifacino and Glick, 2004; Cai et al., 2007) (Fig. 1.9).

Budding: Coat proteins recruited by Arf1/Sar1 GTPases assemble on donor membranes, deforming them into buds and selecting cargo via recognition of sorting signals, ultimately releasing coated vesicles such as clathrin-, COPI-, or COPII-coated carriers (Barlowe et al., 1994; Bonifacino and Lippincott-Schwartz, 2003).

Transport: Newly formed vesicles traverse the cytosol either by Brownian diffusion or via motor proteins (kinesin, dynein, myosin) carrying them along microtubules or actin filaments toward their target compartments (Hammer and Wu, 2002; Matanis et al., 2002).

Tethering: Specific Rab GTPases and their associated tethering factors mediate the initial, long-range contact between vesicles and the appropriate target membrane, ensuring targeting specificity before soluble *N*-ethylmaleimide-sensitive factor attachment protein receptor (SNARE) pairing (Sztul and Lupashin, 2006; Whyte and Munro, 2002).

Fusion: Vesicle-associated SNAREs (v-SNAREs) pair with cognate target cell-associated SNAREs (t-SNAREs) on the target membrane to form a trans-SNARE complex, whose assembly provides the energy to drive lipid bilayer merger and cargo delivery (Hanson et al., 1997; Rothman, 1994).
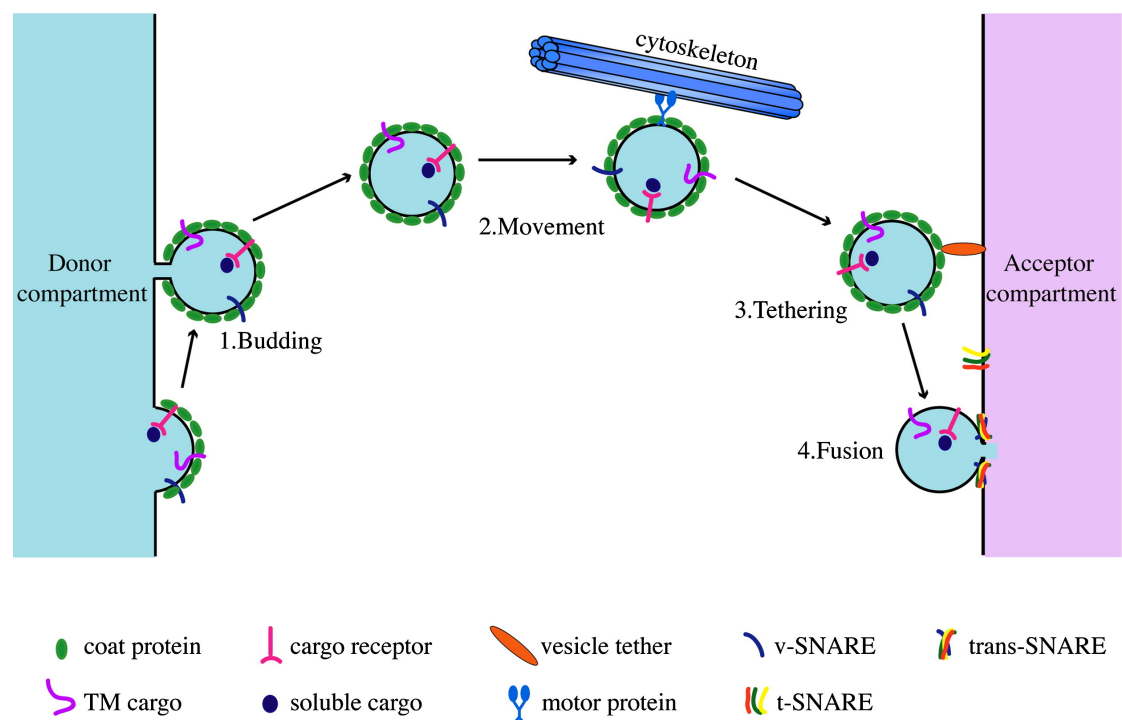
Fig. 1.9 The four essential steps in vesicle transport (Cai et al., 2007).

1.10 SNARE proteins in plant membrane transport

1.10.1 SNARE proteins composition and classification

Eukaryotic cells have evolved SNARE proteins that mediate vesicle fusion between transport vesicles and target membranes (Chen and Scheller, 2001;

Mayer, 2002). SNARE proteins belong to a superfamily of small proteins, typically composed of 100-300 amino acids (Jahn and Scheller, 2006). The SNARE motif, which consists of 60-70 amino acids, is formed by a heptad repeat sequence that assembles into a coiled-coil structure through hetero-oligomeric interactions (Bassham and Blatt, 2008; Jahn and Scheller, 2006; Rehman and Di Sansebastiano, 2013).

The *Arabidopsis thaliana* genome encodes over 60 SNARE genes, whose protein products are distributed across various subcellular compartments (Lipka et al., 2007; Sanderfoot, 2007; Uemura et al., 2004) (Fig. 1.10). Functionally, SNAREs can be classified into v-SNAREs and t-SNAREs (Han et al., 2017; Söllner et al., 1993). Structurally, they are divided based on the conserved glutamine (Q) or arginine (R) residue in the central layer of the SNARE motif into Q- and R-SNAREs (Fasshauer et al., 1998). Technically, SNARE proteins can be classified into four core types, Qa, Qb, Qc, and R, based on their sequence characteristics, each corresponding to one of the four helices forming the functional complex (Kienle et al., 2009; Kloepper et al., 2007; Yadav et al., 2024).
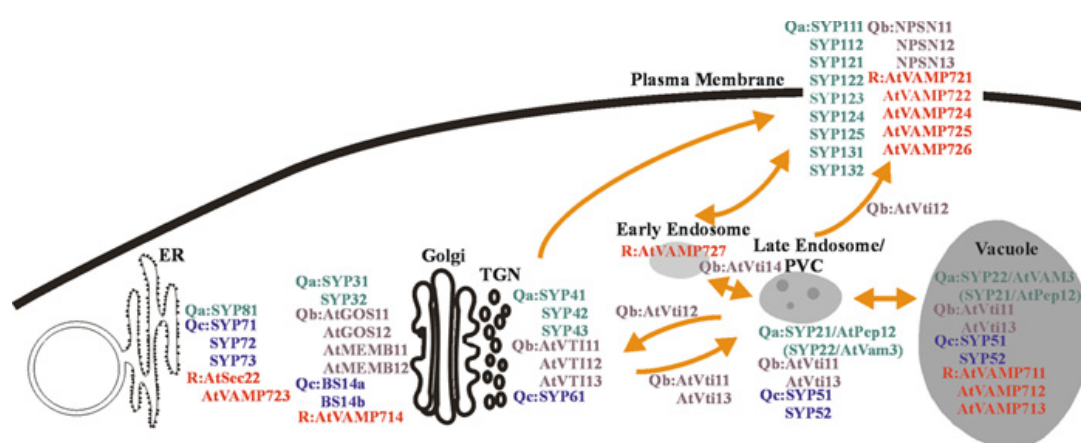
Fig. 1.10 The subcellular location of SNAREs in *Arabidopsis thaliana* (Uemura et al., 2004).

1.10.2 Classification and functional roles of *Arabidopsis thaliana* VAMP7-like R-SNAREs

Plant genomes encode R-SNARE proteins that are classified into three major subfamilies: Sec22-, YKT6-, and vesicle associated membrane protein 7 (VAMP7)-like R-SNAREs (Sanderfoot, 2007). In *Arabidopsis thaliana*, VAMP7-like R-SNAREs are divided into two gene families comprising four and eight members respectively. The four VAMP71 family proteins are involved in endosomal transport (Uemura et al., 2004), while the eight VAMP72 family proteins are implicated in secretion at the plasma membrane (Sanderfoot, 2007; Uemura et al., 2004), with an N-terminal cytosolic region containing the SNARE motif and a C-terminal transmembrane anchor features. In *Arabidopsis thaliana*, VAMP7s are critical for a range of physiological processes, including responses to abiotic stress (Leshem et al., 2010), cytokinesis (El Kasmi et al., 2013; Zhang et al., 2011), and defence responses (Yun et al., 2013).

1.10.3 VAMP714: a potential regulator of salt-stress responses

VAMP714 is a R-SNARE protein revealed by activation tagging to be a key regulator of *Arabidopsis* root growth, acting by mediating the fusion of PIN-containing vesicles at the plasma membrane (Gu et al., 2021). Loss or misexpression of VAMP714 disrupts polar auxin transport, leading to mislocalization of PIN1 and PIN2 and consequent defects in auxin gradient formation, all of which are restored by reintroducing VAMP714 (Gu et al., 2021). Live-cell imaging shows VAMP714-labeled vesicles moving toward the plasma membrane alongside PIN proteins, implicating VAMP714 in both PIN delivery and recycling (Gu et al., 2021). These findings position VAMP714 as an essential component of the vesicle-trafficking machinery that sustains directional auxin flow.

Only a few studies have examined the role of VAMP714 in salt tolerance. One recent study focuses on the histone deacetylase SRT2 and found that it is

induced to deacetylate H4K8 at the *VAMP714* promoter, repressing *VAMP714* transcription and thereby limiting VAMP714-mediated H_2O_2-containing vesicle trafficking to enhance salt tolerance during seed germination (Tang et al., 2022). Another study focuses on VAMP711 but briefly mentioned the potential of VAMP714 to participate in the salt stress response (Leshem et al., 2006).

Together, these findings firmly link VAMP714 to early salt-stress responses at least in some plant tissues but leave unanswered how VAMP714 influences other developmental processes, what phenotypes it mediates, and how its activity is regulated over time and space. To address these gaps, we have undertaken a comprehensive analysis of molecular mechanism of VAMP714, focusing on its contribution to salt tolerance, in *Arabidopsis thaliana*.

The principal hypothesis of this study is that VAMP714 integrates auxin- and reactive oxygen-mediated signalling to mediate salt stress responses in the *Arabidopsis thaliana* root, based on known observations about the function of VAMP714.

Therefore the main aim of the work described in this thesis is to understand better the role of VAMP714 in salt stress in the root of *Arabidopsis*.

This will be addressed through the following objectives:

1. An understanding of the effects of salt stress on *VAMP714* gene expression and subcellular localisation of the VAMP714 protein in roots.

2. An understanding of the role of VAMP714 in auxin-mediated root development under salt stress.

3. A characterisation of VAMP714 protein partners in the salt response.

4. A global transcriptomic survey of VAMP714-linked pathways under salt stress conditions.

Chapter 2: Materials and methods

2.1 Materials

2.1.1 Plant material

Arabidopsis thaliana wild-type (WT) seeds, that is the Columbia ecotype (Col-0) and two *vamp714* loss-of-function mutants, SALK_020516 and GABI_844B05 (hereafter referred to as SALK and GABI, respectively), were obtained from the Nottingham Arabidopsis Stock Centre (Nottingham University, Sutton Bonington, UK). A dominant-negative (DN) mutant of *VAMP714*, was as described (Gu et al., 2021), and only lacked the transmembrane domain while the other domains were retained, allowing it to compete in transgenic plants with functional VAMP714 in SNARE complex formation (Uemura et al., 2005).

Reporter lines with auxin-responsive promoter DR5 driving reporter genes *β*-glucuronidase (GUS) or green fluorescent protein (GFP), abbreviated as *DR5::GUS* and *DR5::GFP* respectively, were kindly provided by Professor Ben Scheres (Wageningen University, Netherlands). *proPIN1::PIN1:GFP* and *proPIN2::PIN2:GFP* were kindly supplied by Dr. Johan Kroon (Durham University, UK). *proVAMP714::GUS*, *proVAMP714::VAMP714:mCherry*, and *pro35S::VAMP714:mCherry* lines were from lab stocks. *pro35S::CTL1:GFP* was kindly provided by Dr. Julien Agneessens (Durham University, UK). One T-DNA insertion line of *CTL1*, SALK_065853C (hereafter referred to as *ctl1*), was obtained from the Nottingham Arabidopsis Stock Centre (Nottingham University, Sutton Bonington, UK). All mutant and reporter lines are homozygous and in the Col-0 background.

2.1.2 Bacteria

Agrobacterium strain GV3101 and competent cells were kindly supplied by Dr. Johan Kroon (Durham University, UK) and NEB® 5-alpha competent *E. coli*

were from New England Biolabs (Ipswich, UK).

2.1.3 Chemicals and kits

Absolute ethanol (Fisher Scientific, Loughborough, UK), acetone (Fisher Scientific, Loughborough, UK), agar (Formedium, Swaffham, UK), calcium chloride ($CaCl_2$) (Merck Life Science UK, Gillingham, UK), dimethyl sulfoxide (DMSO) (Fisher Scientific, Loughborough, UK), glycerol (Fisher Scientific, Loughborough, UK), HNO_3 (Fisher Scientific, Loughborough, UK), hoagland′s No. 2 basal salt mixture (Merck Life Science UK, Gillingham, UK, H2395), hydrochloric acid (HCl) (Merck Life Science UK, Gillingham, UK), Hygromycin B (Merck Life Science UK, Gillingham, UK), IAA (Merck Life Science UK, Gillingham, UK), Kanamycin (Merck Life Science UK, Gillingham, UK), LB (Formedium, Swaffham, UK), L-Kynurenine (Merck Life Science UK, Gillingham, UK, K8625), Murashige and Skoog (MS) (Merck Life Science UK, Gillingham, UK), nitro blue tetrazolium chloride (NBT) (Merck Life Science UK, Gillingham, UK, N6876), *N*-1-naphthylphthalamic acid (NPA) (Merck Life Science UK, Gillingham, UK), sodium chloride (NaCl) (Melford Laboratories, Ipswich, UK), sodium phosphate dibasic (Na_2HPO_4) (Merck Life Science UK, Gillingham, UK), tween20 (Merck Life Science UK, Gillingham, UK), X-Gal (Melford Laboratories, Ipswich, UK), X-Gluc (Melford Laboratories, Ipswich, UK), 3,3'-Diaminobenzidine (DAB) (Merck Life Science UK, Gillingham, UK, D12384), 4-Phenoxyphenylboronic acid (PPBo) (Merck Life Science UK, Gillingham, UK, 480142), and 50 mM sodium phosphate buffer (pH 7.0) (Fisher Scientific, Loughborough, UK, J63791.AP). Other chemicals not mentioned were from Fisher Scientific (Loughborough, UK).

CAT Assay Kit (Merck Life Science UK, Gillingham, UK, MAK531), qPCRBIO SyGreen® Blue Mix Lo-ROX Kit (PCR Biosystems, London, UK, PB20.15), ReliaPrep™ RNA Miniprep Systems Kit (Promega UK, Southampton, UK, Z6111), and UltraScript® cDNA Synthesis Kit (PCR Biosystems, London, UK,

PB30.11).

2.1.4 Instruments and software

Centrifuge (Fisher Scientific, Loughborough, UK), CFX Connect Real-Time PCR Detection System (Bio-Rad Laboratories, California, US), CFX Duet Real-Time PCR System (Bio-Rad Laboratories, California, US), inductively coupled plasma mass spectrometry (ICP-MS) (Department of Chemistry, Durham University, UK), Leica M165FC Stereo Fluor microscope (Lecia Microsystems UK, Miton Keynes, UK), Mini Centrifuge (Fisher Scientific, Loughborough, UK), NanoDrop™1000 Spectrophotometer (Fisher Scientific, Loughborough, UK), pH meter (Fisher Scientific, Loughborough, UK), Real-Time PCR system (Fisher Scientific, Loughborough, UK), Zeiss Axioskop 50 microscope (Carl Zeiss Microscopy, Cambridge, UK), and Zeiss 800 LSCM (Carl Zeiss Microscopy, Cambridge, UK).

Excel (Microsoft, Redmond, US), Fiji (Schindelin et al., 2012), and Prism 10 (GraphPad Software, Boston, US).

2.1.5 Primers

Primers for homozygosis examination, quantitative real time PCR (RT-qPCR), and *VAMP714* DN mutant construction are presented in Appendix I and Appendix II.

2.2 Methods

2.2.1 Plant tissue culture

2.2.1.1 Seed sterilization

1) Seeds were washed with 70-75% (v/v) ethanol for 1 minute, then were treated with 5% (v/v) (final available chlorine 0.5-0.75% (w/v)) bleach (Fisher Scientific, Loughborough, UK, 10-15% (w/v) available chlorine), for

5 to 10 minutes (5 minutes is usually sufficient).

2) Seeds were rinsed three times immediately with sterilized double-distilled water (ddH$_2$O).

3) After the final rinse, the seeds were suspended in sterilized water and transferred to plates.

4) The plates were sealed with Micropore™ tape and the seeds were stratified by placing them at 4°C in the dark for 2 days.

2.2.1.2 Plant growth conditions

Prior to growth, seeds were stratified at 4°C for 2 days to synchronize germination. The seeds were then sown on growth medium sealed with Micropore™ tape. These plates were transferred to a growth cabinet under long-day conditions (16h light/8h dark) at 22°C with a light intensity of approximately 3000 lux (50 µmol m^{-2} s^{-1}), ensuring uniform light exposure by positioning all plates in the same area. Unless otherwise stated, all seedlings for treatment were 5 days post-germination (dpg) aseptically on growth medium in this study.

For soil cultivation, 14 dpg seedlings were transplanted from growth medium into pots filled with F2S Seed & Modular and Sand Compost (ICL professional horticulture), predominantly composed of Sphagnum moss peat. The plants were then grown under long-day conditions at 22°C with a light intensity of approximately 3000 lux (50 µmol m^{-2} s^{-1}), either in a controlled growth room or in a greenhouse.

2.2.1.3 Plant growth medium

Unless otherwise stated, the growth medium in this study refers to 1% (w/v) agar containing half-strength MS solid medium (Murashige and Skoog, 1962). The NaCl growth medium in this study refers to 1% (w/v) agar containing half-strength MS solid medium with different concentrations of NaCl.

1) To prepare the growth medium, 2.2 g of MS powder was dissolved in 900 mL of ddH2O in a beaker, and a magnetic stir bar was added to facilitate thorough mixing. (An additional 2.922 g, 5.844 g, 8.766 g, and 11.688 g NaCl were added to prepare 50, 100, 150, and 200 mM NaCl culture medium, respectively.)

2) The solution was transferred to a 1 L bottle and topped up with water to the 1 L mark.

3) The pH was adjusted to 5.7 by adding 1 M KOH dropwise while monitoring with a pH meter.

4) Next, 10 g of agar was added to the solution, then the medium was sterilized in an autoclave.

5) Once sterilized, the medium was poured into plates, and the plates were stored in a sealed plastic bag at 4°C.

2.2.1.4 Half-strength Hoagland′s No. 2 basal salt mixture liquid solution

1) 0.8 g of half-strength Hoagland′s No. 2 Basal Salt Mixture (Hoagland and Arnon, 1950) powder was dissolved in 900 mL of ddH$_2$O in a beaker, and a magnetic stir bar was added to facilitate thorough mixing. For NaCl treatment, an additional 8.766 g NaCl was added to prepare 150mM NaCl liquid solution.

2) The solution was transferred to a 1 L bottle and topped up with water to the 1 L mark, and labelled the bottle with autoclave tape.

3) The pH was adjusted to 5.7 by adding 1 M KOH dropwise while monitoring with a pH meter.

4) Next, the solution was sterilized in an autoclave and stored at room temperature (RT).

2.2.2 Microorganism culture

2.2.2.1 LB liquid culture medium

This medium was used for microbial cultures.

Reagent	Amount (1 L)
Tryptone	10 g
Yeast Extract	5 g
NaCl	10 g
ddH$_2$O	Up to 1 L

It was used after autoclaving, pH 7.2.

2.2.2.2 *E. coli* transformation

1) 50 µL DH5α competent cells were first allowed to thaw on ice.

2) Next, 4.5 µL of plasmid DNA was gently mixed with the competent cells using a pipette tip to ensure thorough homogenization.

3) The mixture was then incubated on ice for 30 minutes followed by a heat shock at 42°C for 30 seconds.

4) Immediately, the cells were returned to ice for 5 minutes.

5) Subsequently, 950 µL of SOC medium was added, and the culture was incubated at 37°C with shaking at 200 rpm for 1 hour.

6) After incubation, the culture was centrifuged at 12,000 rpm for 1 minute, and 700 µL of the supernatant was removed.

7) The remaining cell suspension was divided into aliquots of 50 µL and 250 µL, which were then evenly plated onto LB selection plates and incubated overnight at 37°C.

2.2.2.3 *Agrobacterium* transformation

1) For *Agrobacterium* GV3101 transformation, the competent cells (50 µL) were thawed on ice for 20 minutes.

2) Then, 3 µL of plasmid DNA containing the desired vector was added and

mixed quickly.

3) The mixture was immediately transferred to liquid nitrogen for 40 seconds, followed by a heat shock at 37°C for 5 minutes before being returned to ice for 1 minute.

4) After this, 1 mL of antibiotic-free LB medium was added, and the culture was incubated at 30°C with shaking at 200 rpm for 3 hours.

5) Finally, an appropriate volume of the bacterial suspension was plated onto LB solid medium supplemented with 50 µg/mL kanamycin, 10 µg/mL gentamicin, and 40 µg/mL rifampicin.

6) The plates were incubated for two days to obtain positive colonies.

2.2.2.4 *Arabidopsis thaliana* transformation by floral dip (based on Clough and Bent, 1998)

1) Validated *Agrobacterium* cultures were first grown in 5 mL LB medium with the appropriate antibiotics at 30°C with shaking overnight and then it was scaled up to 300 mL under the same conditions overnight.

2) The bacterial culture was centrifuged at 4500 rpm for 10 minutes at 25°C, and the supernatant was discarded.

3) The bacterial pellet was then resuspended in 1 L of 5% (w/v) fresh sucrose solution, and Silwet L-77 (v/v) was added to a final concentration of 0.05% (v/v).

4) *Arabidopsis thaliana* plants (5–6 weeks old, with abundant inflorescences) were prepared by removing mature siliques and pollinated flowers to enhance transformation efficiency.

5) The entire inflorescence was then immersed in the *Agrobacterium* suspension for 1 minute.

6) Transformed plants were kept in darkness for one day before being transferred to normal light (approximately 3000 lux (50 µmol m^{-2} s^{-1})) conditions with adequate watering.

7) Seeds were later harvested and screened on selection plates for the

identification of transformants.

2.2.3 Nucleic acids and PCR

2.2.3.1 Genomic DNA extraction

DNA extraction buffer was as follows:

Reagent	Amount (1 L)
CTAB	20 g
NaCl	81.9 g
1.0 M Tris-HCl (pH 8.0)	100 mL
0.5 M EDTA (pH 8.0)	40 mL
ddH$_2$O	Up to 1 L

1) After rapidly freezing in liquid nitrogen, the plant material was ground into a fine powder using a mortar and pestle.

2) Next, 400 µL of CTAB extraction buffer was added to the pulverized tissue in an EP tube and thoroughly mixed.

3) The mixture was incubated in 1 hour 65°C water bath to facilitate extraction.

4) After allowing the sample to RT, 500 µL of chloroform was added and the tube was inverted several times to ensure thorough mixing.

5) The sample was centrifuged at 13,000 rpm for 5 minutes at RT, and the resulting supernatant was carefully transferred to a new EP tube.

6) Subsequently, 400 µL of isopropanol was added, and the tube was inverted to mix the contents.

7) Finally, the sample was centrifuged at 13,000 rpm for 15 minutes at RT, the supernatant was discarded, and an appropriate volume of sterile ddH$_2$O was added to the pellet.

8) A NanoDrop^{TM}1000 Spectrophotometer was used to detect DNA concentration and quality.

2.2.3.2 Total RNA extraction

Total RNA was extracted using the ReliaPrep™ RNA Miniprep Systems Kit following the manufacturer's instructions.

1) Preparation and homogenization:

   All required solutions were prepared according to the technical manual. 1-thioglycerol was added to the LBA Buffer, and then the LBA + TG Buffer was added to the tissue sample. Up to 5 mg of plant tissue was disrupted using a homogenizer, followed by pipetting 7–10 times. The homogenate was cleared by centrifugation at 14,000 × g for 3 minutes, and the supernatant was transferred to a clean tube.

2) RNA precipitation and binding:

   The appropriate volume of 100% (v/v) isopropanol was added to the cleared lysate and was mixed briefly by vortexing for 5 seconds. Next, the lysate was transferred to a Minicolumn placed in a Collection Tube and was centrifuged at 12,000–14,000 × g for 1 minute at RT, which allowed the RNA to bind to the column.

3) Washing, DNase treatment, and elution:

   The flow-through was discarded, and the column was washed by adding 500 µL of RNA Wash Solution, then was centrifuged for 30 seconds. The bound RNA was treated with DNase I solution (applied directly onto the column membrane) and was incubated for 15 minutes to remove any contaminating DNA. This was followed by additional washes using Column Wash Solution and RNA Wash Solution to remove residual impurities. Finally, the column was transferred to an Elution Tube, nuclease-free water was added to elute the RNA, and the column was centrifuged for 1 minute. The column was discarded, and the eluted RNA were stored at –80 °C.

2.2.3.3 Conventional PCR

1) The master mix was prepared as follows:

Reagent	Amount (10 µL reaction)
5x My Taq	2.0 µL
Forward primer (10 µM)	1.0 µL
Reverse primer (10 µM)	1.0 µL
DNA polymerase	1.0 µL
Template DNA	1.0 µL
ddH$_2$O	Up to 10 µL final volume

2) Programme in PCR system:

Cycles	Temperature	Time
1	95 °C	1 min
35	95 °C	15 seconds
	56-65 °C	15 seconds
	72 °C	1 min / 1 kb
1	72 °C	10 mins
	4 °C	-

2.2.3.4 cDNA synthesis

Total RNA was extracted using the UltraScript® cDNA Synthesis Kit following the manufacturer's instructions.

1) The master mix was prepared as follows:

Reagent	Amount (20 µL reaction)
5x cDNA Synthesis Mix	4.0 µL
20x RTase	1.0 µL
Total RNA (between 4.0 pg and 0.4 µg)	X µL
PCR grade dH2O	Up to 20 µL final volume

Master mix was incubated at 42°C for 30 minutes and then incubated at 85°C

for 10 minutes to denature RTase by PCR system.

2.2.3.5 RT-qPCR

RT-qPCR was performed using the qPCRBIO SyGreen® Mix Lo-ROX Kit following the manufacturer's instructions.

1) Master mix:

Reagent	Amount (20 µL reaction)
2x qPCRBIO SyGreen® Mix	10 µL
Forward/Reverse primer (10 µM)	Per 0.8 µL
Template DNA (cDNA)	1 µL
PCR grade dH$_2$O	7.4 µL

2) Programme in CFX Connect Real-Time PCR Detection System or CFX Duet Real-Time PCR System:

Cycles	Temperature	Time
1	95 °C	2 min
40	95 °C	5 seconds
	65 °C	30 seconds
Melt analysis	Default	Default

2.2.4 The identification of mutants

2.2.4.1 The identification of T-DNA mutants

To characterize two T-DNA insertion mutants of *VAMP714*, namely SALK_020516 and GABI_844B05, a three-primer PCR strategy was employed to identify homozygous T-DNA insertion. For the SALK line, genomic primers LP_SALK_020516 and RP_SALK_020516 were used to amplify a wild-type band, while a second combination of the genomic primer RP_SALK_020516 with the T-DNA left border primer LB_SALK amplified the T-DNA flank sequence, thereby confirming the insertion site. Similarly, for the GABI line, two

primer sets, LP_GABI_844B05 with RP_GABI_844B05, and RP_GABI_844B05 with LB_GABI, were utilized to verify the insertion. Subsequently, RT-qPCR analysis confirmed the absence of *VAMP714* mRNA abundance in these mutants. The identification of *CTL1* T-DNA insertion mutant, that is *ctl1*, was kindly provided by Dr Julien Agneessens (Durham University, UK). Subsequently, RT-qPCR analysis confirmed the absence of *CTL1* mRNA abundance in this mutant. Related primers were in Appendix I.

2.2.4.2 Dominant negative (DN) mutants of VAMP714

The wild-type *VAMP714* gene encodes a protein comprising a Longin domain, a SNARE domain, and a transmembrane domain. In the DN, only a non-functional fragment of the *VAMP714* gene was expressed, under the control of the CaMV35S gene promoter (Gu et al., 2021); this fragment contained the Longin and SNARE domains but lacked the transmembrane domain. Despite its deficiency, this truncated fragment is expected to still anchor to the SNARE complex, which is composed of Qa, Qb, and Qc SNARE proteins, thereby interfering with the proper incorporation of the functional VAMP714 protein and ultimately impairing its activity. The mRNA abundance of *VAMP714* in DN was further confirmed by RT-qPCR. Related primers were in Appendix I.

2.2.4.3 The identification of reporter lines

Transgenic positive seedlings for the *proVAMP714::GUS* construct were selected using 50 µg/mL kanamycin, and the selected seedlings were subjected to preliminary experiments to verify that their expression patterns were consistent with previous studies (Gu et al., 2021). The experimental procedure was adapted following modifications described by Harrison et al. (2006). Specifically, seeds obtained after floral dip transformation were sown on culture medium supplemented with 50 µg/mL kanamycin. Following a 2-day stratification period, the plates were transferred to a growth regimen consisting of 6 hours of light, 48 hours of darkness, and an additional 48 hours of light.

Kanamycin-resistant seedlings were easily identified by their green, expanded cotyledons, in contrast to non-resistant seedlings, which exhibited pale, unexpanded cotyledons. Similarly, for the *proVAMP714::VAMP714:mCherry* and *pro35S::VAMP714:mCherry* lines, transgenic positive seedlings were selected using 25 µg/mL hygromycin B. In this case, the experimental protocol was also modified according to Harrison et al. (2006). Seeds were plated on culture medium containing 25 µg/mL hygromycin B after floral dip transformation and underwent a 2-day stratification period followed by 6 hours of light, 48 hours of darkness, and 60 hours of light. Hygromycin B-resistant seedlings were distinguished by their long hypocotyls (0.8–1.0 cm), whereas non-resistant seedlings had short hypocotyls (0.2–0.4 cm). Confocal microscopy was used to check the fluorescence expression pattern of the positive seedlings after screening to verify its consistency with previous studies (Gu et al., 2021). The mRNA abundance of *VAMP714* in these lines was further confirmed by RT-qPCR. The construction of *pro35S::CTL1:GFP* was by Dr Julien Agneessens (Durham University, UK). The mRNA abundance of *AtCTL1* in this mutant was further confirmed by RT-qPCR. Related primers are presented in Appendix I.

2.2.5 Bioinformatics analysis

2.2.5.1 Molecular evolutionary genetics analysis (MEGA)

Here, the *VAMP7* gene family from *Arabidopsis thaliana* was investigated. Relevant sequences were downloaded from the TAIR database (http://www.arabidopsis.org/) using default settings.

1) Bulk protein sequence preparation.

    The TAIR homepage was entered, and 'BULK DATA RETRIEVAL' under 'TOOLS' was selected. 'SEQUENCES' was selected to enter the relevant page. The gene IDs were submitted in the text box, one gene number per line, meanwhile select 'ARAPORT11 PROTEIN SEQUENCES' or 'ARAPORT11 CODING SEQUENCES' under the 'DATASET'. 'GET

SEQUENCE' was clicked, and each sequence was copied and pasted into a TXT format.

2) Sequence alignment.

The MEGA software was opened. 'EDIT/BUILD ALIGNMENT' under 'ALIGN' was selected, and 'CREATE A NEW ALIGNMENT' was clicked. Type was 'PROTEIN' or 'DNA'. 'INSERT SEQUENCES FROM MEGA/FASTA/TEXT/SEQUENCER FILES' was clicked to upload the sequence. 'ALIGN SELECTED BY CODONS USING THE CLUSTALW ALGORITHM' was selected for sequence alignment.

3) Construct the phylogenetic tree.

'PHYLOGENY' was clicked, and the appropriate natural tree construction method was selected, here was unweighted pair group method with arithmetic mean (UPGMA). 'BOOTSTRAP METHOD' under 'TEST OF PHYLOGENY' was clicked and '1000 repetitions' was selected. The phylogenetic tree was constructed.

2.2.5.2 Promoter analysis

Here, promoter sequences of the *AtVAMP7* gene family from *Arabidopsis thaliana* were investigated. Relevant sequences were downloaded from the TAIR database (http://www.arabidopsis.org/) using default settings.

1) The PlantPAN 3.0 homepage (http://plantpan.itps.ncku.edu.tw/index.html) was entered, and 'GENE SEARCH' was selected.

2) 'ARABIDOPSIS THALIANA' was selected to enter the relevant page.

3) The VAMP714 (AT5G22360.1) gene ID was submitted and searched.

4) 'ACCESS PROMOTER ANALYSES' was clicked and 'VISUALIZATION' was chosen.

5) 'ACCESS PROMOTER ANALYSIS (JBROWSE)' was clicked to check the experimental or the predicted binding sites from ChIP-seq data. 'SALT' was submitted to retrieve relevant TFs belong to the subset of promoter analysis & ChIP-seq with the similar score more than 0.950.

6) For co-expression analysis, the menu was returned to step 4) and 'COEXPRESSION ANALYSES' was selected to do next analysis. At this step, TFs with PCC value more than 0.950 were screened.

2.2.5.3 Protein–protein interaction (PPI) analysis

Here, the software was Cytoscape3.10.1. The following procedures all use default settings.

1) 'FILE', 'NEW NETWORK', and 'EMPTY' were clicked one by one.
2) The PPI data were imported from Novogene company directly into the software, using the appropriate Excel version.
3) VAMP714 was selected as the 'SOURCE NODE', and its interactors were set as 'TARGET GENE'.
4) The view was switched to the 'STYLE' page, and the style was changed to 'SAMPLE 1'.
5) The 'EDGE' menu was opened, 'LABEL' was deselected, and the labels were deleted.
6) 'NODE', 'FILL COLOR', 'CODE' under the 'COLUMN', and 'DISCRETE MAPPING' under the 'MAPPING TYPE' were clicked one by one to match the relevant proteins.
7) 'FILE' was clicked, 'EXPORT' was selected, and 'NETWORK TO IMAGE' was chosen to obtain the image.

2.2.5.4 RNA sequencing (RNA-seq)

Col-0 and GABI seedlings were grown on media either supplemented with 150 mM NaCl or under control (salt-free) conditions and were exposed for 0, 3, 9, or 24 hours. After treatment, root tissues were harvested for RNA extraction. Library construction and RNA sequencing were subsequently performed by Novogene (Cambridge, UK). The sequencing process was based on the Illumina platform, which utilized the sequencing-by-synthesis (SBS) method to ensure high throughput and accuracy.

For each genotype and treatment time point, three biological replicates were processed, yielding a total of 24 cDNA libraries. The use of multiple replicates enhanced the statistical robustness of downstream analyses. Novogene carried out the entire library preparation procedure—including mRNA purification using poly-T oligo-attached magnetic beads, cDNA synthesis, end repair, A-tailing, adapter ligation, size selection, and amplification—followed by rigorous quality control using instruments such as Qubit and the Agilent Bioanalyzer.

Following sequencing, Novogene provided comprehensive bioinformatics analyses. These analyses included the identification of differentially expressed genes (DEGs), Gene Ontology (GO) enrichment analysis, Kyoto Encyclopedia of Genes and Genomes (KEGG) pathway mapping, and PPI network analysis. The raw data can be accessed in the GEO database (https://www.ncbi.nlm.nih.gov/geo/, GSE307070).

2.2.6 Salt treatment time points and concentration selection

In *Arabidopsis thaliana*, previous work has shown that the most significant transcriptional alterations occur within the first 24 hours of exposure to 140 mM NaCl, with a stabilization of transcription observed between 24 and 48 hours (Geng et al., 2013). This period is generally categorized into three phases: a quiescent phase (approximately 3 hours, representing the rapid initial response), a recovery phase (8–13 hours), and a homeostasis phase (13–24 hours). Based on these observations, treatment time points were selected at 0, 3, 9, and 24 hours. For salt concentration, 200 mM NaCl was the highest concentration tolerated in short-term experiments, and therefore, a stepwise gradient was applied in 50 mM increments for detailed molecular studies. Unless otherwise stated, all seedlings for treatment were 5 dpg aseptically on growth medium.

2.2.7 Root phenotypic parameters

Root phenotypic parameters were measured as described previously with slight modifications (Fu et al., 2019; Wang et al., 2009). Specifically, primary root length (initial primary root length plus primary root elongation), primary root elongation, lateral root elongation, lateral root density (number of lateral roots divided by the primary root length and was reported as the number of lateral roots per centimetre of primary root, roots cm^{-1}), relative root growth (primary root elongation with treatment divided by primary root elongation without treatment).

2.2.8 Phenotypic assays

2.2.8.1 NaCl stress experiment

5 dpg seedlings were transferred to growth medium containing NaCl at concentrations of 0-200 mM and grown for an additional 7 days.

2.2.8.2 Exogenous IAA and NPA treatment

5 dpg seedlings were transferred to growth medium supplemented with different treatments, namely 150 mM NaCl (control), 150 mM NaCl with 30 nM IAA, or 150 mM NaCl with 10 μM NPA for an additional 7 days. Control was treated with equivalent concentrations of absolute ethanol (final concentration 0.1% (v/v)) and DMSO (final concentration 0.1% (v/v)).

2.2.8.3 CaCl$_2$ rescue experiment

5 dpg seedlings were transferred to growth medium supplemented with different treatments, namely without treatment (control), 3 mM CaCl$_2$, 150 mM NaCl, or 150 mM NaCl with 3 mM CaCl$_2$ for an additional 5 days.

2.2.9 Gene expression analysis

Three independent biological replicates were performed, with each biological replicate containing three technical replicates to ensure reproducibility. RT-

qPCR was then conducted, and the relative expression levels of the target gene were calculated using the 2^-ΔΔCt method.

2.2.9.1 *VAMP714* transcript abundance analysis

Total RNA was extracted from whole seedlings or roots of 5 dpg seedlings on growth medium. *ACTIN2* was chosen as the internal control gene.

2.2.9.2 NaCl stress experiment

Seedlings were transferred to growth medium supplemented with 0-200 mM NaCl for different durations (0, 3, 9, or 24 hours), and root samples were collected for RNA extraction. *UBQ5* was chosen as the internal control gene.

2.2.9.3 IAA and NPA experiment

Seedlings were transferred to growth medium supplemented with four different treatments: without treatment (control), 150 mM NaCl, 150 mM NaCl with 10 µM IAA, or 150 mM NaCl with 10 µM NPA for additional 3 hours, root samples were collected for RNA extraction. Control was treated with equivalent concentrations of absolute ethanol (final concentration 0.1% (v/v)) and DMSO (final concentration 0.1% (v/v)). *UBQ5* was chosen as the internal control gene.

2.2.9.4 Choline experiment

Seedlings were transferred to growth medium supplemented with 10 µM choline, supplied as choline chloride (Merck Life Science UK, Gillingham, UK), or without treatment (control) for an additional 9 hours, and root or whole seedling samples were collected for RNA extraction. *ACTIN2* was chosen as the internal control gene.

2.2.10 Histochemical staining

2.2.10.1 GUS staining

1) Phosphate buffer (pH 7.0):

Reagent	Amount (100 mL)
Na_2HPO_4 (0.2 M)	30.5 mL
NaH_2PO_4 (0.2 M)	19.5 mL
ddH_2O	Up to 100 mL

2) GUS buffer (pH 7.0):

Reagent	Amount (100 mL)	Concentration
EDTA	0.744 g	10 mM
Triton X-100	100 μL	0.1 % (v/v)
Potassium ferricyanide	16.4 mg	0.5 mM
Ferrocyanide	21.1 mg	0.5 mM
Phosphate Buffer	Up to 100 mL	

X-Gluc 20 mM stock: 10.4mg/mL X-Gluc in N-N-dimethylformamide (DMF). GUS staining was carried out by adding 50 μL of X-Gluc stock to 1 mL of GUS buffer, followed by immersing the tissue sample in the resulting staining solution. The sample was then incubated at 37°C overnight to allow sufficient enzymatic reaction. After incubation, the stained tissue was sequentially cleared by a series of ethanol solutions with increasing concentrations. Finally, the tissue was mounted on slides and prepared for Zeiss Axioskop 50 microscope observation.

2.2.10.2 Staining area quantification for GUS staining

Here, staining area quantification was performed using Fiji software. The following procedures all use default settings.

1) One of the experimental images was imported into Fiji, then 'Plugins',

'Macros', and 'Record' were clicked in sequence.

2) 'Image', 'Type', and '8-bit' were selected in turn.

3) 'Image', 'Adjust', and 'Threshold' were clicked in sequence.

4) 'Auto' was selected to identify staining areas.

5) 'Analyze', 'Set Measurements', and 'Area fraction, Limit to threshold, Display label, Area, Mean gray value, and Min & max gray value' were clicked one by one.

6) 'Analyze' and 'Measure' were selected in sequence.

7) 'Process', 'Batch', and 'Macro' were clicked one by one, and then all other experimental images were placed in the same folder.

8) Finally, the code in the Recorder page was copied to the blank area at the bottom of the Batch Process page.

9) Only the '%Area' column was retained for analysis. 0h 0mM NaCl was used as the control to find the average value and perform normalization.

10) Prism 10 was used to visualize.

2.2.10.3 Nitro blue tetrazolium chloride (NBT) staining

For NBT staining, the reagent was first dissolved in 50 mM sodium phosphate buffer (pH 7.0) to prepare a 1 mg/mL solution. The tissue samples were then incubated in the NBT solution for 2 hours at 37°C, followed by three washes with ddH$_2$O to halt the reaction. Subsequent clearing was performed by incubating the samples in 95% (v/v) ethanol for 10 minutes at 37°C, after which the samples were again washed three times with ddH$_2$O to fully terminate the clearing process. Finally, the treated samples were either stored in fresh 50 mM sodium phosphate buffer (pH 7.0) at 4°C for up to 24 hours or directly observed. All steps were carried out under light protection, and a shaker was employed to ensure uniform staining and clearing.

2.2.10.4 3,3'-Diaminobenzidine (DAB) staining

For DAB staining, DAB was initially dissolved in ddH$_2$O, and the pH was adjusted to 3.8 using HCl to achieve a 1 mg/mL solution. Thereafter, a specified amount of Na$_2$HPO$_4$ and Tween20 were added to prepare the final reaction solution, adjusted to pH 7.0. The samples were then incubated in this DAB reaction solution for one hour at RT and subsequently washed three times with ddH$_2$O to stop the reaction. Clearing was accomplished by incubating the samples in 95% (v/v) ethanol for 10 minutes at RT, followed by three additional washes with ddH$_2$O. The processed samples were then either stored in 50% (v/v) glycerol at RT for up to 24 hours or directly examined. As with the NBT staining procedure, all DAB staining steps were performed under light protection with the use of a shaker to ensure consistent staining and clearing throughout the process.

2.2.10.5 Staining intensity quantification for NBT and DAB staining

Meristem (the main site of auxin and VAMP714 functional activity in the root tip) stretches up to 200 μm away from the junction between root and root cap (Verbelen et al., 2006).

Here, staining intensity quantification was performed using Fiji. The following procedures all use default settings.

1) The image with the scale bar (200 μm) was imported into Fiji, and then the straight line was used to measure 200 μm in length.

2) The shortcut tool 'Polygon selections' was clicked to select the specific range to be measured.

3) 'Process', 'Subtract Background', and 'OK' with Light background and 50.0 pixels of Rolling ball radius (that is the default setting) were selected in turn. This made the background blacker later, making the measurement result more accurate.

4) 'Image', 'Type', '8-bit', 'Edit', 'Invert', 'Analyze', 'Set Measurements', and

'Integrated density, Limit to threshold, Display label, Area, Mean gray value, and Min & max gray value' were clicked sequentially.

5) 'Analyze' and 'Measure' were selected one by one to make the Results page pop up.

6) After that, each image was processed through step 3) - 5) one by one.

7) Only the 'Mean' were retained. *Col-0* without treatment was used as the control to find the average value and perform normalization.

8) Prism 10 was used to visualize.

2.2.11 CAT assay

ROS scavenging activity was quantified in roots samples using the CAT Assay Kit following the manufacturer's protocol. One unit is the amount of catalase that decomposes 1 µmole of H_2O_2 per min at pH 7.0 and RT.

2.2.12 Inductively coupled plasma-mass spectrometry (ICP-MS) for elemental (Na^+, K^+, Ca^{2+}) analysis

Three-week-old seedlings grown on solid medium were transferred into containers filled with half-strength Hoagland's No. 2 Basal Salt Mixture liquid solution for one week to refresh the ionic environment. During this acclimation period, the liquid solution was replaced every 3.5 days (Wang et al., 2020), after which the seedlings were deemed ready for subsequent treatments.

For the hormone experiments, the seedlings were exposed to four distinct treatments in half-strength Hoagland's No. 2 Basal Salt Mixture liquid medium for an additional 24 hours: a Mock treatment (with equivalent concentrations of absolute ethanol (final concentration 0.1% (v/v)) and DMSO (final concentration 0.1% (v/v)), 150 mM NaCl, 150 mM NaCl combined with 10 µM IAA, and 150 mM NaCl combined with 10 µM NPA. In a similar manner, for the auxin biosynthesis inhibitor experiments, four treatments were applied for 24 hours: a Mock treatment (with equivalent concentrations of DMSO (final concentration

0.1% (v/v)) and acetone (final concentration 0.1% (v/v)), 150 mM NaCl, 150 mM NaCl supplemented with 30 µM L-kynurenine, and 150 mM NaCl supplemented with 30 µM PPBo.

After the treatment period, whole seedlings were harvested and dried at 65°C for three days. The dry weight of each sample was recorded to ensure consistency among replicates. Subsequently, the dried samples were digested in 1 mL of 65% (v/v) HNO_3 by heating at 72°C for two hours, followed by an overnight incubation at RT (Fu et al., 2019). The resulting digest was then diluted 1000-fold in 2.5% (v/v) HNO_3 containing beryllium (Be), indium (In), and silver (Ag) as internal standards. Finally, the concentrations of Na^+, K^+, and Ca^{2+} were quantified using ICP-MS at the Department of Chemistry, Durham University, UK.

2.2.13 Statistical analysis

All data were presented as mean ± SD from three biological replicates. Statistical significance was determined using Student's *t*-test ($p < 0.05$).

Chapter 3: VAMP714 as a central mediator of salt-stress-induced auxin reprogramming of roots in *Arabidopsis thaliana*

3.1 Introduction

The VAMP7 protein family is particularly noteworthy for its involvement in vesicle-mediated processes that are essential for *Arabidopsis thaliana* responses under abiotic stress. For example, VAMP711-4 are linked to salt stress (Leshem et al., 2006) and VAMP711 also participates in drought stress regulation (Leshem et al., 2010; Xue et al., 2018). Moreover, a microarray analysis of *VAMP71* gene expression suggests that *VAMP714* transcript level is influenced by salt stress, indicating a potential regulatory role (Leshem et al., 2006). Furthermore, research by Tang et al. (2022) demonstrates that the histone deacetylase SRT2 regulates salt tolerance during seed germination through VAMP714. Although these studies do not exclusively focus on VAMP714, they provide compelling evidence of its possible function as a regulator in the salt stress response. A recent study from this lab reveals that VAMP714 is critical for the polarization of PIN proteins, which are important to the auxin transport system (Gu et al., 2021). Based on these findings, this chapter aims to explore the hypothesis that VAMP714 acts as a pivotal connection between auxin signalling and salt stress responses in roots of *Arabidopsis thaliana*. In this chapter, "WT" refers to the Col-0 ecotype, and 5 dpg seedlings serve as material for treatment or analysis.

3.2 Preliminary bioinformatics analysis of VAMP714

3.2.1 VAMP7 family homology analysis

In *Arabidopsis thaliana*, the *VAMP7* gene family is organized into two distinct subfamilies based on sequence similarities: the *VAMP71* subfamily comprises

VAMP711-4, and the *VAMP72* subfamily includes *VAMP721-8* (Sanderfoot, 2007; Uemura et al., 2004). Analysis of both the coding DNA sequences (Fig. 3.1a) and the protein sequences (Fig. 3.1b) revealed that they could be segregated into two distinct groups. This division highlighted the evolutionary divergence within the family. Interestingly, VAMP714 displayed markedly lower homology compared to other members of the subfamily (Fig. 3.1a-b). These results indicate that, despite sharing some common functional attributes, the various members of the *VAMP7* gene family also possess distinct molecular characteristics. This divergence likely contributes to their specialized roles in vesicle trafficking and other processes.
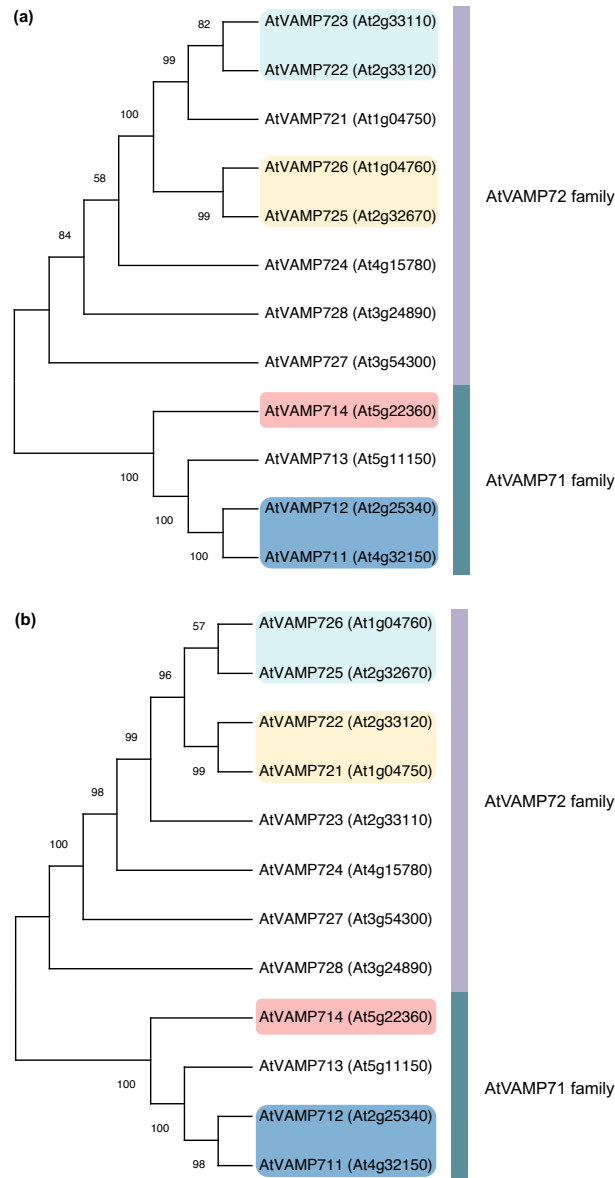
Fig. 3.1 VAMP7 family homology analysis.

Homology analysis based on coding DNA sequence **(a)** and protein sequence **(b)**. UPGMA, 1000 repetitions.

3.2.2 *VAMP714* gene promoter analysis

A detailed examination of the *VAMP714* gene promoter revealed that it contains multiple binding sites for salt stress related transcription factors, including *DIV2* (Fang et al., 2018), *HAT22* (Seok et al., 2022), *NF-YB2* (Li et al., 2024) and *RD26* (Chung et al., 2014) (Fig. 3.2). This finding implies that the regulation of *VAMP714* expression is potentially influenced by salt stress conditions.
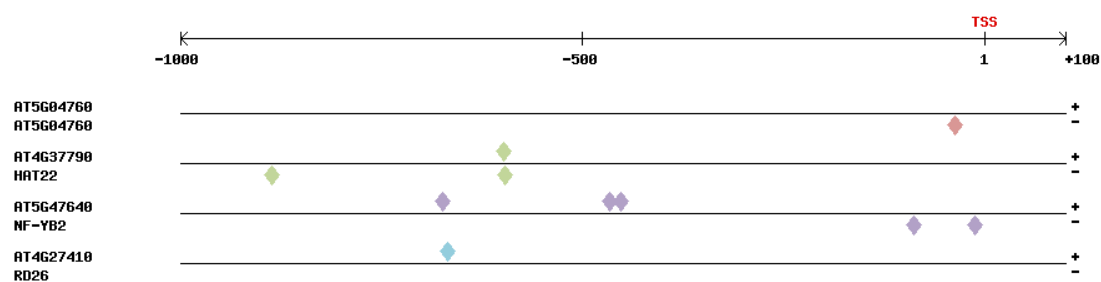
Fig. 3.2 *VAMP714* gene promoter analysis.

The top horizontal line is the promoter region of *VAMP714*, and TSS is transcription start site.

'+' is the sense strand and '-' is the antisense strand, similar score ≥ 0.95.

3.2.3 *VAMP714* gene co-expression analysis

The co-expression analysis of *VAMP714* (Table 3.1) indicated that it was closely linked with salt stress related genes *RR12* (Mason et al., 2010) and *GRP2* (Park et al., 2009). This strong association suggests that *VAMP714* shares common regulatory networks with other salt stress-responsive genes, implying a potential functional role in stress adaptation. Collectively, these findings imply that *VAMP714* is involved in modulating plant responses to salt stress.

Table 3.1 *VAMP714* gene co-expressed analysis.

Symbol	Position (Strand)	PCC value
RR12 (AT2G25180)	-683 (+), -472 (-)	0.98
GRP2 (AT4G38680)	67 (+)	0.95

(+) is the sense strand, (-) is the antisense strand. (PCC value ≥ 0.95).

3.3 Identification and molecular characterisation of mutants of *VAMP714*

3.3.1 *VAMP714* T-DNA insertion mutant identification

T-DNA insertion lines have established themselves as an indispensable asset in plant molecular genetics and functional genomics, particularly within the model organism *Arabidopsis thaliana* (Radhamony et al., 2005). One of the

primary advantages of these lines is their capacity to generate stable and heritable gene knockouts (Wang, 2008). Moreover, comprehensive T-DNA insertion libraries have been developed that encompass a significant portion of the *Arabidopsis thaliana* genome (Alonso et al., 2003; Galbiati et al., 2000).

The functional disruption of the *VAMP714* gene was verified by performing PCR on assumed T-DNA insertion mutants, namely SALK_020516 and GABI_844B05. For the SALK line, a 1212 bp wild-type band was successfully amplified from the WT using the primers LP_SALK_020516 and RP_SALK_020516 (Fig. 3.3 and Appendix I). In parallel, a 649 bp T-DNA-specific fragment was amplified exclusively from the SALK line using the T-DNA-associated primers LB_SALK and RP_SALK_020516 (Fig. 3.3). Similarly, for the GABI line, an 1187 bp wild-type band was obtained from WT with the primers LP_GABI_844B05 and RP_GABI_844B05, while a 550 bp T-DNA flank was specifically amplified from GABI using the primers LB_GABI and RP_GABI_844B05 (Fig. 3.3). These PCR results unequivocally demonstrated that both T-DNA insertion lines are homozygous for the disrupted *VAMP714*.

Fig. 3.3 SALK_020516 and GABI_844B05 identification.

Furthermore, RT-qPCR was employed to assess the *VAMP714* mRNA abundance in both roots and whole seedlings of SALK and GABI lines. Using conventional RT-qPCR primers, results revealed that the *VAMP714* mRNA abundance in both T-DNA insertion lines had fallen to nearly undetectable

levels (Fig. 3.4).
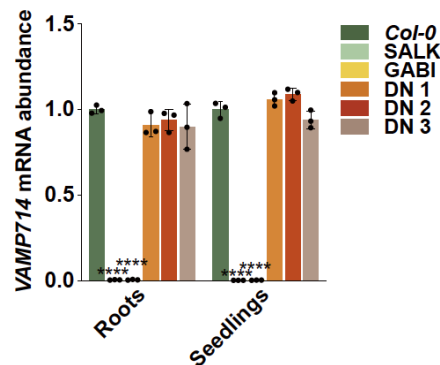
Fig. 3.4 *VAMP714* mRNA abundance in roots and whole seedlings of 5 dpg *VAMP714* loss-of-function mutants by conventional primers.

ACTIN2 was used as an internal reference, and *Col-0* (WT) served as the control for statistical comparisons. Data presented were means ± SD, n = 3 biological replicates, each with three technical replicates. *, $p < 0.05$, **, $p < 0.01$, ***, $p < 0.001$, ****, $p < 0.0001$, Student's *t*-test.

3.3.2 *VAMP714* dominant negative mutant identification

DN mutants offer distinct advantages in molecular genetics and functional studies (Gerasimavicius et al., 2022; Sheppard, 1994; Veitia, 2007). Specifically, one key benefit is that they allow for the effective inhibition of wild-type protein function even when the normal allele is present. For the DN construct, only the Longin and SNARE domains of the *VAMP714* gene were amplified, deliberately excluding the transmembrane domain, to generate a peptide fragment lacking normal functionality (Fig. 3.5; Gu et al., 2021). The expectation is that it would bind to the SNARE complex competitively with full-length VAMP714 protein, leading to a loss of functional VAMP714.
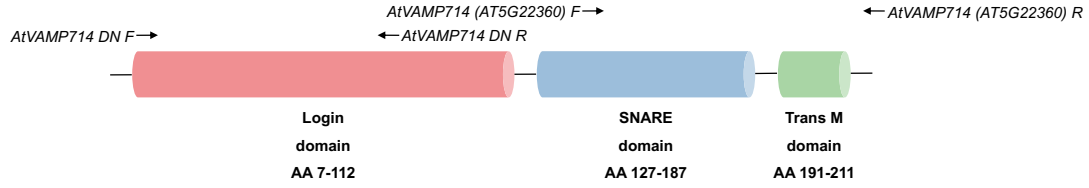
Fig. 3.5 The structural domains of *VAMP714* and the relevant RT-qPCR primers.

VAMP714 (AT5G22360) F and *R* represent conventional RT-qPCR primers, and *VAMP714 DN F* and *R* represent DN RT-qPCR primers. AA is amino acid.

Subsequently, RT-qPCR was employed to assess the *VAMP714* mRNA abundance in both roots and whole seedlings of DN lines. When using DN-specific primers, among the three DN lines examined, only the DN 1 line exhibited a significant overexpression of the peptide fragment (Fig. 3.6). In parallel, RT-qPCR analysis with conventional primers clarified that the DN construct did not affect endogenous *VAMP714* mRNA abundance (Fig. 3.4). Based on this information, it was confirmed that DN 1 represented a successfully constructed *VAMP714* DN line, which was employed in subsequent experiments.
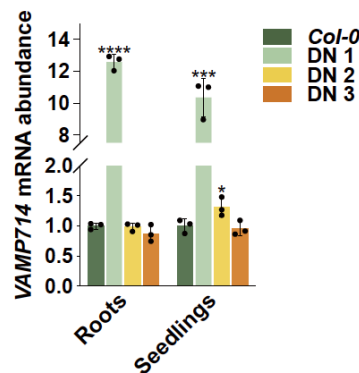
Fig. 3.6 *VAMP714* mRNA abundance in roots and whole seedlings of 5 dpg *VAMP714* DN mutants by DN-specific primers.

ACTIN2 was used as an internal reference, and *Col-0* (WT) at each group served as the control for statistical comparisons. Data presented were means ± SD, n = 3 biological replicates, each with three technical replicates. *, $p < 0.05$, **, $p < 0.01$, ***, $p < 0.001$, ****, $p < 0.0001$, Student's t-test.

3.3.3 *VAMP714* reporter line identification

Overexpression mutants are invaluable tools for dissecting gene function, and their design often involves driving the gene of interest with either a constitutive promoter, such as the CaMV35S promoter, or a natural (endogenous) promoter. The CaMV35S promoter is widely used due to its strong and constitutive activity in most tissues and developmental stages (Amack and Antunes, 2020; Holtorf et al., 1995; Hull et al., 2000). In contrast, overexpression driven by natural promoter preserves the inherent spatial and temporal expression patterns (Dey et al., 2015). Using a natural promoter reduces the risk of artifacts that may arise from ectopic or excessively high levels of expression, thereby minimizing unintended pleiotropic effects (Dey et al., 2015).

For the *VAMP714* reporter lines, several independent transgenic lines were generated using two different promoter constructs: one driven by the CaMV35S promoter (*pro35S::VAMP714:mCherry*) and the other one by the native *VAMP714* promoter (*proVAMP714::VAMP714:mCherry*) (Gu et al., 2021). Homozygous lines were isolated through antibiotic selection (see Section 2.2.4.3 for details), and fluorescence detection by confocal microscopy confirmed the successful establishment of three homozygous lines for each construct. Subsequently, RT-qPCR were employed to quantify the *VAMP714* mRNA abundance in both roots and whole seedlings of these lines. The results reveal that all lines exhibited constitutive overexpression of *VAMP714* (Fig. 3.7). Moreover, the *pro35S::VAMP714:mCherry* lines displayed higher *VAMP714* mRNA abundance compared to the *proVAMP714::VAMP714:mCherry* lines (Fig. 3.7), thereby demonstrating the effectiveness of the CaMV35S promoter in driving stronger expression.
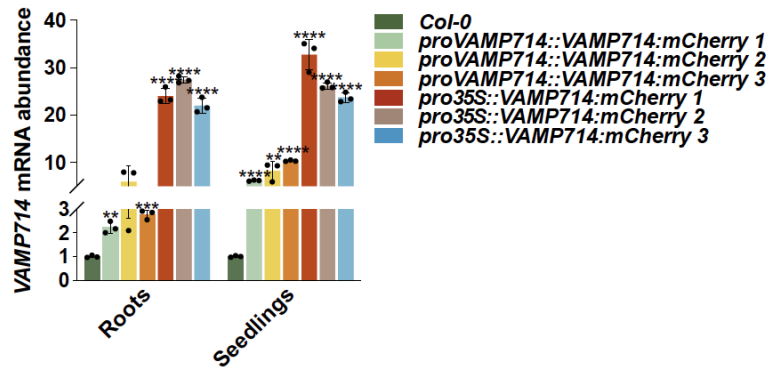
Fig. 3.7 *VAMP714* mRNA abundance in roots and whole seedlings of 5 dpg *VAMP714* reporter lines.

ACTIN2 was used as an internal reference gene, and *Col-0* (WT) at each group served as the control for statistical comparisons. Data presented were means ± SD, n = 3 biological replicates, each with three technical replicates. *, $p < 0.05$, **, $p < 0.01$, ***, $p < 0.001$, ****, $p < 0.0001$, Student's *t*-test.

3.4 Salt stress perturbs auxin distribution patterns

To assess whether auxin distribution patterns are altered by saline conditions, the experiment employed the widely used synthetic reporter DR5, originally derived from a soybean GH3 promoter and engineered to maximize sensitivity to endogenous auxin levels (Ulmasov et al., 1997; Das et al., 2021). This system has enabled cell-level visualization of auxin distribution in diverse species, under a variety of developmental and stress contexts (Xiao et al., 2020; Jedličková et al., 2022).

Under 200 mM NaCl treatment for 24 h, a reorganization of the auxin response was observed. Under non-stress conditions, the staining of *DR5::GUS* extended broadly across the QC and columella of the root tip (Fig. 3.8a), and the fluorescence of *DR5::GFP* marked a similar pattern (Fig. 3.8b). In contrast salt-treated roots showed a dramatic restriction of both GUS staining and GFP signal to the root cap alone (Fig. 3.8a, b). Quantitative image analysis confirmed that DR5 expression zones areas were significantly more restricted in NaCl-

exposed roots compared to controls (Fig. 3.8c, d), indicating a substantial loss of auxin response activity in the elongation and meristematic zones. Collectively, these findings demonstrate that salt stress rapidly disrupts the auxin distribution pattern, confining active auxin response to more distal root tissues.
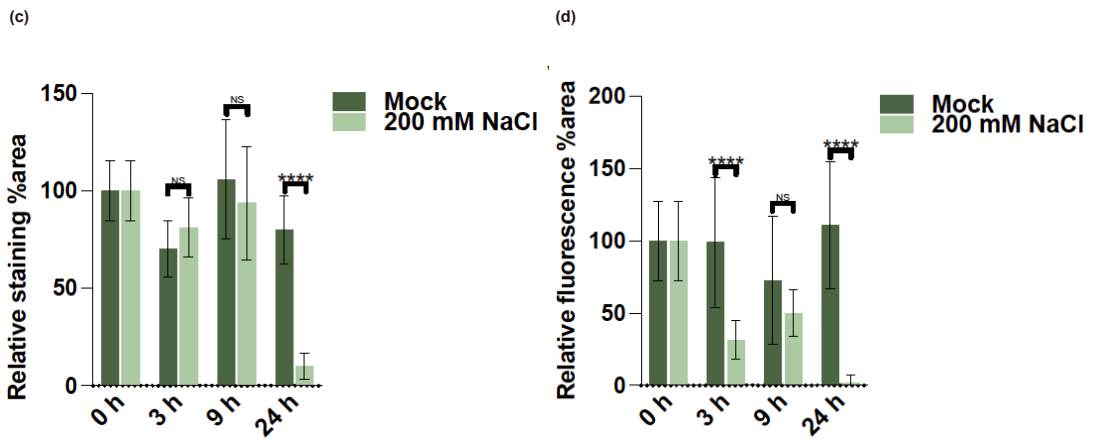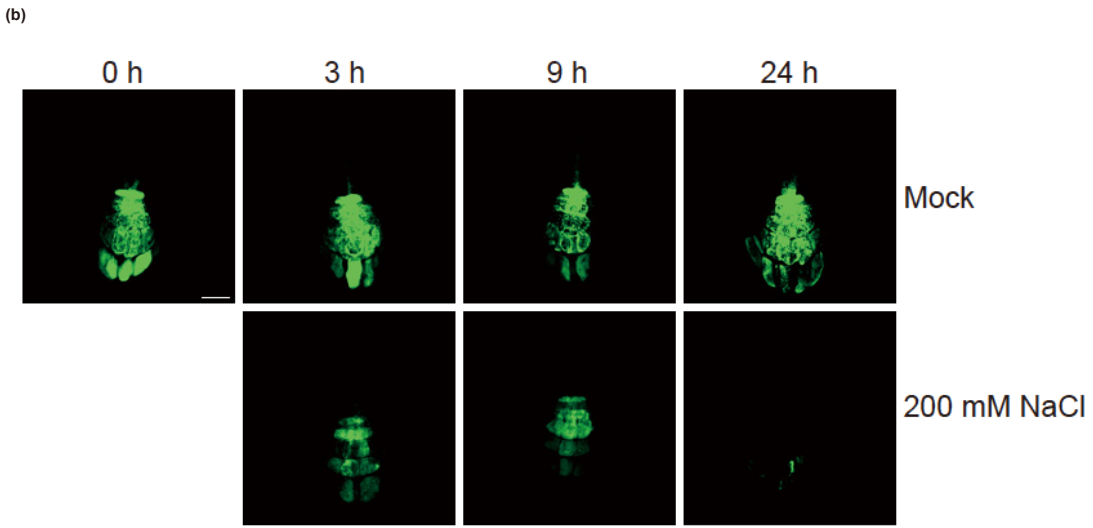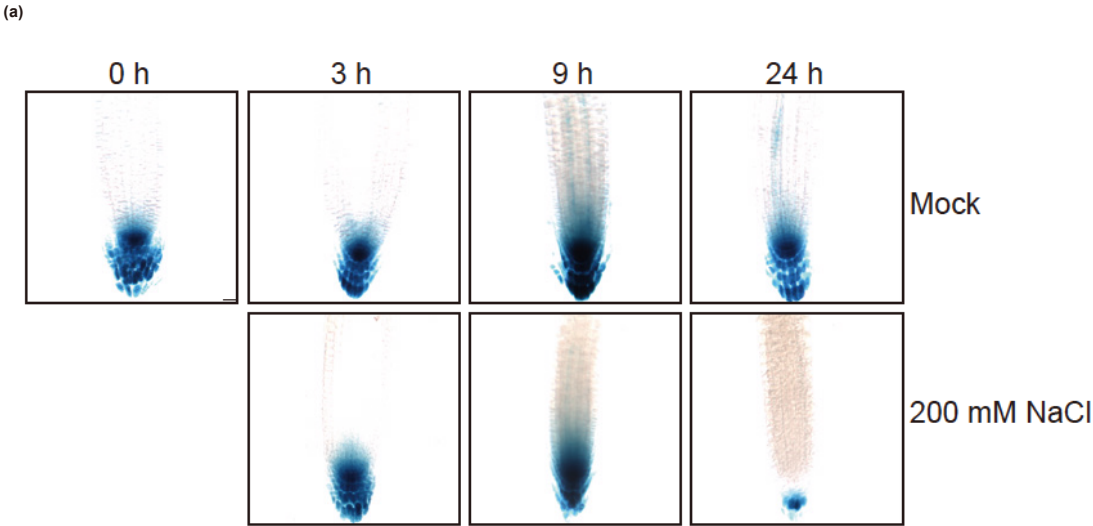
Fig. 3.8 Salt stress perturbs auxin distribution patterns.

(a, b) The root tip expression pattern of 5 dpg *DR5::GUS* **(a)** and *DR5::GFP* **(b)** on growth medium supplemented with 200 mM NaCl for additional 0, 3, 9, or 24 hours. Each treatment with at least 12 roots. Bars = 20 μm. **(c, d)** The staining/fluorescence area in *DR5::GUS* and *DR5::GFP* were determined by Fiji. The area without NaCl treatment was taken as 100%. Data presented were means ± SD. *, $p < 0.05$, **, $p < 0.01$, ***, $p < 0.001$, ****, $p < 0.0001$, Student's *t*-test.

3.5 Salt stress disrupts polar auxin transportation

Polar auxin transport in *Arabidopsis thaliana* is established by the asymmetric localization of PIN proteins at the plasma membrane, which creates the cellular auxin distribution patterns essential for root development (Michniewicz et al., 2007). PIN1 is polarly localized to the basal plasma membrane of provascular cells, where it functions as an auxin efflux carrier to drive directional auxin flow and establish intercellular auxin gradients for tissue patterning (Křeček et al., 2009). Meanwhile, PIN2 is targeted to the apical plasma membrane of root epidermal and cortical cells, mediating shootward auxin transport that is essential for root gravitropic responses (Křeček et al., 2009).

proPIN1::PIN1:GFP and *proPIN2::PIN2:GFP* were used to characterize the polar auxin transport pathways under high salinity. Under 200 mM NaCl exposure, a loss of PIN1:GFP polarity as early as 9 h after treatment was observed, with the fluorescent fusion protein losing its sharp plasma-membrane localization and becoming increasingly diffuse within the cytoplasm over time (Fig. 3.9a). Similarly, 24 h exposure abolished membrane-specific localization of PIN2:GFP, resulting in a homogeneous, non-polar fluorescence signal (Fig. 3.9b). Together, these findings demonstrate that salt stress rapidly dismantles the polarized distribution of both PIN1 and PIN2, thereby compromising the polar auxin transport mechanisms that are vital for root

development under saline stress.
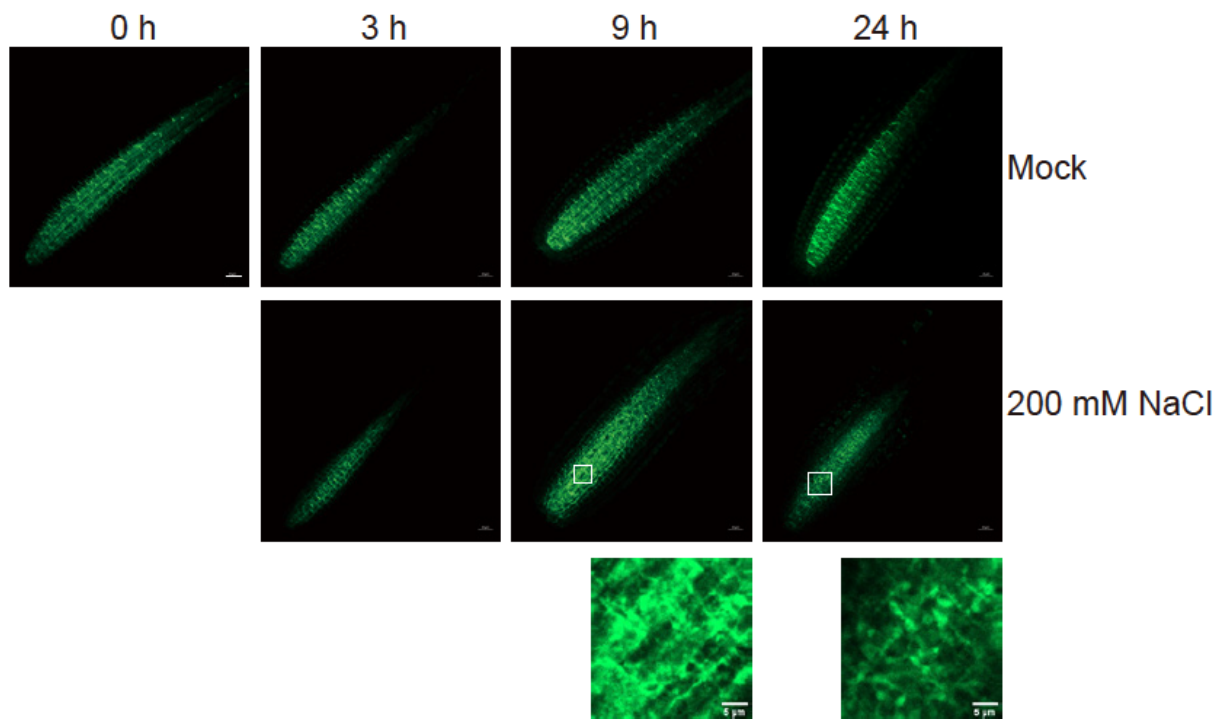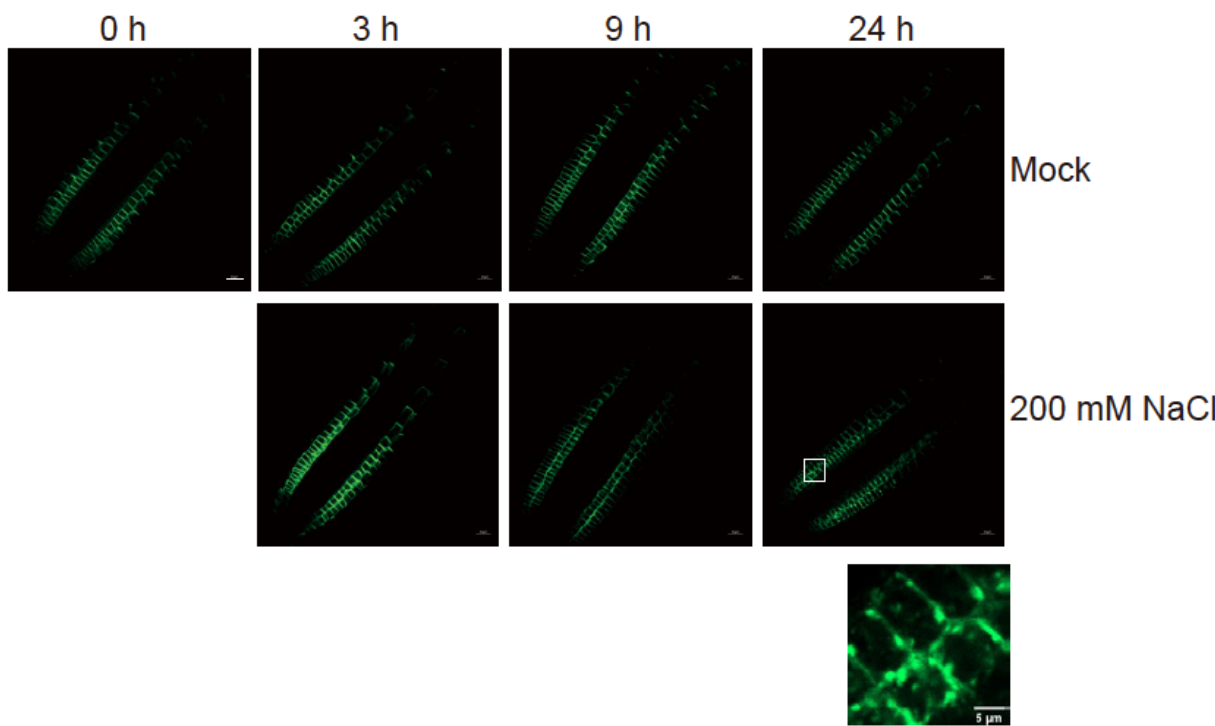
Fig. 3.9 Salt stress disrupts polar auxin transportation.

(a, b) The root tip expression pattern of **(a)** 5 dpg *proPIN1::PIN1:GFP* and **(b)** *proPIN2::PIN2:GFP* on growth medium supplemented with 200 mM NaCl for additional 0, 3, 9, or 24 hours. Below is a close-up of the area inside the rectangle. Each treatment with at least 12 roots. Bars = 20 µm. Scale bar in the below = 5 µm.

3.6 Salt stress alters auxin signal transduction in roots

In *Arabidopsis thaliana*, auxin uptake into cells is mediated primarily by the AUX1/LAX influx-carrier family, with AUX1 functioning as a high-affinity proton–IAA symporter at the plasma membrane to import auxin into root cells (Carrier et al., 2008; Swarup and Péret, 2012; Yang et al., 2006). Auxin is perceived by TIR1/AFB F-box receptors, which, upon binding auxin, recruit and ubiquitinate Aux/IAA repressors for proteasomal degradation, thereby liberating ARF transcription factors to modulate auxin-responsive gene expression (Calderón Villalobos et al., 2012; Lavenus et al., 2013; Tan et al., 2007; Worley et al., 2000). Transcript dynamics of key components within auxin signalling transduction were monitored in roots of WT, to understand how high salinity influenced its cascade, under 200 mM NaCl within 24 h.

Remarkably, *AUX1* mRNA abundance almost remained essentially constant throughout the treatment, indicating that the capacity for auxin uptake is preserved even under salt stress (Fig. 3.10). In contrast, both *IAA1* and *IAA2* mRNA abundance surged to peak levels at 9 h before declining, while *PIN1* mirrored this pattern with its highest expression at 9 h (Fig. 3.10). Notably, *PIN2* responded even more swiftly, reaching maximum expression just 3 h after salt application (Fig. 3.10). These temporally distinct profiles correspond closely with the three phases of the early salt-stress response in *Arabidopsis thaliana*, which are initial quiescent phase (~0–3 h), recovery phase (8–13 h), and homeostasis phase (13–24 h) (Geng et al., 2013). These results suggest that

rapid modulation of auxin efflux (via PIN2) during the quiescent phase may facilitate immediate adjustment of hormone gradients, while coordinated activation of IAA1, IAA2, and PIN1 during recovery helps reestablish signalling equilibrium under prolonged saline conditions.However, given the restriction of auxin distribution in the root tip over prolonged salt exposure, as monitored by DR5 activity and PIN localization (Figs. 3.8, 3.9), correct polar auxin transport is not maintained.

Auxin also underpins the integrity of the root stem-cell niche, with the QC serving as an organizing hub that maintains adjacent stem cells (Della Rovere et al., 2016). SHR and SCR form a heterodimer that regulates downstream targets necessary for QC specification and stem-cell maintenance (Cui et al., 2007; Nakajima et al., 2001; Sabatini et al., 2003; Sarkar et al., 2007; Yoon et al., 2016). Results showed that *SHR* mRNA abundance dropped precipitously within the first few hours and remained low through 24 h, whereas *SCR* mRNA abundance showed no significant deviation from control levels (Fig. 3.10). This uncoupling implies a buffering mechanism within the SHR–SCR regulatory module: while early *SHR* downregulation may have served as a rapid cue to modulate meristem activity and adapt root growth under salt stress, continued *SCR* expression likely preserved QC stability and prevented stem-cell loss. Such regulatory resilience ensures that the stem-cell niche remains functional even as upstream signals recalibrate developmental programs to cope with environmental challenges. Moreover, the identity of the QC is regulated by the auxin-induced PLETHORA factors (Aida et al., 2004). Under saline conditions, *PLT1* expression remained stable, whereas *PLT2* exhibited a transient up-regulation at 3 h (Fig. 3.10), suggesting that salt stress primarily elicits a short-lived *PLT2* response. Given that *PLT* transcription factors are crucial for maintaining root meristem activity and stem cell fate (Aida et al., 2004; Blilou et al., 2005; Galinha et al., 2007), such stability of *PLT1/2* expression is likely important for preserving meristem function and improving plant resilience to salt
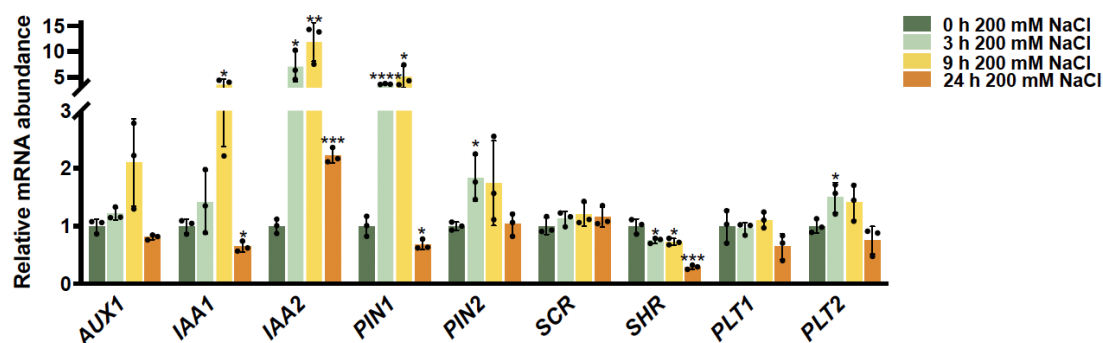
stress.

Fig. 3.10 Salt stress alters auxin signalling transduction in roots.

Relative mRNA abundance of auxin signalling transduction in roots of 5 dpg *Col-0* (WT) on growth medium supplemented with 200 mM NaCl for additional 0, 3, 9, or 24 hours by RT-qPCR. *UBQ5* was used as an internal reference, and without NaCl treatment served as the control for statistical comparisons. Data presented were means ± SD, *n* = 3, each with three technical replicates. *, $p < 0.05$, **, $p < 0.01$, ***, $p < 0.001$, ****, $p < 0.0001$, Student's *t*-test.

3.7 Salt stress induces *VAMP714* mRNA abundance in roots

To explore whether VAMP714 links auxin signalling with cellular response to salinity, *VAMP71* gene family (*VAMP711–714*) mRNA abundance was analysed under salt stress. Results showed that only *VAMP713* mRNA abundance remained stable over the course of the treatment. In contrast, both *VAMP711* and *VAMP712* mRNA abundances exhibited a marked induction beginning at 9 h post-treatment, with their expression continuing to rise through subsequent time points (Fig. 3.11). The time-dependent accumulation of these transcripts reinforced the notion that a subset of *VAMP71* family is mobilized during the salt-stress response, thereby implicating *VAMP714* as a candidate for further investigation.
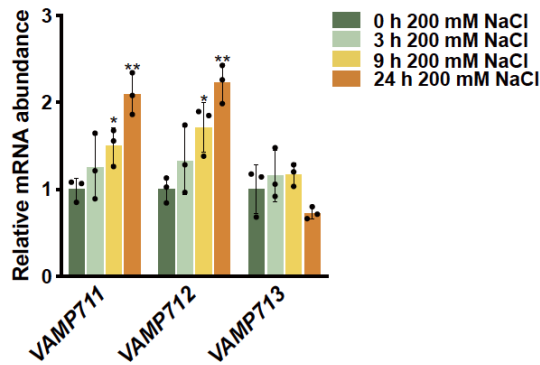
Fig. 3.11 Salt stress alters *VAMP71* genes family transduction in roots.

Relative mRNA abundance of *VAMP71* genes family in roots of 5 dpg *Col-0* (WT) on growth medium supplemented with 200 mM NaCl for additional 0, 3, 9, or 24 hours by RT-qPCR. *UBQ5* was used as an internal reference, and without NaCl treatment served as the control for statistical comparisons. Data presented were means ± SD, n = 3, each with three technical replicates. *, $p < 0.05$, **, $p < 0.01$, ***, $p < 0.001$, ****, $p < 0.0001$, Student's *t*-test.

To characterize the salt-induced transcriptional dynamics of *VAMP714*, we designed a comprehensive time-course and dose–response experiment. WT seedlings were exposed to a NaCl gradient (0, 50, 100, 150, and 200 mM) and harvested at 0, 3, 9, and 24 h for mRNA quantification. Across all tested concentrations, *VAMP714* mRNA abundance was significantly elevated relative to the untreated control (Fig. 3.12). Moreover, a clear dose–response relationship emerged: 50 mM required the full 24 h to elicit detectable induction, whereas 100 mM and high (150–200 mM) salt levels triggered earlier upregulation at 9 h and 3 h respectively. Interestingly, *VAMP714* mRNA abundance peaked at 9 h under all salt conditions except 50 mM NaCl before declining by 24 h, which was similar to the transient induction profiles reported for key auxin transport and transduction signalling components (*IAA1*, *IAA2*, *PIN1*, and *PIN2*) as described above (Fig. 3.10). This transient 'early-response' behaviour aligns closely with the rapid transcriptional reprogramming described in *Arabidopsis thaliana* during the initial phase of salt stress (Geng et al., 2013), suggesting that *VAMP714* is integrated into the immediate gene regulatory

network for coping with high salinity.
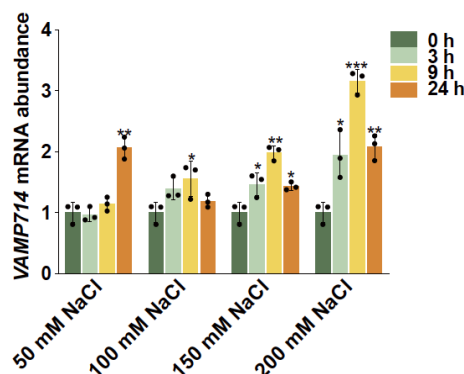
Fig. 3.12 Salt stress induces *VAMP714* mRNA abundance in roots.

VAMP714 mRNA abundance in roots of 5 dpg *Col-0* (WT) on growth medium supplemented with 0-200 mM NaCl for additional 0, 3, 9, or 24 hours by RT-qPCR. *UBQ5* was used as an internal reference, and without NaCl treatment served as the control for statistical comparisons. Data presented were means ± SD, $n = 3$, each with three technical replicates. *, $p < 0.05$, **, $p < 0.01$, ***, $p < 0.001$, ****, $p < 0.0001$, Student's *t*-test.

3.8 Salt stress disrupts VAMP714 localization

VAMP714 plays a pivotal role in establishing PIN protein polarity and mediating auxin signalling cascades in roots of *Arabidopsis thaliana* (Gu et al., 2021). To chart its dynamic response to salinity, two reporter lines: *proVAMP714::GUS* were employed for monitoring promoter activity and *proVAMP714::VAMP714:mCherry* for revealing fusion protein expression and localization.

Under non-stress conditions, the GUS signal of roots in *proVAMP714::GUS* was located at the root apical meristem and elongation zone (Fig. 3.13a). VAMP714:mCherry of roots expressing *proVAMP714::VAMP714:mCherry* was predominantly associated with vesicular compartments and the plasma membrane within the same location (Fig. 3.13b). These results are consistent with the previous study (Gu et al., 2021). Under 200 mM NaCl treatment for 3,

9, and 24 h, histochemical staining of *proVAMP714::GUS* revealed a detectable shift in GUS signal distribution as early as 3 h post-treatment, with staining area reduced in a time-dependent manner (Fig. 3.13a). By 24 h, GUS activity was sharply confined to the root cap, like the GUS signal of *DR5::GUS* under identical salinity conditions (Fig. 3.8a) and indicated a salt-triggered reprogramming of *VAMP714* transcription in distal root tissues. In parallel, confocal microscopy of *proVAMP714::VAMP714:mCherry* demonstrated that characteristic membrane tethering was progressively lost following salt exposure (Fig. 3.13b). Within 9 h, the VAMP714:mCherry exhibited a marked reduction in plasma membrane localization, becoming increasingly diffuse throughout the cytoplasm; this dispersion was more pronounced by 24 h (Fig. 3.13b). Given that VAMP714 normally colocalizes with PIN1 and PIN2 (Gu et al., 2021), its mislocalization under high salinity likely underpinned the loss of PIN1:GFP and PIN2:GFP polarity observed before (Fig. 3.9a–b). Collectively, these findings suggest that salt stress disrupts VAMP714 distribution and thereby compromises the vesicle-mediated polar auxin transport.

(b)

Col-0

AT1G07400

0 h

63×

3 h

63×

9 h

63×

24 h

63×

10 μM IAA + 200 mM NaCl

200 mM NaCl

10 μM IAA

Mock

Relative mRNA level

85
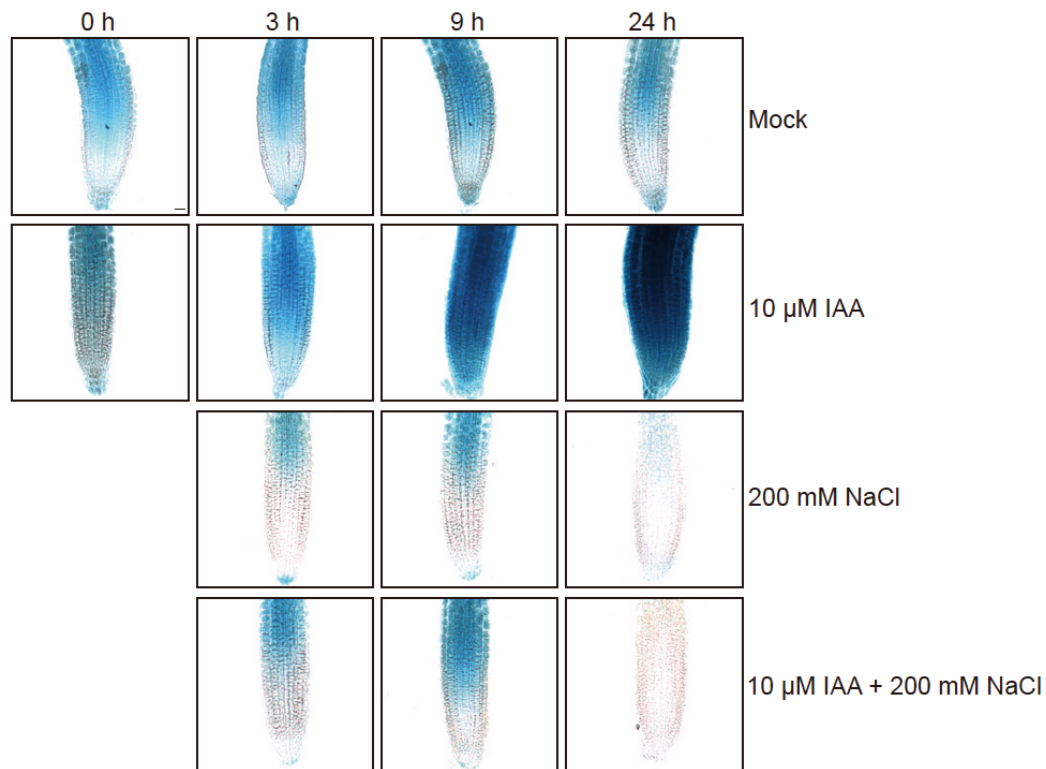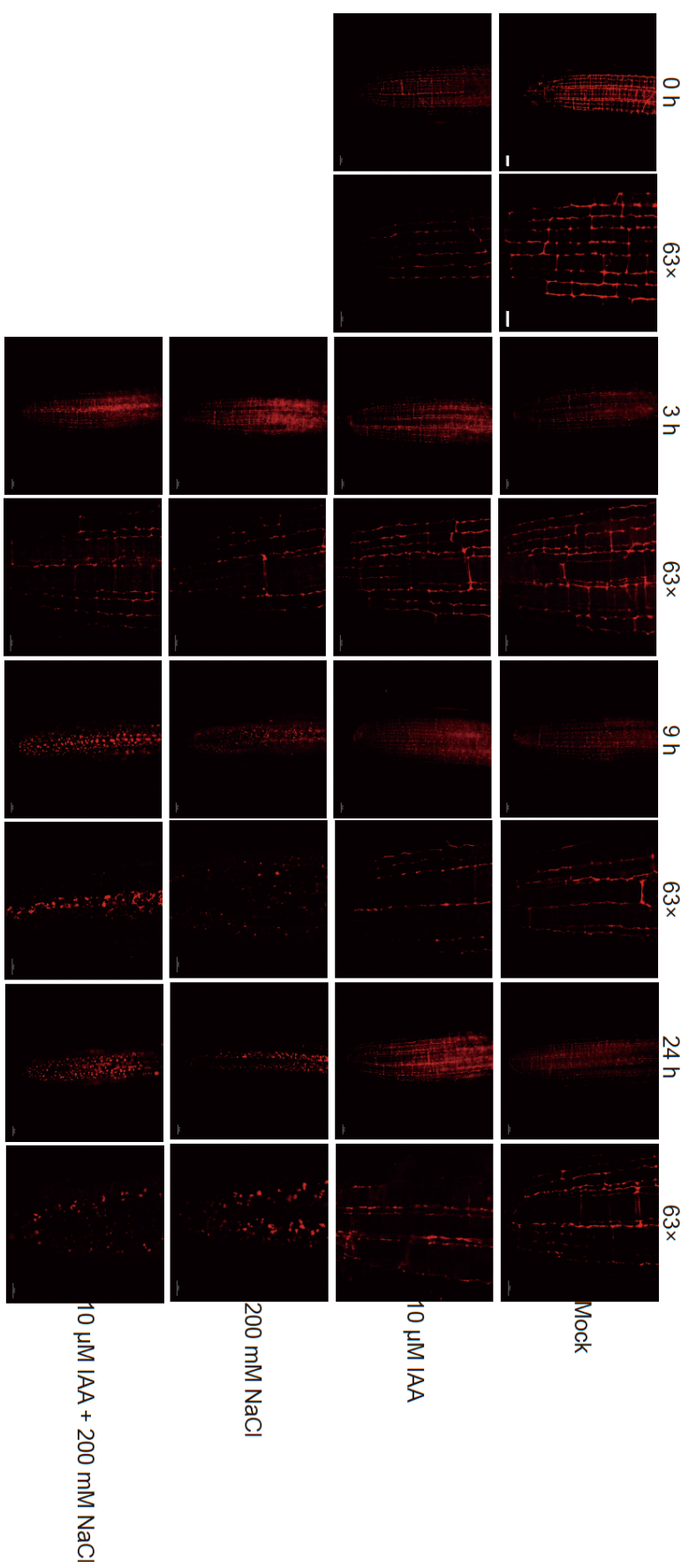
Fig. 3.13 Salt stress shifts VAMP714 location.

(a, b) The root tip expression pattern of 5 dpg *proVAMP714::GUS* **(a)** and *proVAMP714::VAMP714:mCherry* **(b)** on growth medium supplemented with different treatments for additional 0, 3, 9, or 24 hours. Each treatment with at least 3 roots. Bars = 20 µm in **(a)**. Bars = 20 µm for 20x or Bars = 10 µm for 63x in **(b)**.

3.9 Exogenous auxin fails to prevent salt-induced VAMP714 mislocalization

Building on the results presented in Section 3.8, 10 µM exogenous IAA was applied to assess the role of auxin availability in the response of VAMP714 to salt stress. Histochemical staining revealed a gradual, time-dependent increase in VAMP714:GUS activity over the treatment period (Fig. 3.13a), indicating that exogenous IAA alone could drive *VAMP714* transcription. In parallel, VAMP714:mCherry maintained its characteristic association with the plasma membrane, with no detectable relocalization following IAA treatment alone (Fig. 3.13b). However, when co-treated with 10 µM IAA and 200 mM NaCl, the salt-induced redistribution of GUS activity, marked by its confinement to the root cap, persisted, and the VAMP714:mCherry remained diffuse rather than membrane-localized (Fig. 3.13a–b).

Together, these data demonstrate that, although *VAMP714* expression and membrane targeting of its protein are auxin-responsive under non-stress conditions, high salinity overrides this regulation. Thus, VAMP714 appears to act as an early responder to salt stress signals, and simply restoring auxin levels is insufficient to rescue its changed localization or transcriptional activation in a high saline environment.

3.10 Summary

In this chapter, the objective was to define how VAMP714 links salt stress to auxin dynamics in roots of *Arabidopsis thaliana*. First, sequence comparisons and promoter analyses were used to show that *VAMP714* is genetically distinct within the *VAMP7* family and carries salt-responsive transcription factor binding sites, suggesting direct regulation by salinity. Co-expression data further connected *VAMP714* with established salt-stress genes. T-DNA and dominant-negative lines were confirmed by PCR and RT-qPCR, and mCherry-tagged overexpressors were generated. Under salt stress, DR5 reporter analysis revealed that auxin responses became confined to the root cap, and GFP-tagged PIN1/PIN2 rapidly lost polar localization, demonstrating that salt disrupts auxin distribution and its polar transportation. Moreover, transcript profiling showed a transient surge in *AUX/IAA* and *PIN* expression aligned with early stress phases, while *SHR* (but not *SCR*) was downregulated, indicating niche robustness. Finally, it was shown that salt induces a dose- and time-dependent rise in *VAMP714* transcript levels and shifted the protein from membrane-associated vesicles into the cytoplasm. Exogenous IAA could not restore its localization, implying that high salinity directly overrides auxin inputs. Together, the results position VAMP714 as a critical sensor and coordinator of vesicle-mediated auxin reprogramming under salt stress.

Chapter 4: VAMP714-driven salt tolerance and CTL1 interaction in *Arabidopsis thaliana*

4.1 Introduction

The root system underpins the capacity of plants for water and nutrient uptake (Koevoets et al., 2016). Analysing its architectural traits could uncover the basis of plastic responses that enable efficient foraging in saline-alkaline soils (Duan et al., 2014), informing our understanding of adaptive modifications to root development (Galvan-Ampudia and Testerink, 2011) and guiding breeding strategies for stress-resilient cultivars (Lombardi et al., 2024). Building on these insights into the critical roles of root system architecture in plant salt tolerance, the work described in this chapter undertakes a comprehensive phenotypic characterization of mutant lines of *VAMP714* under graded NaCl treatments. By systematically measuring primary root length, primary root elongation, lateral root elongation, lateral root density, and relative root growth (see Section 2.2.7 for parameter definitions), the objective was to determine a possible role for VAMP714 in the root adaptations that underpin salinity resilience in *Arabidopsis thaliana*. In this chapter, "WT" refers to Col-0, and 5 dpg seedlings serve as material for treatment or analysis.

4.2 Mild *VAMP714* overexpression enhances salt tolerance

The salt tolerance of *vamp714* mutants, *VAMP714* overexpressers and WT was assessed by culturing seedlings on growth medium supplemented with 0, 50, 100, 150, or 200 mM NaCl for an additional 7 days. Under non-stress conditions, all genotypes exhibited a similar developmental phenotype (Fig. 4.1-4.3). These results are partially consistent with earlier work of our lab (Gu et al., 2021). The intergenerational variability in transgene-driven phenotypes can arise from a complex and often unpredictable interplay of mechanisms, including transcriptional compensation, genetic redundancy, and epigenetic

silencing, that have been documented in many plants (Chalfun-Junior et al., 2003; Gao and Zhao, 2013; Jupe et al., 2019; Mlotshwa et al., 2010; Osabe et al., 2017; Raabe et al., 2024; Stokes et al., 2002; Weinhold et al., 2013). Crucially, these data demonstrate that mutation of *VAMP714* did not significantly impair baseline growth under non-stress conditions. At the highest salinity (200 mM NaCl), nearly all genotypes developed pronounced leaf chlorosis and failed to survive the treatment period (Fig. 4.1-4.3). In contrast, seedlings remained viable at 50-150 mM NaCl, indicating that these salinity levels did not exceed the tolerance capacity (Fig. 4.1-4.3). These results reflect a threshold of salt sensitivity that is consistent with prior reports on the role of the related gene *VAMP711* in salinity responses (Leshem et al., 2006). Specifically, both *VAMP711* overexpressing and wild-type plants died under 200 mM NaCl within 5-7 days, and under 150 mM NaCl within 10-14 days, rather than within 7 days.

4.2.1 *VAMP714* loss-of-function mutants preserve baseline salt tolerance

Firstly, it is necessary to assess salt tolerance in three independent *vamp714* loss-of-function mutants, two homozygous T-DNA insertion lines (SALK and GABI) and a dominant-negative line (DN 1). Across 50-150 mM salt concentrations, none of the metrics (primary root length, primary root elongation, lateral root elongation, lateral root density, and relative root growth) differed significantly between mutants and WT (Fig. 4.1a-b). These data demonstrate that insufficient VAMP714 function neither compromised seedling viability under salt stress nor altered root architectural plasticity, suggesting potential functional redundancy or activation of alternative compensatory pathways in maintaining salinity tolerance.

(a)

Col-0 SALK GABI DN

Mock

50 mM NaCl

100 mM NaCl

150 mM NaCl

200 mM NaCl

(b)

Legend:
- Col-0 (orange circle)
- SALK (purple square)
- GABI (red triangle)
- DN (teal inverted triangle)

Relative root growth (%) vs NaCl (mM)

Primary root elongation (cm) vs NaCl (mM)

Lateral root density (roots cm⁻¹) vs NaCl (mM)

Lateral root elongation (cm) vs NaCl (mM)

Primary root length (cm) vs NaCl (mM)

Grouped: Entering replicate data

90

Fig. 4.1 *VAMP714* loss-of-function mutants preserve baseline salt tolerance.

(a) The root growth of 5 dpg WT and *VAMP714* loss-of-function mutants on growth medium supplemented with 0-200 mM NaCl for additional 7 days. Bars = 1 cm. **(b)** The relevant phenotypic parameters. *Col-0* (WT) at each group served as the control for statistical comparisons. Data presented were means ± SD, $n = 3$, each with 10 roots. *, $p < 0.05$, **, $p < 0.01$, ***, $p < 0.001$, ****, $p < 0.0001$, Student's *t*-test.

4.2.2 Native promoter-driven *VAMP714* overexpression enhances salt tolerance

Secondly, salt tolerance was assessed using three independent *VAMP714* over-abundance lines driven by the native promoter (*proVAMP714::VAMP714:mCherry*). Across 50-100 mM NaCl concentrations, none of the root metrics differed significantly from WT (Fig. 4.2a-b). However all three independent over-expression lines exhibited significantly enhanced salt tolerance at 150 mM NaCl (Fig. 4.2a-b). Specifically, they had a longer primary root elongation and higher relative root growth with reduced lateral root elongation and lateral root density compared to WT, while primary root length remained unchanged (Fig. 4.2a-b). These findings demonstrate that moderate overexpression of *VAMP714* enhanced the adaptive remodelling of the root system under high salinity, enabling plants to maintain functional root architecture when challenged with salt stress. This trait would be associated with deeper soil exploration, while limiting lateral root proliferation, which may help minimize exposure to toxic ions in the upper soil layers.

(a)

proVAMP714::VAMP714:mCherry

Col-0   1   2   3

Mock

50 mM NaCl

100 mM NaCl

150 mM NaCl

200 mM NaCl

(b)

- Col-0
- proVAMP714::VAMP714:mCherry 1
- proVAMP714::VAMP714:mCherry 2
- proVAMP714::VAMP714:mCherry 3

92
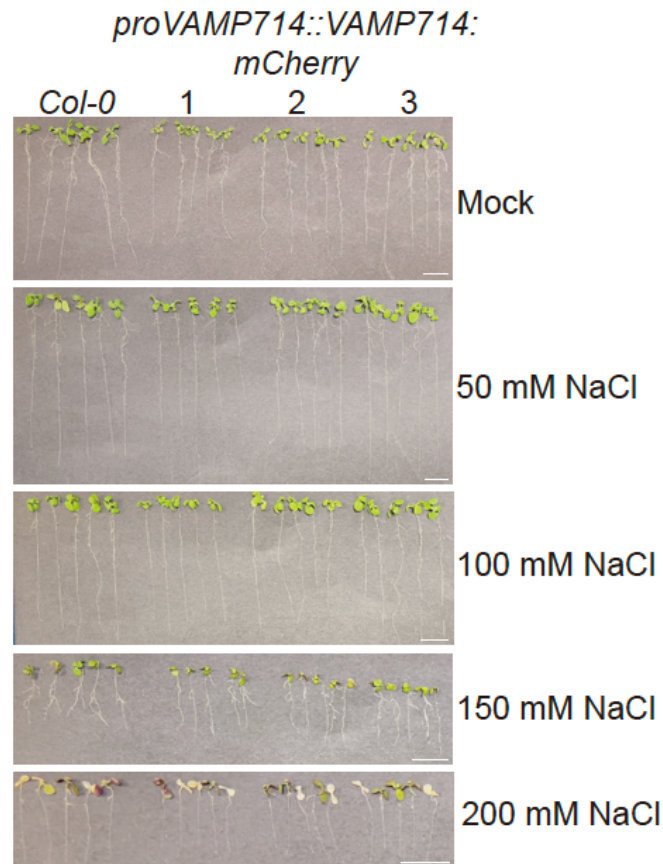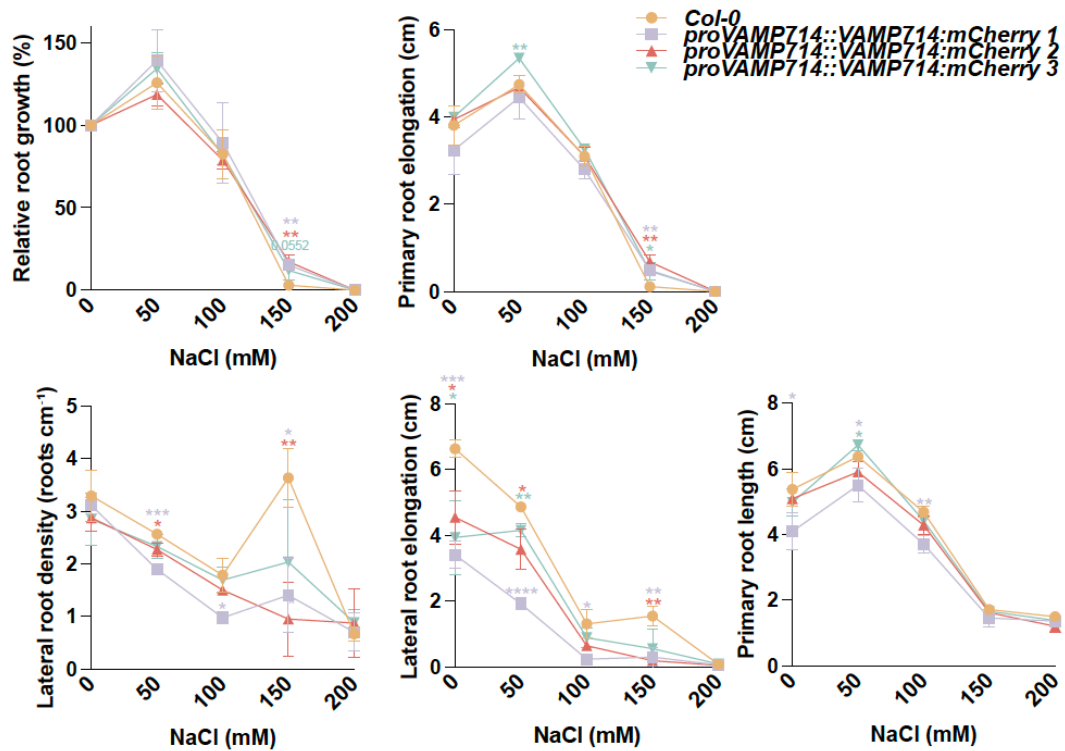
Fig. 4.2 *VAMP714* native promoter-driven overexpression mutants enhance salt tolerance.

(a) The root growth of 5 dpg WT and *VAMP714* native promoter-driven overexpression mutants on growth medium supplemented with 0-200 mM NaCl for additional 7 days. Bars = 1 cm. **(b)** The relevant phenotypic parameters. *Col-0* (WT) at each group served as the control for statistical comparisons. Data presented were means ± SD, n = 3, each with 10 roots. *, $p <$ 0.05, **, $p < 0.01$, ***, $p < 0.001$, ****, $p < 0.0001$, Student's *t*-test.

4.2.3 Constitutive 35S-driven *VAMP714* overexpression preserves baseline salt tolerance

Finally, salt tolerance was assessed in three independent *VAMP714* over-abundance lines driven by the 35S promoter (*pro35S::VAMP714:mCherry*). Across 50-150 mM salt concentrations, none of the metrics differed significantly between overexpressers and WT (Fig. 4.3a-b). These results further underscore that only a finely tuned constitutive overexpression of *VAMP714* conferred optimal benefits to root system remodelling and maintenance under saline conditions. Excessive *VAMP714* expression could disrupt endogenous vesicle trafficking pathways, whereas insufficient upregulation may fail to support the necessary adaptive shifts in root architecture. Previous results have shown that *Arabidopsis* seedlings expressing the *VAMP714* gene under the control of the CaMV35S promoter show a gain-of-function mutant phenotype associated with PIN protein mis-localisation and defective polar auxin transport in roots (Gu et al., 2021). Thus, achieving the appropriate expression threshold is critical for harnessing protective effects of VAMP714 and enhancing plant resilience to salt stress.

(a)

pro35S::VAMP714:mCherry

Col-0 1 2 3

Mock

50 mM NaCl

100 mM NaCl

150 mM NaCl

200 mM NaCl

(b)

Legend:
- ● *Col-0*
- ■ *pro35S::VAMP714:mCherry 1*
- ▲ *pro35S::VAMP714:mCherry 2*
- ▼ *pro35S::VAMP714:mCherry 3*

Grouped: Entering replicate data
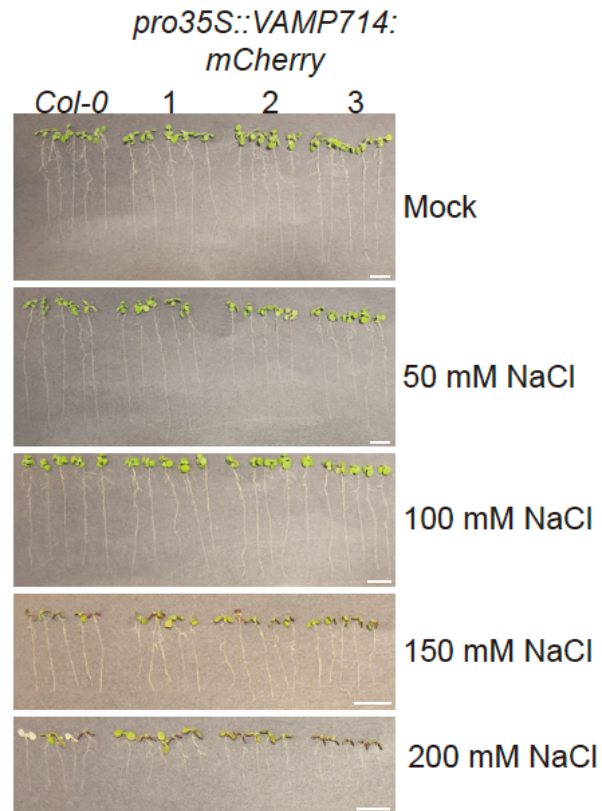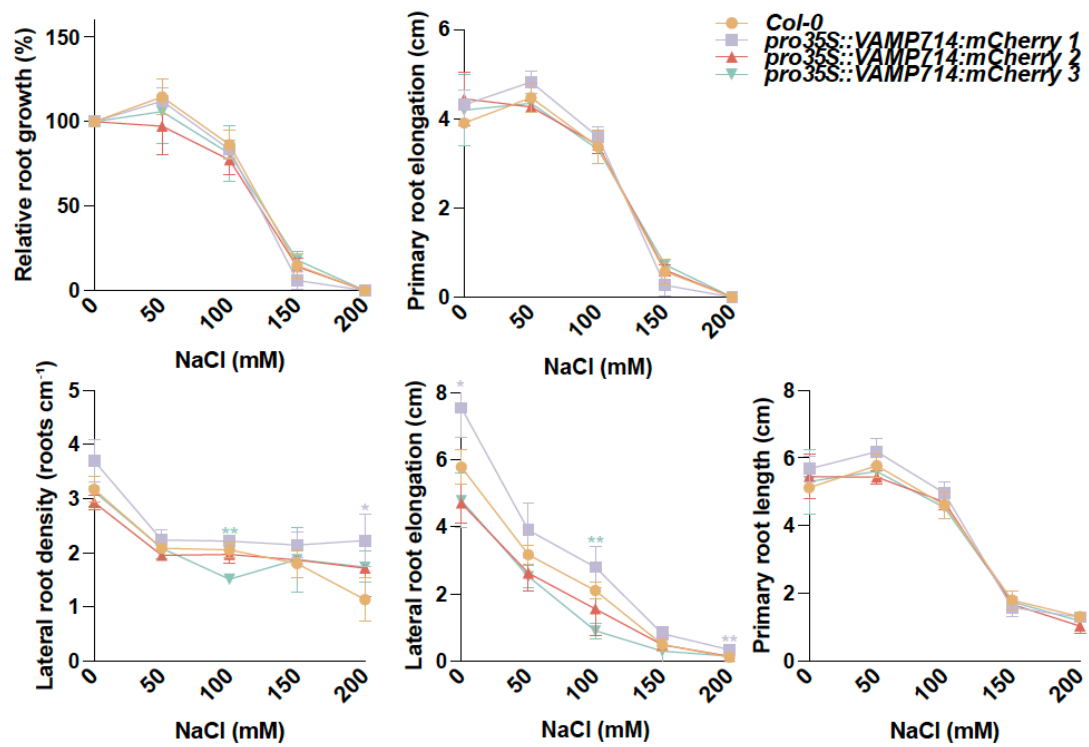
Fig. 4.3 *VAMP714* constitutive 35S-driven overexpression mutants preserve baseline salt tolerance.

(a) The root growth of 5 dpg WT and *VAMP714* constitutive 35S-driven overexpression mutants on growth medium supplemented with 0-200 mM NaCl for additional 7 days. Bars = 1 cm. **(b)** The relevant phenotypic parameters. *Col-0* (WT) at each group served as the control for statistical comparisons. Data presented were means ± SD, $n = 3$, each with 10 roots. *, $p < 0.05$, **, $p < 0.01$, ***, $p < 0.001$, ****, $p < 0.0001$, Student's *t*-test.

4.3 Native promoter-driven *VAMP714* overexpression maintains polar auxin transport to confer salt tolerance

To assess the contribution of auxin redistribution to salt-stress adaptation, the experiment co-applied 30 nM IAA, a concentration known to suppress primary root elongation (Rahman et al., 2007), to *proVAMP714::VAMP714:mCherry* mild overexpresser transgenics and WT under 150 mM NaCl for additional 7 days. In WT, exogenous IAA did not alleviate salt-induced growth inhibition (Fig. 4.4a-b). In contrast, *proVAMP714::VAMP714:mCherry* maintained certain primary root elongation and relative root growth, despite both metrics declining relative to NaCl treatment alone (Fig. 4.4a-b). The transgenics also exhibited significant increases in lateral root density and lateral root elongation, although they did not reach untreated WT levels (Fig. 4.4a-b). These findings indicate that moderate *VAMP714* overexpression provided at least partial retention of auxin-mediated developmental responses during salt stress. Next, it was examined whether polar auxin transport was necessary for this enhanced tolerance by co-treating seedlings with 10 µM NPA, a polar auxin transport inhibitor that does not disrupt PIN1 or PIN2 protein localization (Rahman et al., 2007). Results showed that both *proVAMP714::VAMP714:mCherry* and WT showed severe suppression of all metrics except primary root length under NPA/salt co-treatment (Fig. 4.4a-b). Together, these results demonstrate that appropriate, constitutive overexpression of VAMP714 supports auxin

redistribution and its polar transportation, which contributes to the observed salt-tolerant phenotype.
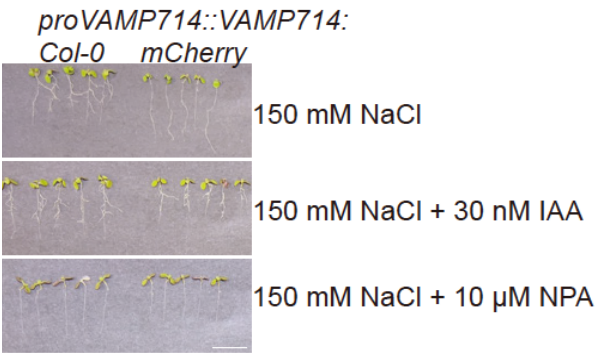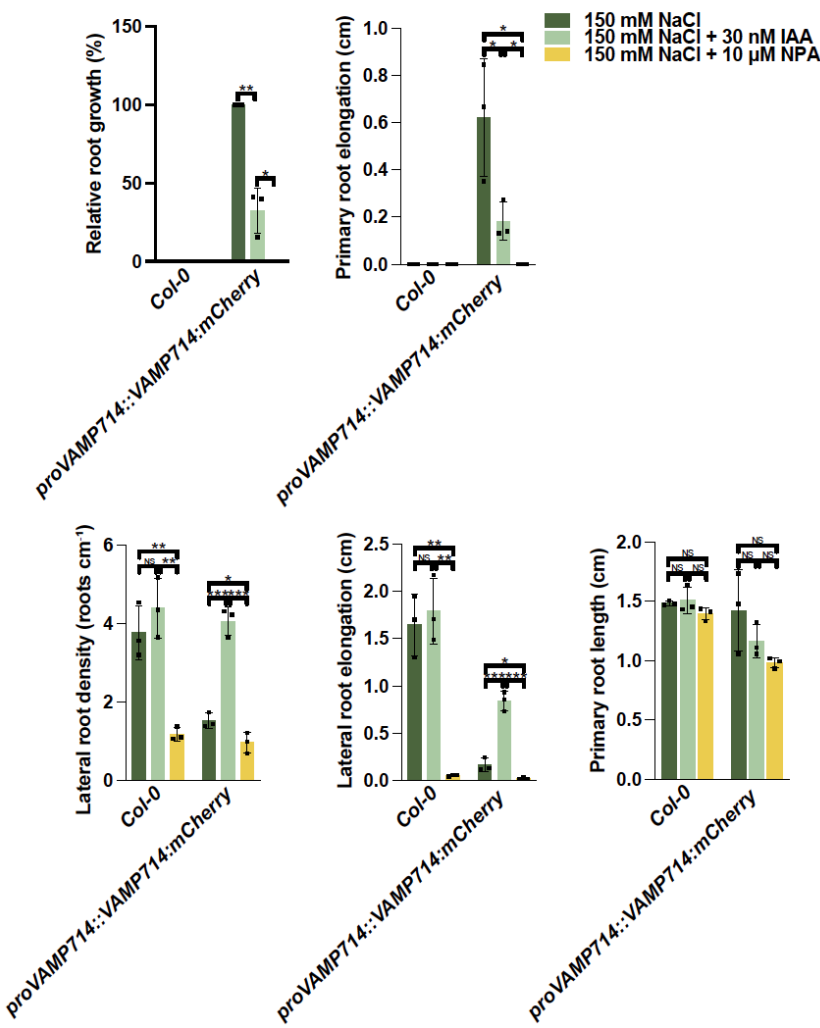
Fig. 4.4 Native promoter-driven *VAMP714* overexpression maintains auxin redistribution and its polar transportation to confer salt tolerance.

(a) The root growth of 5 dpg WT and *proVAMP714::VAMP714:mCherry* on growth medium supplemented with exogenous IAA or NPA treatments under 150 mM NaCl for additional 7 days. Bars = 1 cm. **(b)** The relevant phenotypic parameters. 150 mM NaCl treatment at each group served as the control for statistical comparisons. Data presented were means ± SD, n = 3 biological replicates, each with 10 roots. *, $p < 0.05$, **, $p < 0.01$, ***, $p < 0.001$, ****, $p < 0.0001$, Student's *t*-test.

4.4 CTL1 and VAMP714 cooperate in vesicle trafficking and auxin homeostasis

Choline transporter-like 1 (CTL1) (At3g15380), is a multi-pass transmembrane protein that mediates high-affinity choline uptake, a precursor for the synthesis of phosphatidylcholine and sphingolipids essential for membrane integrity and signalling (Dettmer et al., 2014; Nakamura et al., 2010). CTL1 predominantly localizes to the trans-Golgi network and early endosome compartments, where it transiently associates with forming cell plates during cytokinesis in root meristematic cells (Dettmer et al., 2014; Nakamura et al., 2010). Functionally, CTL1 not only mediates high-affinity choline uptake for phosphatidylcholine and sphingolipid biosynthesis (Gao et al., 2017) but also plays a pivotal role in establishing auxin distribution patterns via vesicle trafficking (Wang et al., 2017). Moreover, CTL1 participates in leaf plasmodesmata composition (Kraner et al., 2017) and root epidermal ion-transporter recycling and ion homeostasis (Gao et al., 2017). Collectively, CTL1 integrates choline transport with membrane lipid remodelling, hormone distribution, and vesicle trafficking to support critical developmental and physiological processes in *Arabidopsis thaliana*.

4.4.1 Co-operation of CTL1 and VAMP714 in vesicle trafficking and auxin distribution

Our lab member Dr. Agneessens has demonstrated a direct or very tight binding between CTL1 and VAMP714 protein by FRET-FLIM (Agneessens, 2024). Moreover, he localized by BiFC this interaction to discrete, punctate "cycling hubs," identified as trans-Golgi network/early endosome compartments where vesicle fusion and cargo sorting converge (Agneessens, 2024). Functionally, CTL1-mediated choline homeostasis is critical for maintaining proper subcellular distribution of VAMP714 (Agneessens, 2024). While VAMP714 is required for the polarity of both PIN1 and PIN2, CTL1 and thus choline levels selectively influence PIN1 localization without perturbing PIN2 (Agneessens, 2024). Such specificity suggests that CTL1 primes or recruits VAMP714-containing vesicles for PIN1 exocytosis in particular cell types, whereas PIN2 trafficking can proceed via CTL1-independent pathways.

4.4.2 *ctl1* mutant identification

The *CTL1* T-DNA insertion mutant line, *ctl1* (SALK_065853C), was obtained from the Nottingham Arabidopsis Stock Centre. Dr. Agneessens generated two independent *pro35S::CTL1:GFP* lines as described (Agneessens, 2024). Homozygosity was confirmed by Dr. Agneessens. Furthermore, RT-qPCR was employed to assess the mRNA abundance of *CTL1* in both the roots and whole seedlings of these lines. In *ctl1*, *CTL1* mRNA abundance was reduced to an undetectable level (Fig. 4.5), confirming effective gene disruption. Conversely, two *pro35S::CTL1:GFP* lines exhibited constitutive overexpression of *CTL1*, with line 1 showing higher transcript accumulation than line 2 (Fig. 4.5). Based on its stronger and more consistent overexpression, line 1 was selected for all subsequent functional analyses.

Fig. 4.5 *CTL1* mRNA abundance in roots and whole seedlings of mutants of *CTL1*.

ACTIN2 was used as an internal reference, and *Col-0* (WT) at each group served as the control for statistical comparisons. Data presented were means ± SD, n = 3 biological replicates, each with three technical replicates. *, $p < 0.05$, **, $p < 0.01$, ***, $p < 0.001$, ****, $p < 0.0001$, Student's *t*-test.

4.4.3 Bidirectional and tissue-specific feedback regulation between CTL1 and VAMP714

The above results prompted the examination of whether CTL1 and VAMP714 exert reciprocal control over each other's expression. Firstly, the experiment checked *CTL1* mRNA abundance in both roots and whole seedlings of mutants of *VAMP714* (Fig. 4.6a-b). In *vamp714* loss-of-function lines, *CTL1* mRNA abundance remained statistically indistinguishable from WT in roots and whole seedlings, indicating that elimination *VAMP714* does not regulated *CTL1* transcription. Similarly, roots of *VAMP714* gain-of-function lines showed no alteration in *CTL1* mRNA abundance. However, whole seedlings of gain-of-function lines displayed a reproducible, significant decrease in *CTL1* mRNA abundance, pointing to a tissue-specific, negative regulation of *CTL1* by VAMP714 that operates outside the root environment.
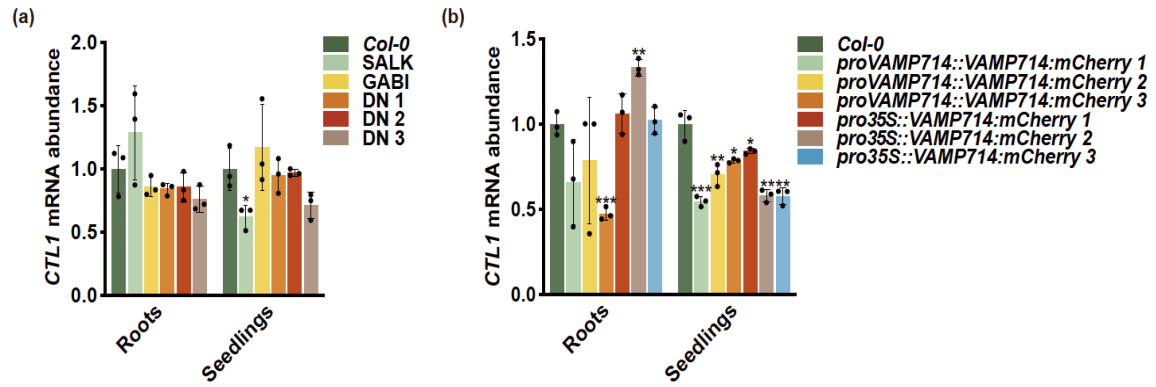
Fig. 4.6 *CTL1* mRNA abundance in roots and whole seedlings of mutants of *VAMP714*.

(a-b) *CTL1* mRNA abundance in roots and whole seedlings of *VAMP714* loss-of-function mutants **(a)** and gain-of-function mutants **(b)**. *ACTIN2* was used as an internal reference, and *Col-0* (WT) at each group served as the control for statistical comparisons. Data presented were means ± SD, n = 3 biological replicates, each with three technical replicates. *, $p < 0.05$, **, $p < 0.01$, ***, $p < 0.001$, ****, $p < 0.0001$, Student's *t*-test.

To determine whether *CTL1* likewise modulates *VAMP714* mRNA abundance, we profiled *VAMP714* mRNA abundance in mutants of *CTL1*. Results showed a consistent upregulation of *VAMP714* mRNA abundance in both roots and whole seedlings in *ctl1*, whereas overexpressing line 1 caused a significant downregulation of *VAMP714* mRNA abundance (Fig. 4.7). In contrast, the weakly overexpressing line 2 failed to elicit this response, suggesting that feedback suppression of *VAMP714* requires a threshold level of *CTL1* activity (Fig. 4.7). Collectively, these findings reveal a bidirectional, organ-contextual regulatory circuit between *CTL1* and *VAMP714*, with the change of *CTL1* regulating *VAMP714* expression in non-tissues manner and *VAMP714* overexpression selectively repressing *CTL1* in above-ground tissues.

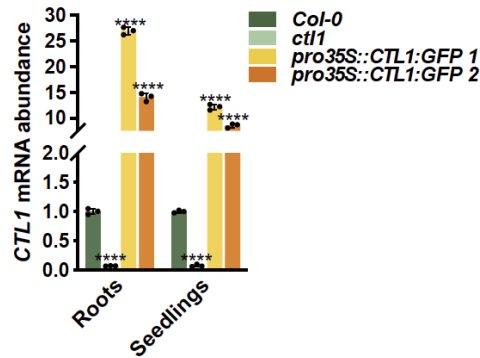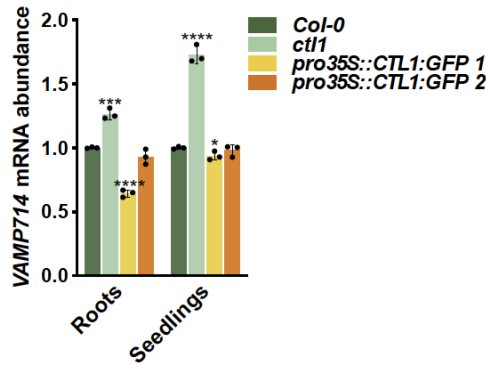**Fig. 4.7** ***VAMP714* mRNA abundance in roots and whole seedlings of mutants of *CTL1*.**

ACTIN2 was used as an internal reference, and *Col-0* (WT) at each group served as the control for statistical comparisons. Data presented were means ± SD, n = 3 biological replicates, each with three technical replicates. *, $p < 0.05$, **, $p < 0.01$, ***, $p < 0.001$, ****, $p < 0.0001$, Student's *t*-test.

4.4.4 Root-specific modulation of the VAMP714-CTL1 feedback circuit by exogenous choline

To test whether exogenous choline supply influences the reciprocal regulation between CTL1 and VAMP714, mutants of *CTL1* were exposed to 10 µM choline for additional 9 hours. Root analysis revealed that choline treatment elicited a pronounced increase in *CTL1* mRNA abundance in both WT and *pro35S::CTL1:GFP* but not in *ctl1*, showing that constitutive *CTL1* overexpression does not abrogate its response to choline (Fig. 4.8a). Interestingly, exogenous choline did not regulate *VAMP714* mRNA abundance in WT (Fig. 4.8b). This shows that under physiological conditions, VAMP714 did not respond to exogenous choline. Meanwhile, in *ctl1 VAMP714* mRNA abundance was significantly elevated. This indicates that the VAMP714-CTL1 feedback loop remains operational. By contrast, in *pro35S::CTL1:GFP*, which responded to exogenous choline, *VAMP714* mRNA abundance was likewise markedly increased, an outcome that runs counter to the VAMP714-CTL1 feedback mechanism. These findings imply that exogenous choline perturbs this feedback circuit through alternative pathways. Whole-seedling analysis

illustrated that neither *CTL1* nor *VAMP714* mRNA abundances were significantly altered by choline treatment (Fig. 4.8a-b). This tissue-specific effect demonstrated that exogenous choline selectively modulates the CTL1 and VAMP714 regulatory circuit in roots while leaving their expression unperturbed in aerial or non-root tissues.
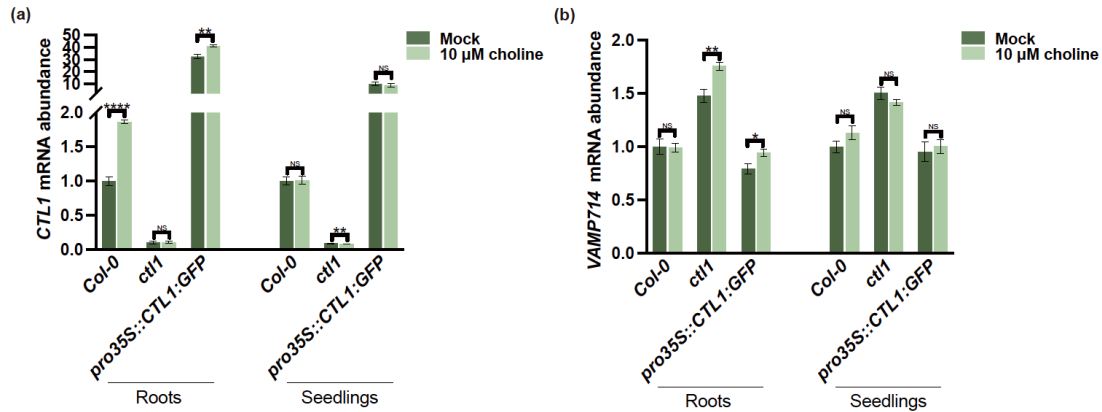
Fig. 4.8 Root-specific modulation of the VAMP714-CTL1 feedback circuit by exogenous choline.

(a) *CTL1* and **(b)** *VAMP714* mRNA abundance of 5 dpg WT and mutants of *CTL1* on growth medium supplemented with exogenous choline for additional 9 h. Without treatment at each group served as the control for statistical comparisons. Data presented were means ± SD, *n* = 3 biological replicates, each with three technical replicates. *, $p < 0.05$, **, $p < 0.01$, ***, $p < 0.001$, ****, $p < 0.0001$, Student's *t*-test.

4.5 Salt stress induces *CTL1* transcriptional level in roots

Given the close functional relationship between CTL1 and VAMP714, it is easy to hypothesize that mutants of *CTL1* would exhibit a similar salt-induced expression. Accordingly, we subjected the mRNA abundance of mutants of *CTL1* to the same set of expression assays, that is culturing seedlings on growth medium supplemented with 0-200 mM NaCl for an additional 0, 3, 9, or 24 hours described in Section 3.7. The results indicated that, while a 50 mM NaCl treatment failed to significantly alter *CTL1* mRNA abundance, exposure

to 100-200 mM NaCl for just 3 h elicited a pronounced increase in *CTL1* transcripts, which remained elevated at 9 h (Fig. 4.9). After 24 h, only the 150 mM NaCl treatment sustained this induction, whereas transcript levels under 100 mM and 200 mM reverted toward baseline (Fig. 4.9). These observations revealed that the spatiotemporal pattern of salt-induced *CTL1* expression closely parallels that of *VAMP714* and key auxin signalling induction genes as described in Section 3.6 and 3.7, consistent with the early-phase salt-stress regulatory program in *Arabidopsis thaliana* (Geng et al., 2013). This finding further corroborates a tight functional linkage between CTL1 and VAMP714.
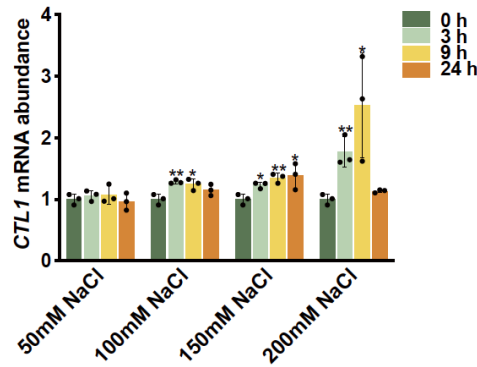
Fig. 4.9 Salt stress induces *CTL1* mRNA abundance in roots.

CTL1 mRNA abundance in roots of 5 dpg *Col-0* (WT) on growth medium supplemented with 0-200 mM NaCl for additional 0, 3, 9, or 24 hours by RT-qPCR. *UBQ5* was used as an internal reference, and without NaCl treatment served as the control for statistical comparisons. Data presented were means ± SD, n = 3 biological replicates, each with three technical replicates. *, $p < 0.05$, **, $p < 0.01$, ***, $p < 0.001$, ****, $p < 0.0001$, Student's *t*-test.

4.6 CTL1 modulates root salt tolerance parallel to VAMP714

It hypothesized that mutants of *CTL1* would exhibit a similar salt-response phenotype to *vamp714*. Accordingly, the experiment subjected *ctl1* mutants to the same set of phenotypic assays, that is culturing seedlings on growth medium supplemented with 0, 50, 100, 150, or 200 mM NaCl for an additional

7 days described in Section 4.2. Under non-stress conditions, *ctl1*, but not *pro35S::CTL1:GFP*, exhibited significantly shorter primary root lengths than WT, confirming that CTL1 was required for primary root elongation, and its overexpression does not impair baseline growth. However, this also meant that the phenotype caused by salt treatment in *ctl1* may be affected by its already reduced growth, while *pro35S::CTL1:GFP* was not affected. Exposure to 200 mM NaCl proved lethal for all genotypes (Fig. 4.10a-b), as previously observed for mutants of *VAMP714*. Between 50 and 100 mM NaCl, *ctl1* primary root elongation remained significantly below that of WT, and primary root length was predictably reduced. In contrast, *pro35S::CTL1:GFP* displayed a striking salt-tolerant profile at 150 mM NaCl, with significantly greater primary root elongation than WT. This coincided with markedly lower lateral root density and lateral root elongation, mirroring the response seen for *proVAMP714::VAMP714:mCherry* transgenic seedlings, further supporting a model in which CTL1 levels modulate root architectural plasticity under salt stress.

(a)

Col-0   ctl1   *pro35S::CTL1:GFP*

Col-0

Relative mRNA level
3000
2000
1000
100
80
60
40
20

Mock

50 mM NaCl

100 mM NaCl

Col-0

150 mM NaCl

200 mM NaCl

AtZF14   *AT1G07400*

1G07400

Col-0

Col-0

(b)

- ● *Col-0*
- ■ *ctl1*
- ▲ *pro35S::CTL1:GFP*

Relative root growth (%) vs NaCl (mM)

Primary root elongation (cm) vs NaCl (mM)

Lateral root density (roots cm⁻¹) vs NaCl (mM)

Lateral root elongation (cm) vs NaCl (mM)

Primary root length (cm) vs NaCl (mM)

AtVAMP714   *AtEDL3*   *AtCML37*   *AtZF14*   *AT1G07400*

AtMYB42

mRNA level
3000
2000
1000

Grouped: Entering replicate data

105

Fig. 4.10 *CTL1* modulates root salt tolerance parallel to *VAMP714*.

(a) The root growth of 5 dpg WT and mutants of *CTL1* on growth medium supplemented with 0-200 mM NaCl for additional 7 days. Bars = 1 cm. **(b)** The relevant phenotypic parameters. *Col-0* (WT) at each group served as the control for statistical comparisons. Data presented were means ± SD, n = 3 biological replicates, each with 10 roots. *, $p < 0.05$, **, $p < 0.01$, ***, $p < 0.001$, ****, $p < 0.0001$, Student's t-test.

4.7 Summary

In this chapter, analysis was carried out as to how VAMP714 expression levels might influence salt tolerance, by integrating root architectural measurements and molecular analyses. Firstly, it was found that mild overexpression of *VAMP714* under its native promoter significantly improves primary root growth at moderately high salinity. In contrast loss-of-function and 35S driven constitutive overexpression seedlings maintained limited baseline tolerance. Secondly, it was demonstrated that this improved performance depends on polar auxin transport. Specifically, co-application of low-dose IAA revealed that native-promoter overexpressors partially retained auxin-mediated growth under salt stress, and inhibition of polar auxin transport abolished this advantage. Thirdly, there was found to be a close functional relationship between VAMP714 and CTL1. CTL1 was previously found to physically interacts with VAMP714 in trans-Golgi/endosomal hubs, and is required for proper VAMP714 localization and PIN1 polarity. Reciprocal, tissue-specific feedback was observed: *CTL1* expression was repressed in above-ground tissues of *VAMP714* overexpressors, and *VAMP714* was upregulated in *ctl1* but downregulated in *CTL1* overexpressor in non-tissue manner. Exogenous choline selectively induced this feedback in roots. Finally, *CTL1* mRNA abundance was rapidly induced by 100-200 mM NaCl in roots, paralleling *VAMP714*, and *pro35S::CTL1:GFP* exhibited root salt tolerance, underscoring their coordinated roles in vesicle-mediated auxin reprogramming under salinity.

Chapter 5: VAMP714 orchestrates vesicle fusion, ROS homeostasis, and SOS pathway activation during early salt-stress response

5.1 Introduction

Work described so far has employed a range of assays to characterize the baseline salt tolerance and adaptive root phenotypes of *vamp714* mutants, demonstrating that misexpression of *VAMP714* alters root system architecture under salt stress. However, these results stopped short of revealing the underlying molecular mechanisms.

In this chapter, the objective is bridge that gap by combining global transcriptomic profiling with targeted physiological experiments. By correlating salt-induced changes in gene expression with VAMP714-dependent alterations in auxin distribution, root growth dynamics, and vesicle trafficking, a comprehensive model is assembled of how VAMP714 integrates vesicle fusion events into hormone-driven salt-stress adaptation. This integrated approach reveals SNARE-dependent signalling circuits as central components of salinity responses in *Arabidopsis thaliana*. In this chapter, "WT" refers to Col-0. 5 dpg seedlings are the material for treatment, with roots sampled except in Sections 5.5-5.7.

5.2 Transcriptomic profiling uncovers VAMP714-linked pathways are affected by salt stress

5.2.1 Experimental design and transcriptome profiling

Firstly, 5 dpg GABI *vamp714* mutant and WT seedlings were each subjected to 150 mM NaCl for an additional 0, 3, 9, and 24 h, to delineate the signalling

networks involving VAMP714 under high saline conditions. Overexpression lines often exhibit novel functions not found in nature (Zhang, 2003), therefore, the loss-of-function mutant was used for the RNA-seq analysis. 24 cDNA libraries (two genotypes × four time points × three biological replicates) were generated and Illumina RNA-seq was performed based on SBS (Appendix III). Correlation analysis and principal component analysis (PCA) confirmed strong reproducibility between replicate samples (Fig. 5.1a-b) based on Fragments Per Kilobase of transcript sequence per Millions base pairs sequenced (FPKM) normalization (Bray et al., 2016; Mortazavi et al., 2008; Trapnell et al., 2010). PCA clearly distinguished control and NaCl treatment groups for both mutant and WT, indicating a substantial salt-induced shift in the transcriptome (Fig. 5.1b). Differential expression analysis validated that GABI showed no *VAMP714* expression (Appendix IV), and cluster analysis (Fig. 5.1c) reinforced sample consistency. In total, 41 differentially expressed genes (including *VAMP714*) that were common to all treatments (plus and minus salt, 0-24 hours; Fig. 5.2a; Appendix V) and 29 genes were found to be specifically altered by salt treatment (Fig. 5.2a-b; Appendix V). These genes potentially represent salt-regulated genes that are dependent on VAMP714 function.

(a) Pearson correlation between samples

(b) Grouped: Entering replicate data
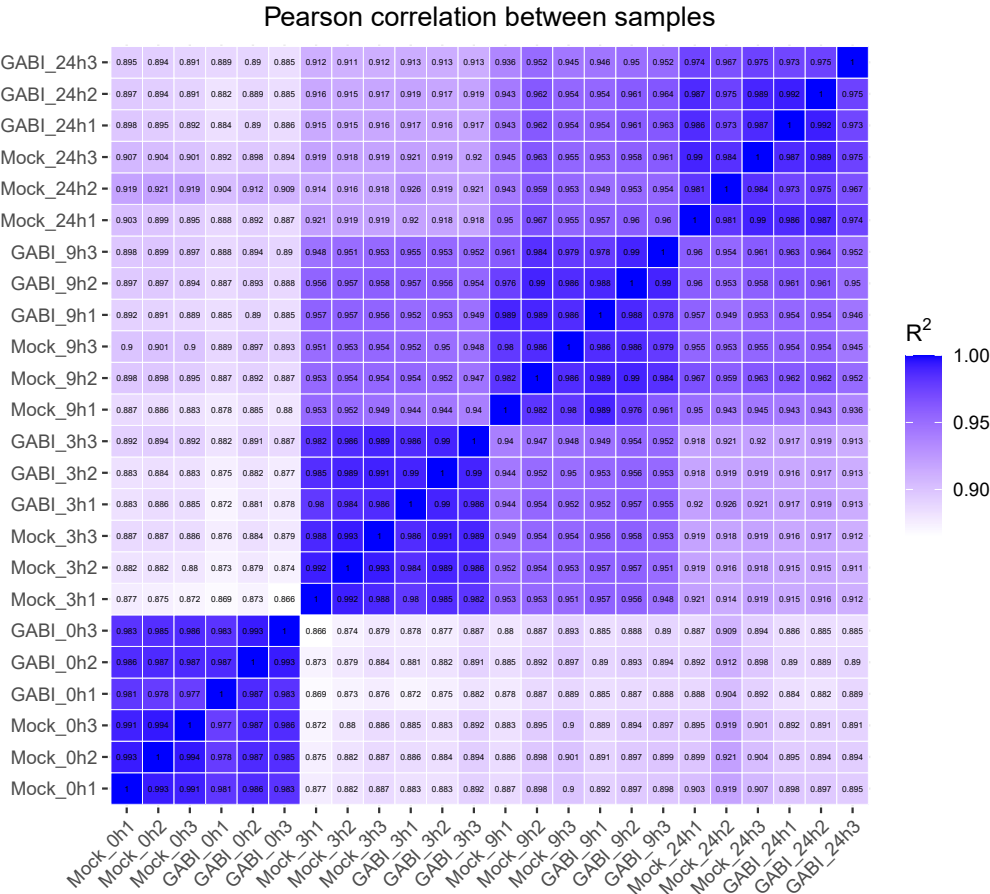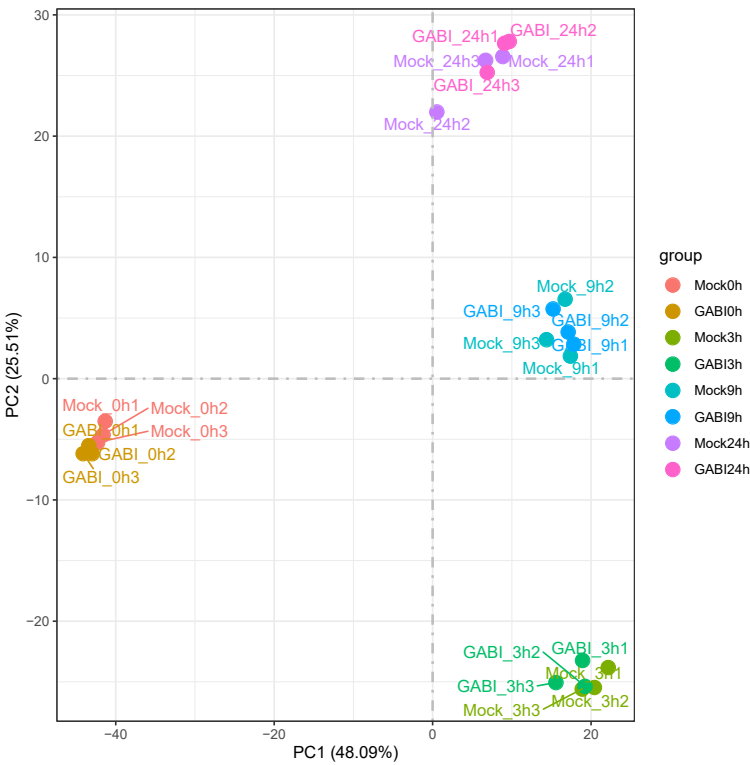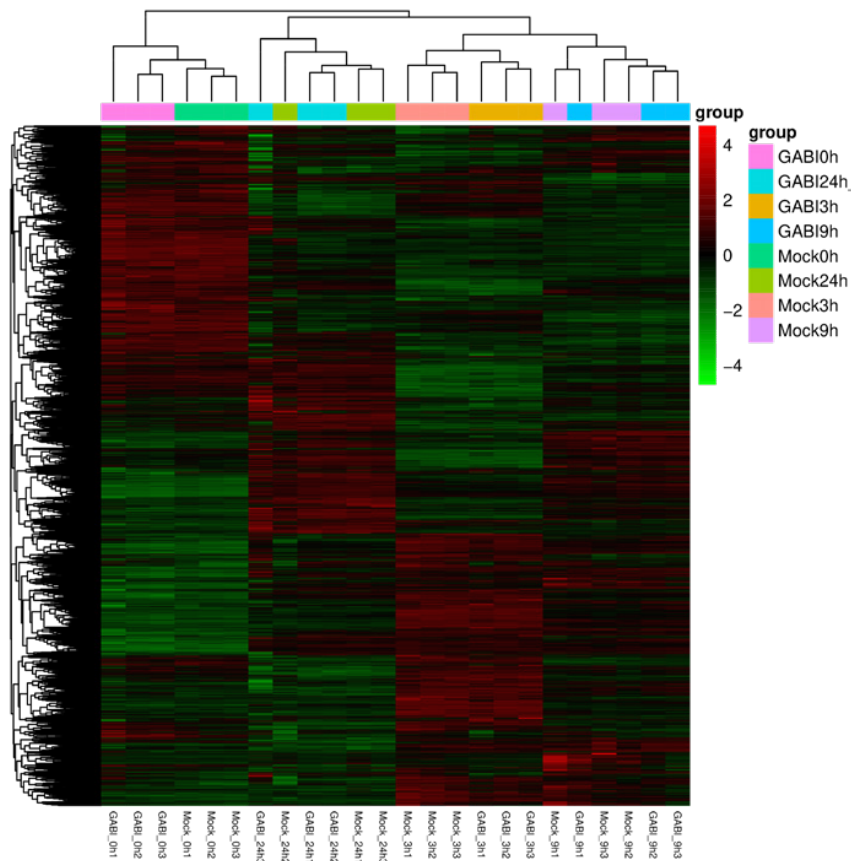
Fig. 5.1 Correlation analysis (a), PCA (b), and cluster analysis (c) of RNA-seq.
GABI = *vamp714* mutant, Mock = wild type (Col-0).

5.2.2 Dynamic pathway enrichment during early salt response

Gene Ontology (GO) enrichment analysis (Ashburner et al., 2000; Fig. 5.2c) revealed that under control conditions, biological process (BP) terms such as 'response to oxidative stress', 'oxygen levels', 'hypoxia', and 'response to water' were significantly enriched in the *vamp714* mutant (Fig. 5.2c). This suggests that VAMP714 is required for regulated hormonal and oxygen-related signaling and is consistent with observations indicating that VAMP714-associated vesicles translocate both PIN proteins and H_2O_2 between intracellular membrane compartments. The mutant is disrupted in auxin transport and so likely auxin-dependent signaling networks (Gu et al., 2021), and is expected to accumulate less H_2O_2 in the vacuole but more in 'megavesicles' in the cytoplasm (Leshem et al., 2006, Tang et al., 2022). At 3 hours of salt treatment,

110

genes associated with 'oxygen levels' were also enriched in the mutant. At 9 hours, enrichment of pathways related to secondary metabolites indicated the onset of plant adaptation (Geng et al., 2013), while at 24 hours, terms related to 'response to oxidative stress' and 'cell wall' were predominant. KEGG enrichment analysis (Kanehisa and Goto, 2000) produced similar trends. Under control conditions 'plant hormone signal transduction' was enriched in the *vamp714* mutant, which is consistent with the known function of VAMP714; at 3 hours of salt treatment, the 'ribosome' pathway was prominent, indicative of effects on protein synthesis; at 9 hours, primary metabolism and defence pathways dominated, suggesting plant adaptation; and at 24 hours, cell wall-related pathways were most differentially expressed (Fig. 5.2d). For further analysis we focused on the 3-hour time point to identify rapid changes in response pathways.

(a)

(b)

(c)
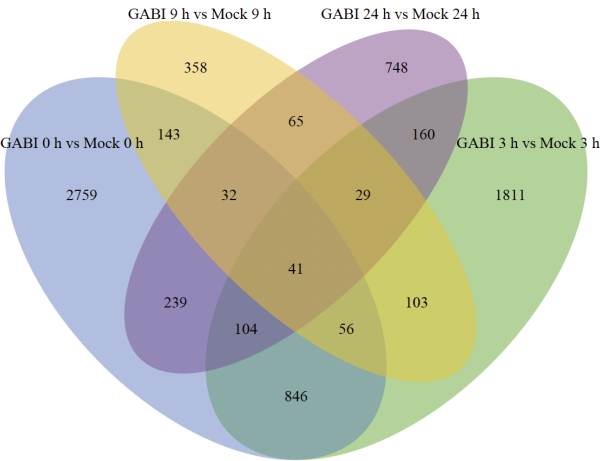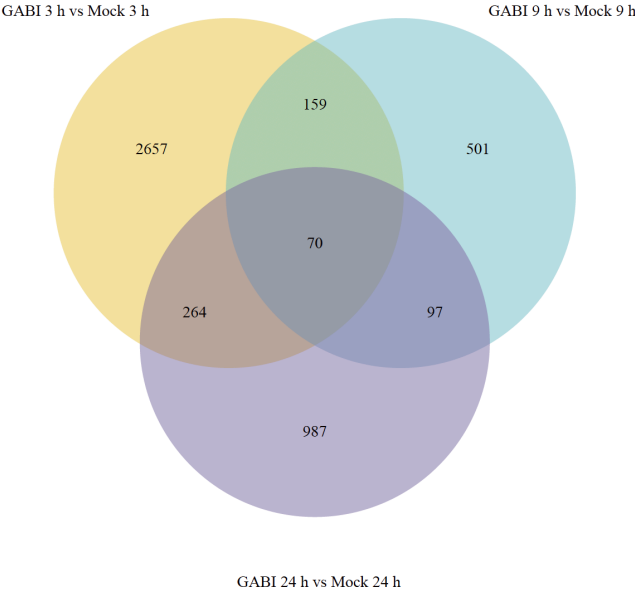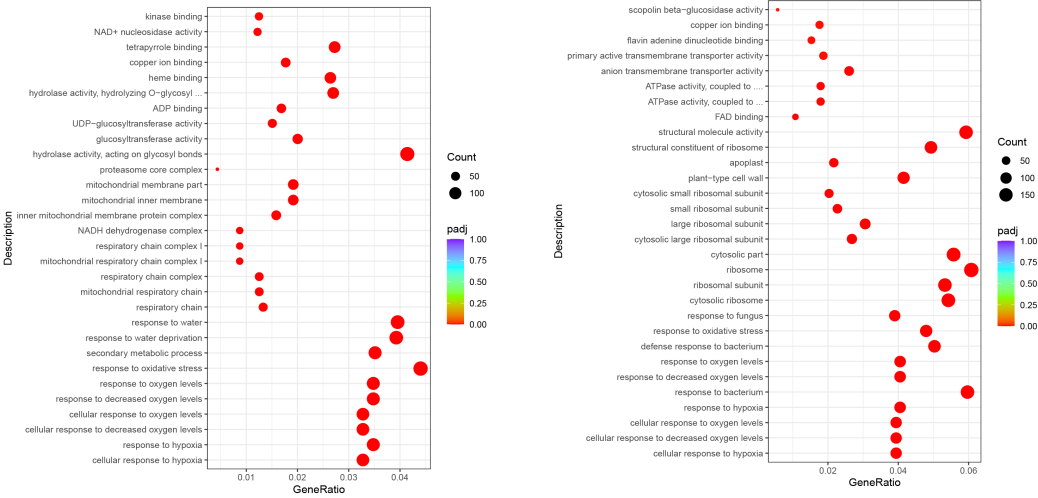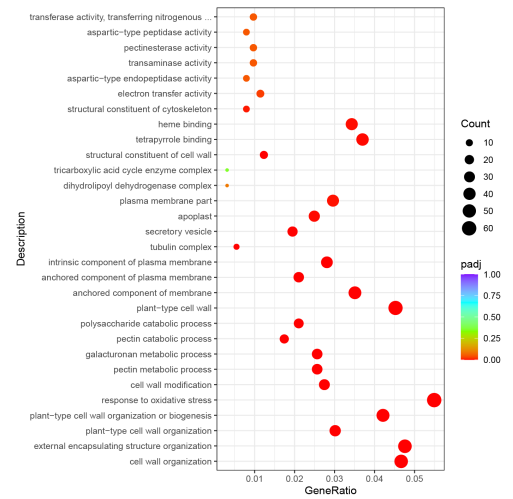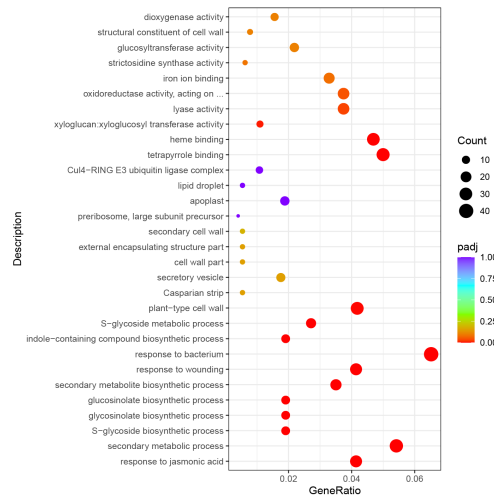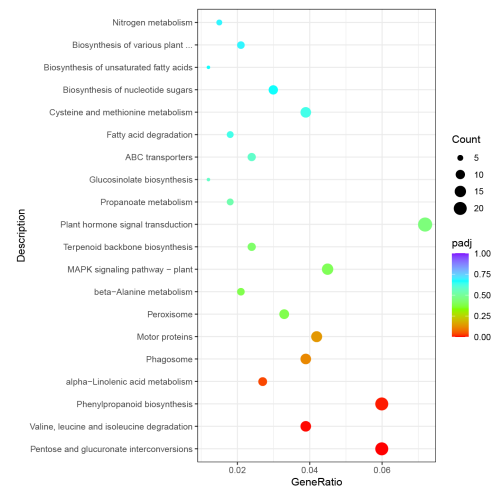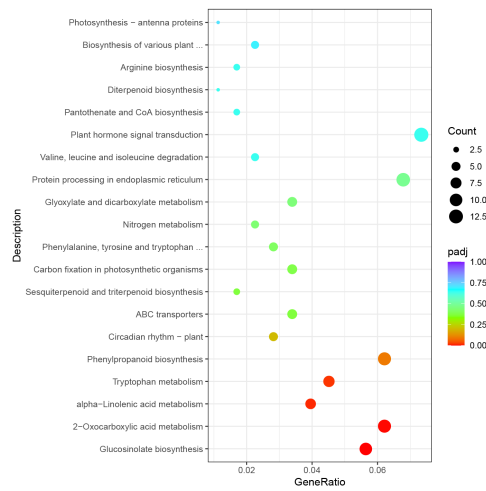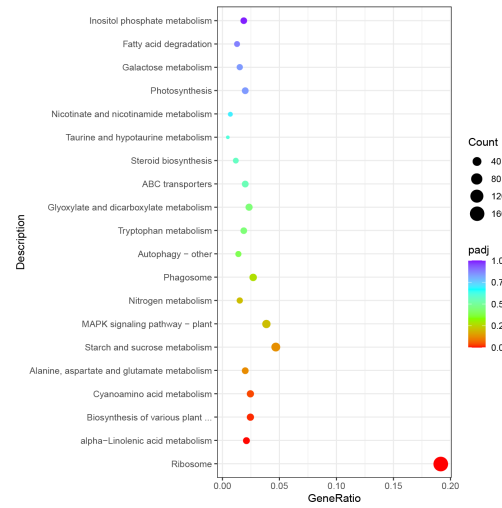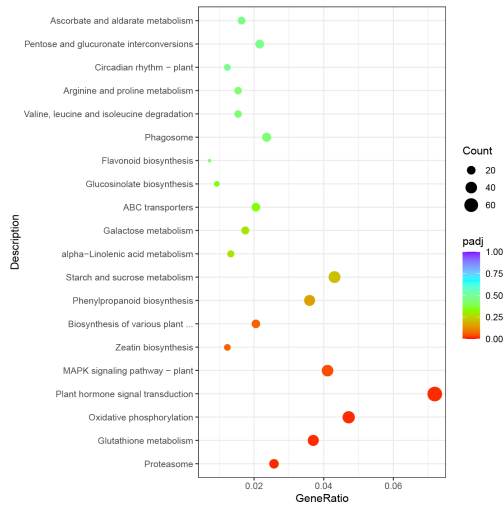
Fig. 5.2 Dynamic pathway enrichment during salt response.

GABI = *vamp714* mutant, Mock = wild type (Col-0). **(a-b)** The differentially expressed genes of 5 dpg *vamp714* mutant and WT on growth medium supplemented with 150 mM NaCl for additional 0, 3, 9, and 24 hours. **(a)** The differential genes of GABI 0 h vs Mock 0 h, GABI 3 h vs Mock 3 h, GABI 9 h vs Mock 9 h, and GABI 24 h vs Mock 24 h. **(b)** The differential genes of GABI 3 h vs Mock 3 h, GABI 9 h vs Mock 9 h, and GABI 24 h vs Mock 24 h. The sum of all the numbers in the circle represents the total number in the compared groups, and the overlapping area indicates the number of differential genes shared between the groups. **(c-d)** GO **(c)** and KEGG **(d)** enrichment analysis scatter plot. From left to right, they are the results of GABI 0 h vs Mock 0 h, GABI 3 h vs Mock 3 h, GABI 9 h vs Mock 9 h, and GABI 24 h vs Mock 24 h. In the **(c)**, the abscissa is the ratio of the number of differential genes linked with the GO Term to the total number of differential genes, and the ordinate is GO Term. The size of a point represents the number of genes annotated to a specific GO Term, and the color from red to purple represents the significant level of the enrichment. In the **(d)**, the abscissa is the ratio of the number of differential genes linked with the KEGG pathway to the total number of differential genes. The ordinate is KEGG Pathway. The size of a point represents the number of genes annotated to a specific KEGG pathway. The colour from red to purple represents the significant level of the enrichment. **(a-d)** n = 3, each with three technical replicates. Related analysis software and thresholds are detailed in (Appendix III).

5.2.3 Candidate genes selection and validation of early salt responses

Ten candidate genes (including *VAMP714*) have been selected from 41 DEGs (baseline and salt treatment) based on their GO annotations in TAIR as 'salt or hormone related' and 'oxygen related' (https://www.arabidopsis.org/; Appendix V) for further validation by RT-qPCR. Following 150 mM salt treatment for 3 hours, the four "salt or hormone related" genes (*EDL3*, *CML37*, *ZF14*, and *AT1G07400*) and five "oxygen related" genes (*GDPD2*, *GSTF7*, *IRT1*, *NIT2* and *PMSR1*) showed consistent trends between WT and GABI (Fig. 5.3). This shows that salt-induction of these genes is not dependent on VAMP714. These

results confirm the reliability of our RNA-seq data and justify mining VAMP714 candidate targets from the 29 salt-specific DEGs. Screen then applied the following selection criteria: in WT samples, expression at 3, 9, and 24 h must be significantly higher than at 0 h, while in the *vamp714* mutant, expression at those time points must remain unchanged. Using these filters, there is no identified candidate gene (Appendix VI). However, *CYP96A12 (AT4G39510)* is persistently downregulated in the WT, while unchanged in the *vamp714* mutant (Appendix VI). *CYP96A12* is predicted to participate in redox processes (https://www.arabidopsis.org/). This suggests an association between VAMP714 and redox processes.
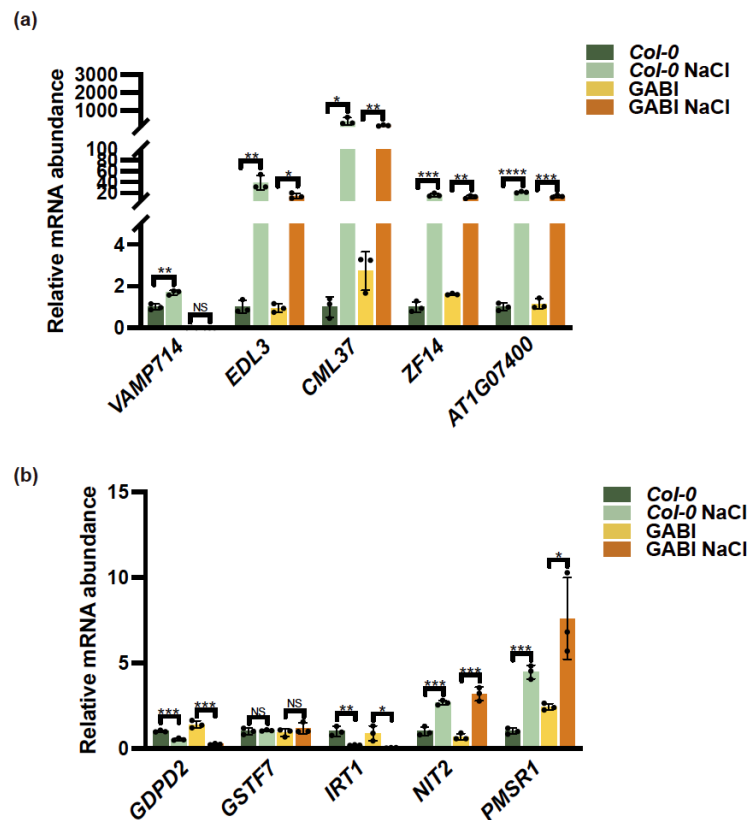
Fig. 5.3 Ten candidate genes validation of early salt responses.

(a-b) RT-qPCR analysis of relative mRNA abundance of selected differentially expressed genes in roots of 5 dpg wild type and *vamp714* mutant on half MS medium supplemented with 150 mM NaCl for additional 3 hours. *UBQ5* was used as an internal reference, and seedlings grown without NaCl served as the control for each group for statistical comparisons. Data

represent means ± SD, *n* = 3 biological replicates, each with three technical replicates. *, $p <$ 0.05, **, $p < 0.01$, ***, $p < 0.001$, ****, $p < 0.0001$, Student's *t*-test.

Furthermore, PPI mapping under 150 mM NaCl treatment defined a spatiotemporal framework for the engagement of VAMP714 with its partners (Fig. 5.4). Under non-stress conditions VAMP714 likely interacts with AP-3 and SNAP29; after 3 h of salt exposure interactors include AP-3, SNAP29, and SYP23; at 9 h with SNAP29; and by 24 h with MEMB11. All these four proteins are related to vesicle fusion or transport based on *TAIR* GO annotations (https://www.arabidopsis.org/). The persistence of this complex suggests that the functional activity of VAMP714, both under non-stress conditions and salt stress, is fundamentally driven by its role in mediating vesicle trafficking. Further, VAMP714 likely ensures efficient cargo delivery and membrane recycling critical for salt-adaptive signalling and auxin redistribution.
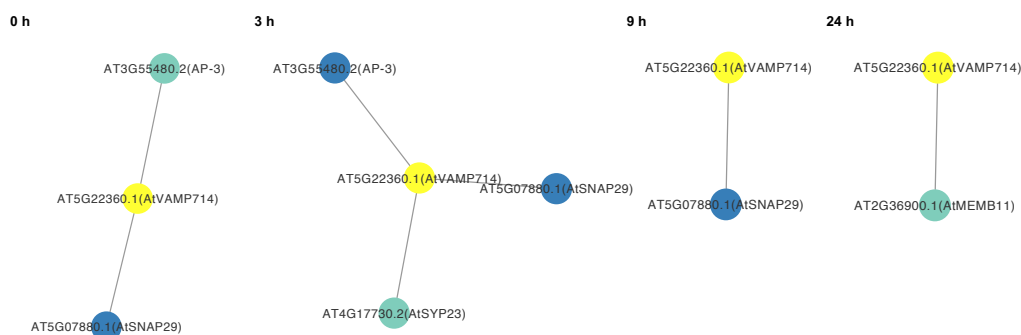
Fig. 5.4 PPI of VAMP714 under salt stress.

From left to right, the PPI networks of VAMP714 under salt stress at 0 h, 3 h, 9 h, and 24 h are shown as visualized using Cytoscape (v3.10.1). Edges represent protein–protein associations derived from the STRING database (https://string-db.org/), including experimentally determined and database-annotated interactions, as well as predicted functional associations. Yellow nodes indicate VAMP714, green nodes denote interactors without significant differences in protein abundance between GABI and WT, and blue nodes represent interactors with significantly decreased protein abundance in GABI compared with WT. Related analysis software and thresholds are detailed in (Appendix III).

5.3 VAMP714 influences ROS homeostasis under salt stress

Since ROS are classical components of the salt stress response and plant abiotic stress in general (Apel and Hirt, 2004), and the results above suggest a role for VAMP714 in the regulation of ROS homeostasis-related gene expression under salt stress. Based on this, the mRNA abundance of key ROS biosynthetic genes *RBOHD* and *RBOHF* and scavenging genes (*CAT1*, *GSTF6* and *MSD1*) in roots of *vamp714* mutant and WT have been measured after 3 hours of control or 150 mM NaCl treatment (Fig. 5.5). *RBOHD*, *RBOHF* and *CAT1* were upregulated in WT and mutant under salt stress, although *RBOHD* had an upward trend but with no significant difference in *vamp714* mutant on salt (Fig. 5.5). Similarly, *MSD1* showed no significant differences between WT and mutant under salt stress. Interestingly, *GSTF6* was not up-regulated under salt stress in WT but was in the *vamp714* mutant, indicating VAMP714 represses expression of this gene under salt stress.
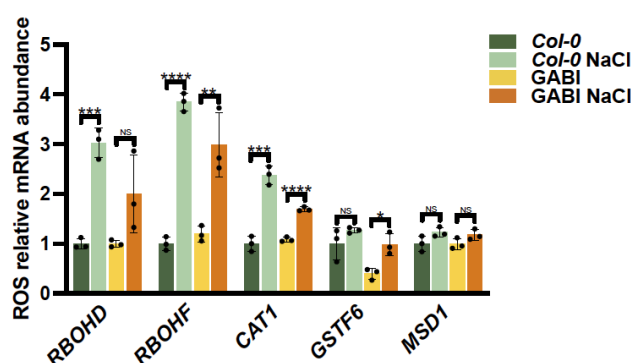
Fig. 5.5 Relative ROS Homeostasis genes mRNA abundance under salt stress.

RT-qPCR analysis of relative mRNA abundance of selected ROS pathway genes in roots of 5 dpg wild type and *vamp714* mutant on half MS medium supplemented with 150 mM NaCl for an additional 3 hours. *UBQ5* was used as an internal reference, and seedlings grown without NaCl served as the control for each group for statistical comparisons. Data represent means ± SD, *n* = 3 biological replicates each with three technical replicates.

To corroborate these transcriptional changes at the biochemical level, ROS

histochemistry in roots has been performed. NBT staining, which detects superoxide, showed no significant differences between WT and *vamp714* mutant (Fig. 5.6a, c), suggesting *VAMP714* expression level does not influence superoxide accumulation. In contrast, DAB staining, which reveals H_2O_2 accumulation, showed that *vamp714* mutant roots accumulated significantly more H_2O_2 than WT in the presence of salt (Fig. 5.6b, d). We assayed catalase (CAT) enzyme activity, involved in ROS scavenging, and found that under control (no salt) conditions CAT activity was reduced in the *vamp714* mutant, but salt treatment increased CAT activity in mutant but not WT (Fig. 5.6e). These results are consistent with the data showing that *vamp714* and WT have similar salt sensitivity (Fig. 4.1). These results are consistent with previous observations that CAT activity does not undergo dynamic changes during the initial stages of salt stress (Apel and Hirt, 2004; Ellouzi, et al., 2011; Nabi et al., 2025).
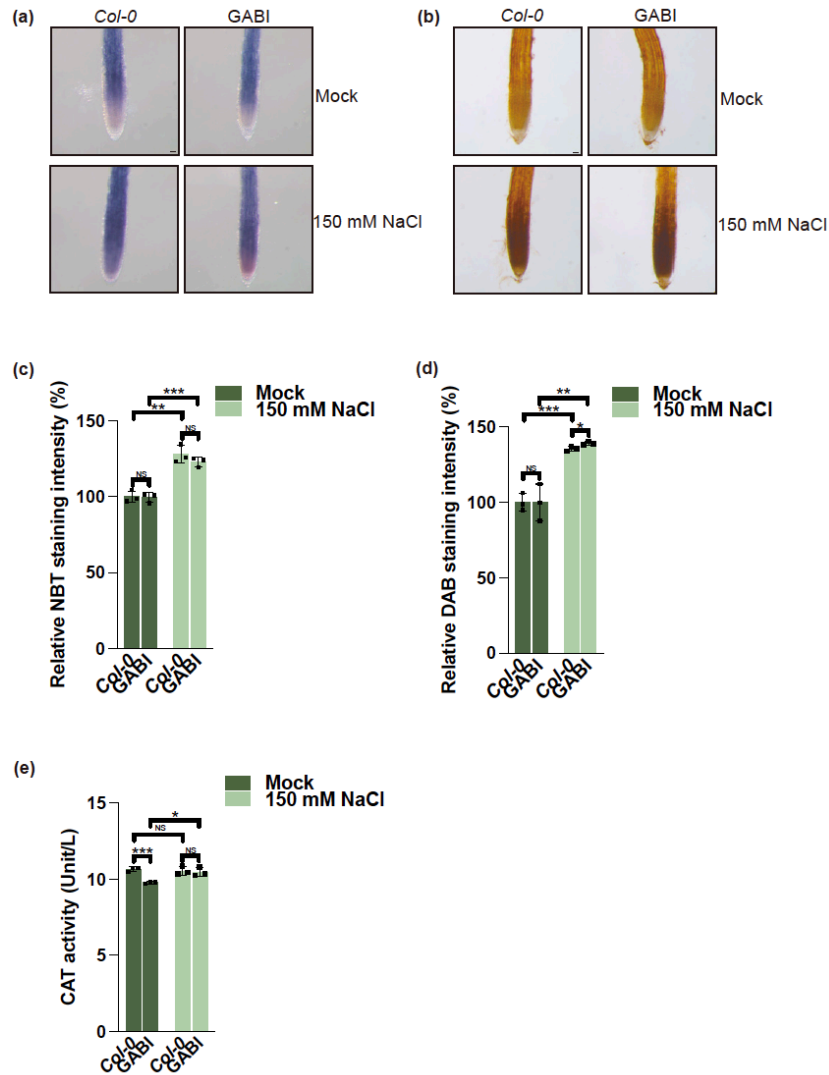
Fig. 5.6 VAMP714 influences ROS homeostasis under salt stress.

(a,c) NBT staining, **(b,d)** DAB staining, and **(e)** catalase (CAT) enzyme activities of roots of 5 dpg WT and *vamp714* mutant seedlings on half MS medium (Mock) and half MS medium supplemented with 150 mM NaCl for an additional 3 hours. **(a-b)** Bars = 20 μm. **(c-d)** The intensities of NBT staining **(c)** and DAB staining **(d)** were determined using Fiji image analysis software. The intensity in mock treatment samples was taken as 100%. **(c-e)** Data represents means ± SD, n = 3 biological replicates, each with at least 5 seedlings for NBT staining, at least 10 seedlings for DAB staining and three technical replicates for CAT. *, $p < 0.05$, **, $p < 0.01$, ***, $p < 0.001$, ****, $p < 0.0001$, Student's *t*-test.

5.4 VAMP714 is associated with the SOS pathway

Salt stress directly impacts Na^+ homeostasis. In *Arabidopsis* roots, Na^+ is taken up by HKT1 (Platten et al., 2006), then partly stored in the vacuole by NHX1 (Apse et al., 2003), and the remainder expelled by the Na^+/H^+ antiporter SOS1 (SALT OVERLY SENSITIVE1; Shi et al., 2000), a key component of the salt response pathway (Ali et al., 2023). A problem is that whether VAMP714 regulates the SOS pathway. Results presented in Fig. 5.7a showed that salt treatment significantly decreased the mRNA abundance of *HKT1* and increased *NHX1* in all genotypes, showing their regulation is independent of VAMP714. However, salt treatment significantly increased the mRNA abundance of *SOS1* in WT but not the *vamp714* mutant (Fig. 5.7a), suggesting the *VAMP714* is associated with Na^+ efflux. We further examined expression of the SOS pathway-related genes *SOS2*, *SOS3*, *CBL10*, *HIS1-3* and *WRKY1* under salt stress (Fig. 5.7b). *SOS2*, *HIS1-3* and *WRKY1* exhibited VAMP714-associated expression patterns, similar to *SOS1*, while *SOS3* showed no VAMP714-associated. Further analysis revealed that SOS3-associated gene *PLATZ2* (Fig. 5.7c) and *SOS2*-associated genes *UBC1* and *UBC2*, similarly paralleled the expression patterns of *SOS2*, *HIS1-3*, *WRKY1* and *SOS1* (Fig. 5.7d); though SOS1-associated genes *RSA1* and *AT3G06590* (Fig. 5.7c), and other SOS2-associated genes *MPK4* and *MYB42* (Fig. 5.7d) showed no VAMP714 dependency. Given that salt-activated SOS2 phosphorylates PLT1/2 proteins via their conserved C-terminal motifs to stabilize them and maintain root meristem activity under stress (Hao et al., 2023), our results not only confirm SOS2 activation under salinity but also explain the stabilization of PLT1/2 observed in Fig. 3.10.
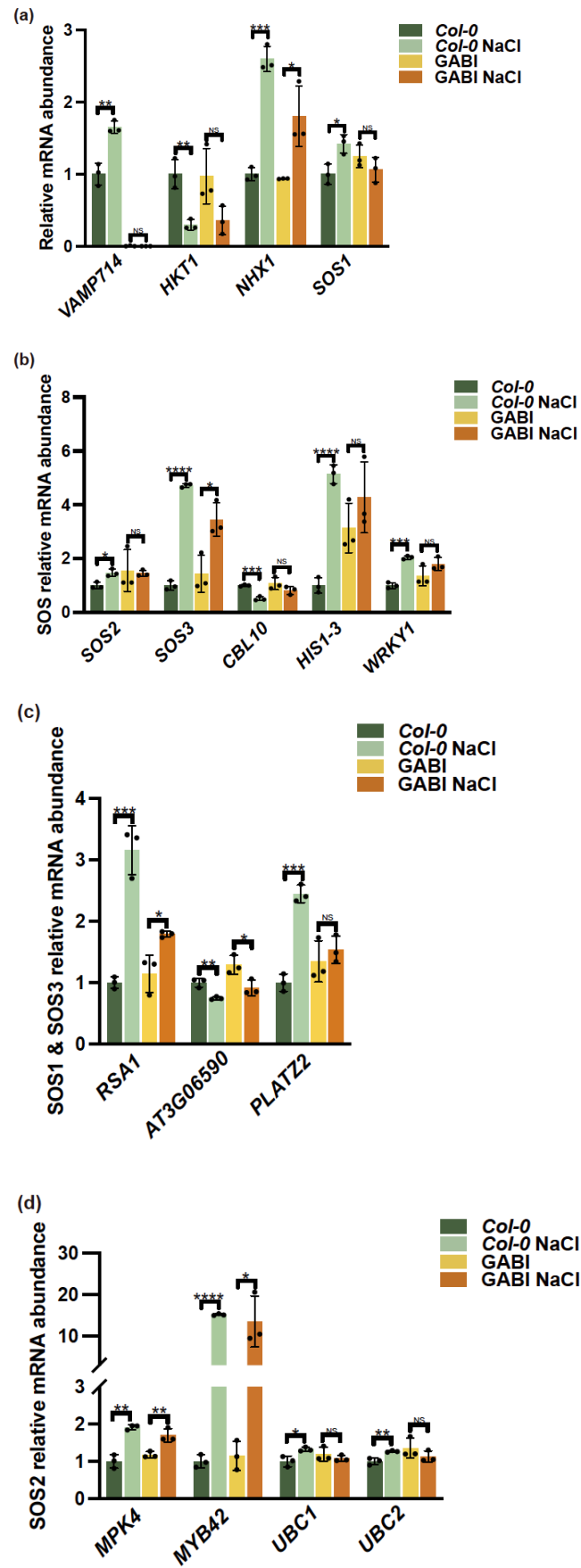
Fig. 5.7 Relative SOS signalling pathway genes mRNA abundance under salt stress.
RT-qPCR measurements of relative mRNA abundance of SOS pathway genes in roots of 5 dpg *Col-0* (WT) on half MS medium supplemented with 150 mM NaCl for an additional 3 hours. *UBQ5* was used as an internal reference, and seedlings grown without NaCl served as the control for each group for statistical comparisons. Data represent means ± SD, n = 3 biological replicates, each with three technical replicates. *, $p < 0.05$, **, $p < 0.01$, ***, $p < 0.001$, ****, $p < 0.0001$, Student's t-test.

5.5 VAMP714 fails to restore ion homeostasis under salt stress

The SOS signaling pathway affects ion homeostasis directly by regulating Na^+ and K^+ contents and the second messenger Ca^{2+} (Gong et al., 2004). To investigate ion homeostasis in mutant and WT seedlings under salt stress, we measured Na^+, K^+ and Ca^{2+} contents in 28 dpg whole plants after 24 hours of 150 mM NaCl treatment (See Section 2.2.12 for details). Salt treatment led to dramatically increased Na^+ contents in both WT and mutant plants (Fig. 5.8-5.9). In WT, K^+ and Ca^{2+} showed a downward trend by salt treatment but both were variable in the *vamp714* mutant (Fig. 5.8-5.9).

5.6 Auxin redistribution activates downstream Ca^{2+} signalling pathways independently of VAMP714

Previous studies indicate that the SOS pathway regulates the redistribution of auxin to mediate changes in root development under salt stress (Zhao et al., 2011). To assess whether auxin plays a role in regulating ionic balance, we exposed seedlings to 150 mM NaCl together with either 10 µM IAA or 10 µM NPA. The application of exogenous IAA or NPA did not rescue the ion imbalance in both WT and mutant plants caused by salt stress (Fig. 5.8). However, IAA co-treatment led to a significant increase in Ca^{2+} content in both WT and mutant plants compared to salt stress alone (Fig. 5.8). This suggests that auxin distribution could activate downstream Ca^{2+} signaling pathways

independently of VAMP714 under salt stress.
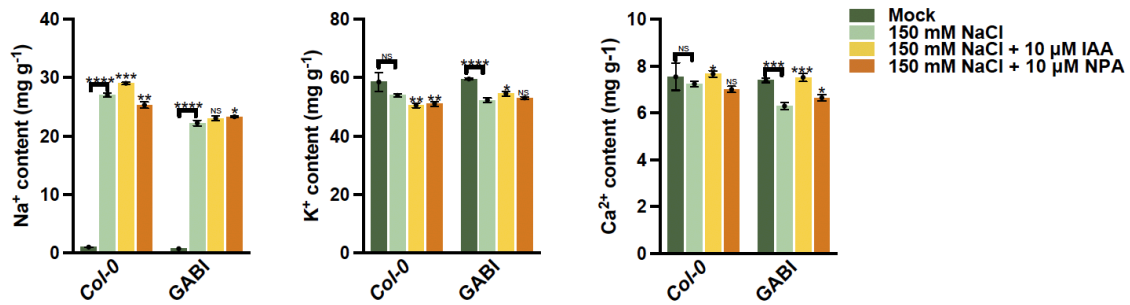
Fig. 5.8 Auxin redistribution activates downstream Ca²⁺ signalling pathways independently of VAMP714.

Ion contents were determined for 28 dpg whole seedlings of wild type (*Col-0*) and *vamp714* (GABI) mutant grown on half-strength Hoagland's No. 2 Basal Salt Mixture liquid solution supplemented with different treatments for an additional 24 hours. Wild type or 150 mM NaCl treatment served as the controls for each group for statistical comparisons. Data represent means ± SD, n = 3 biological replicates, each with three technical replicates. *, $p < 0.05$, **, $p < 0.01$, ***, $p < 0.001$, ****, $p < 0.0001$, Student's *t*-test.

5.7 VAMP714 is required for auxin biosynthesis–mediated regulation of ion homeostasis

To determine whether auxin biosynthesis as well as transport is important for ion homeostasis, we blocked endogenous auxin biosynthesis using 30 µM L-kynurenine (inhibiting TAA1/TARs to block the Trp-IPyA step) (He et al., 2011) and 30 µM PPBo (inhibiting YUCCAs to block the subsequent conversion of IPyA to IAA) (Kakei et al., 2015; Koike et al., 2020). In WT, addition of L-kynurenine with 150 mM NaCl did not significantly change Na⁺, K⁺, or Ca²⁺ contents relative to salt treatment alone, whereas PPBo treatment led to increases in all three ions (Fig. 5.9). This finding implies that blocking the YUCCA-mediated final biosynthetic step, rather than the upstream TAA1/TAR-catalyzed reaction, affects ion homeostasis under salt stress. In the *vamp714* mutant, L-kynurenine/salt co-treatment led to marked decreases in Na⁺, K⁺, and

Ca^{2+} contents (Fig. 5.9). Likewise, under PPBo treatment, the *vamp714* mutant showed reductions in Na^+ and K^+ contents with stable Ca^{2+} content (Fig. 5.9). These responses show that VAMP714 is essential for the effect of auxin biosynthesis on ion homeostasis, presumably due to its role in regulating auxin distribution.
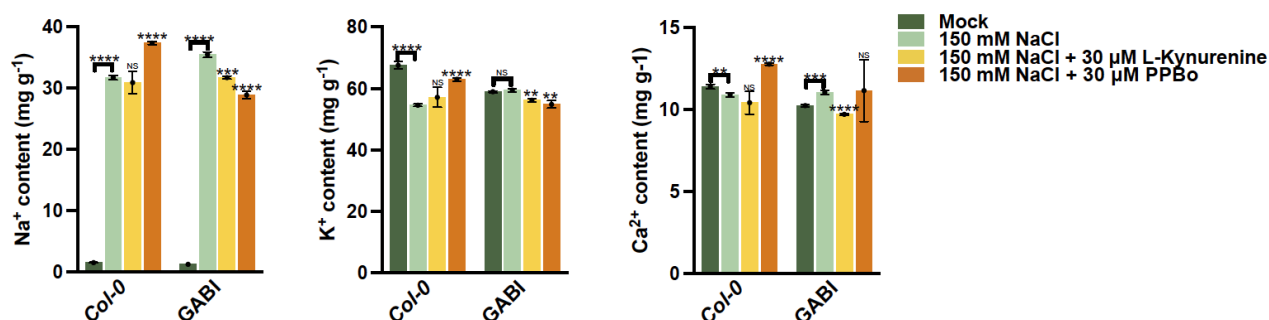
Fig. 5.9 VAMP714 is required for auxin biosynthesis–mediated regulation of ion homeostasis.

Ion contents were determined for 28 dpg whole seedlings of wild type (*Col-0*) and *vamp714* (GABI) mutant grown on half-strength Hoagland's No. 2 Basal Salt Mixture liquid solution supplemented with different treatments for an additional 24 hours. Wild type or 150 mM NaCl treatment served as the controls for each group for statistical comparisons. Data represent means ± SD, n = 3 biological replicates, each with three technical replicates. *, $p < 0.05$, **, $p < 0.01$, ***, $p < 0.001$, ****, $p < 0.0001$, Student's *t*-test.

5.8 Calcium treatment partially restores root development independently of VAMP714

The above results and other data (Manishankar et al., 2018) show the importance of Ca^{2+} in salt stress responses, so we investigated whether $CaCl_2$ treatment affects *Arabidopsis* seedlings root growth under salt stress. Under normal conditions, high Ca^{2+} had almost no effect on root growth in either WT or *vamp714* mutant (Fig. 5.10). Under salt stress, high Ca^{2+} partially rescued root growth by maintaining primary root elongation, but not lateral root growth,

and the effect was independent of VAMP714 (Fig. 5.10). This suggests the role of Ca^{2+} in the salt stress response works in parallel to the polar auxin transport pathway mediated by VAMP714-dependent vesicle trafficking.
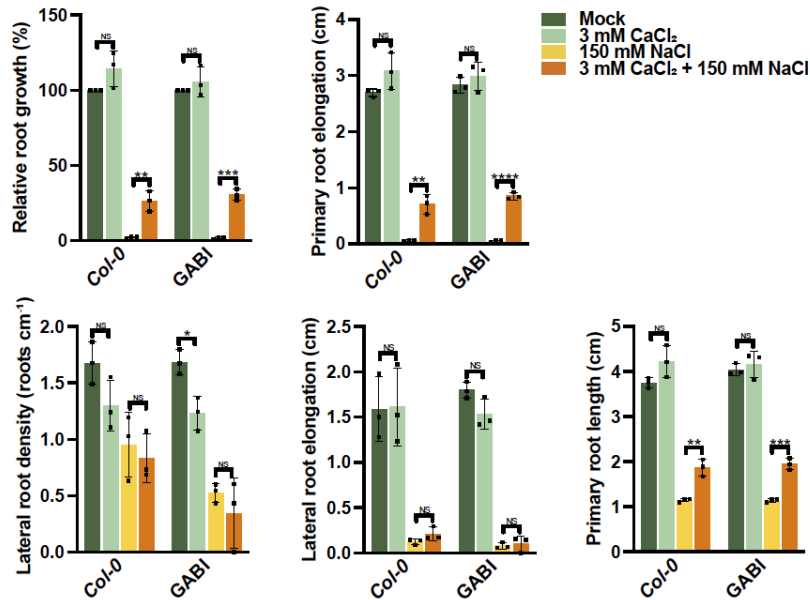
Fig. 5.10 Calcium treatment partially restores root development independently of VAMP714.

Root growth of 5 dpg wild type (*Col-0*) and *vamp714* (GABI) mutant seedlings grown on half MS medium supplemented with different treatments for an additional 5 days. Seedlings grown without NaCl served as the control for each group for statistical comparisons. Data represent means ± SD, *n* = 3 biological replicates, each with 10 roots. *, $p < 0.05$, **, $p < 0.01$, ***, $p < 0.001$, ****, $p < 0.0001$, Student's *t*-test.

5.9 Summary

In this chapter, transcriptomic and physiological analyses were integrated to elucidate how VAMP714 contributes to the early salt-stress response in Arabidopsis. RNA-seq of *vamp714* mutant and WT at 0, 3, 9, and 24 h after 150 mM NaCl treatment revealed 41 baseline DEGs and 29 salt-specific DEGs. GO and KEGG enrichment analysis highlighted changes in oxidative-stress responses, hormone signalling, and cell-wall remodelling over the treatment

time course, with the most rapid transcriptional reprogramming occurring at 3 h. Of the 41 DEGs, 10 candidates with "salt or hormone" and "oxygen" annotations were validated by RT-qPCR; only *CYP96A12*, a redox-related gene, exhibited VAMP714-dependent expression, suggesting a link between VAMP714 and redox metabolism. Protein-protein interaction mapping under salt stress showed that VAMP714 may partner dynamically with vesicle-fusion factors (AP-3, SNAP29, SYP23, and MEMB11), underscoring its role in trafficking.

ROS homeostasis studies show both WT and mutant genotypes exhibited induced *RBOHD*, *RBOHF*, and *CAT1* under salt, but only the mutant upregulated *GSTF6*, implying that VAMP714 normally represses this scavenger under salt stress. Histochemical staining confirmed no change in superoxide accumulation, while H_2O_2 levels rose markedly in the mutant under salinity. Correspondingly, CAT was reduced in the mutant compared to WT but increased upon salt treatment, indicating enhanced scavenging capacity despite elevated H_2O_2. A potential basis for the observation that the mutant has a similar salt sensitivity to WT is that, although loss of *VAMP714* leads to increased H_2O_2 accumulation, it also accelerates ROS scavenging and CAT activity.

Assessing the SOS pathway, it was found that salt-induced downregulation of *HKT1* and upregulation of *NHX1* were VAMP714-independent, whereas induction of *SOS1*, *SOS2*, *HIS1-3*, *WRKY1*, and their associated regulators (*PLATZ2*, *UBC1*, *UBC2*) is associated with VAMP714. Ion-content assays demonstrated that loss of VAMP714 destabilizes K^+ and Ca^{2+} under salt stress and abrogates the effects of blocking auxin biosynthesis on ion balance. By contrast, supplemental Ca^{2+} partially rescued root growth independently of VAMP714. Together, these findings position VAMP714 at the nexus of vesicle fusion, ROS regulation, ion-homeostasis signalling, and auxin-mediated adaptation during early salt stress.

Chapter 6: Discussion

In this study, VAMP714 was identified as a central mediator linking salt-stress signalling to auxin reprogramming and ROS homeostasis in *Arabidopsis thaliana*. The multidisciplinary approach used combines bioinformatics analyses, genetic perturbations, reporter assays, transcript profiling, and physiological measurements to unravel how VAMP714 coordinates vesicle trafficking, hormone distribution, and ionic homeostasis under saline conditions. Below is discussed the findings in seven thematic sections: (1) Genetic distinctiveness and salt-responsive regulation of VAMP714, (2) Salt stress reprograms auxin distribution via disruption of vesicle trafficking, (3) Functional consequences of manipulating VAMP714 expression, (4) Partnership between VAMP714 and CTL1 in vesicle-mediated auxin homeostasis, (5,6) VAMP714-driven ROS/SOS-pathway responses during early salt adaptation, and (7) Integration of auxin, vesicle trafficking, and ionic signalling in VAMP714.

6.1 Genetic distinctiveness and salt-responsive regulation of VAMP714

Bioinformatic and promoter analyses indicate that VAMP714 is a structurally divergent member of the VAMP7 subfamily, distinguished by its unique transcriptional regulation under saline conditions. This divergence is consistent with the evolutionary trend of SNARE proteins acquiring functional specialisation (Jahn and Scheller, 2006). Notably, the rapid and transient induction of VAMP714 resembles the dynamic expression profiles of auxin-related and early stress genes (Geng et al., 2013), positioning VAMP714 as an early sensor–effector node in salt adaptation.

The salt inducibility of VAMP714 adds a new dimension to the understanding of VAMP71 family members, since earlier studies largely focused on

VAMP711/712 (Leshem et al., 2006). These findings extend previous insights by showing that VAMP714 transcription integrates both stress-responsive transcription factors, such as NF-YB2 and RD26, and auxin-related modules. This suggests that VAMP714 functions as a mechanistic bridge between stress signalling and developmental regulation of the root meristem, a concept not previously recognised.

6.2 Salt stress reprograms auxin distribution via disruption of vesicle trafficking

The disruption of PIN polarity and auxin gradients by salt stress confirms prior reports (Fu et al., 2019; Liu et al., 2015) but also demonstrates that VAMP714 directly participates in this process. PIN proteins undergo continual endocytic and exocytic cycling between the plasma membrane and endosomal compartments (Goldsmith, 1977; Chen et al., 1998). This trafficking is crucial for establishing the directional auxin gradients that underpin root meristem function and organ formation (Friml et al., 2003a, 2003b). SNAREs facilitate vesicle–membrane fusion events (Jahn et al., 2024; Koike and Jahn, 2022). The loss of VAMP714 localisation at endomembrane puncta under salinity implies that VAMP714 functions as a checkpoint in vesicle fusion, ensuring directional auxin flow.

This direct sensing of salt cues by VAMP714 suggests that it may act as a regulator of PIN relocalization events, serving as a vesicle-fusion checkpoint under stress. Auxin could regulate its own transport by regulating the expression of PINs (Benjamins et al., 2005), our results reinforce the view that the cellular machinery responsible for vesicle fusion, including SNARE complexes, must be intact to maintain proper auxin distribution under stress (Marhava, 2022). This observation is significant because it reframes salt-induced auxin mislocalisation not simply as a passive consequence of stress,

but as an actively mediated process dependent on trafficking machinery. The inability of exogenous auxin to rescue VAMP714 mislocalisation indicates that vesicle fusion machinery, rather than auxin signalling alone, is the limiting factor during early stress. This provides a new mechanistic insight: auxin redistribution under salt stress requires intact SNARE complexes, with VAMP714 acting as a vesicle-fusion regulator responsive to environmental cues.

6.3 Functional consequences of manipulating *VAMP714* expression

Manipulation of *VAMP714* expression demonstrates its physiological relevance. Mild overexpression under the native promoter enhances primary root elongation under salt stress, whereas ubiquitous overexpression via the CaMV35S promoter proves ineffective, underscoring the necessity for fine-tuned expression. These findings are consistent with broader principles of SNARE biology, where correct spatiotemporal regulation is critical for function (Surpin et al., 2003; Zhang et al., 2011).

The absence of strong phenotypes in knockout mutants suggests functional redundancy, consistent with the overlapping roles reported for other SNAREs (Zhang et al., 2011). Nevertheless, the enhanced tolerance conferred by native overexpression highlights that VAMP714 is not dispensable but operates within a buffering network. The balance between redundancy and specific contribution illustrates how plants maintain robustness in essential trafficking pathways while still allowing individual SNAREs to provide unique adaptive advantages. Salt exposure in *Arabidopsis thaliana* is known to impair primary root extension and reduce overall root length, effects that become more pronounced at higher NaCl concentrations (Lombardi et al., 2024; Smolko et al., 2021). Lateral root development is also frequently suppressed under salinity (Zolla et al., 2010), although a transient increase in lateral root initiation has been reported as a

compensatory strategy (Julkowska et al., 2014; Zolla et al., 2010). The degree of lateral root response varies with genetic background, treatment regime, and seedling developmental stage, with some genotypes or conditions exhibiting strong inhibition of lateral root formation (Smolko et al., 2021). In this context, *VAMP714* mild overexpression enhances salt tolerance by favouring primary root growth over lateral root proliferation, a pattern that mirrors its expression profile: high in vascular tissues, the meristem, and the elongation zone, but low in the quiescent centre (Gu et al., 2021).

Constitutive overexpression of *VAMP714* under the CaMV35S promoter does not enhance salt tolerance, indicating that simply increasing transcript levels does not yield proportionate stress resilience. A similar lack of benefit has been observed for 35S-driven VAMP711 overexpression (Leshem et al., 2006). Tang et al. (2022) likewise demonstrated that only precise expression of VAMP714 improves salt-stress performance during seed germination. Native regulation likely ensures the appropriate spatial, temporal, and quantitative control of VAMP SNARE activity, whereas ubiquitous overexpression may perturb the finely tuned vesicle-trafficking network and negate adaptive advantages. Furthermore, *VAMP714* loss-of-function mutants do not display heightened salt sensitivity relative to WT, which may reflect redundancy within the SNARE family. For example, AtVAMP721 and VAMP722 can substitute for each other's roles (Zhang et al., 2011), and the related VTI11 and VTI12 isoforms share overlapping functions in vesicle fusion (Surpin et al., 2003). Leshem et al. (2006) further reported that, despite the absence of transcriptional compensation among VAMP71 family members, deletion of VAMP714 reduces VAMP713 expression. It is therefore plausible that other SNAREs compensate for the absence of VAMP714, thereby masking a potential phenotype. Notably, Leshem et al. (2006) described enhanced tolerance in a VAMP714 T-DNA mutant, a discrepancy that may arise from differences in seedling age or NaCl concentration.

The ability of exogenous IAA to enhance salt tolerance in *proVAMP714::VAMP714:mCherry* lines, coupled with the loss of this advantage upon NPA treatment, underscores that VAMP714-mediated tolerance depends on the maintenance of polar auxin transport rather than auxin abundance per se. This finding aligns with the established view that directional auxin flow, sustained by PIN cycling, is the critical determinant of root developmental plasticity under stress (Fu et al., 2019; Zhao et al., 2011). Within this framework, precise VAMP714 expression appears to safeguard the fidelity of vesicle trafficking required for PIN localisation, thereby enabling auxin redistribution to function as an adaptive signal. Thus, VAMP714 acts not as a generic enhancer of auxin responses but as a regulator that secures the machinery of polar transport, providing a mechanistic explanation for why only native promoter-driven overexpression confers tolerance.

6.4 Partnership between VAMP714 and CTL1 in vesicle-mediated auxin homeostasis

CTL1 orchestrates membrane lipid biosynthesis and regulates vesicle dynamics (Dettmer et al., 2014; Gao et al., 2017; Nakamura et al., 2010; Wang et al., 2017). FRET-FLIM and BiFC studies localize a direct CTL1–VAMP714 interaction to trans-Golgi/early endosome "cycling hubs" (Agneessens, 2024). Functional assays further delineate that CTL1 is requisite for VAMP714 and PIN1 polarity but dispensable for PIN2 trafficking, suggesting cargo-specific SNARE recruitment (Agneessens, 2024). The interaction between VAMP714 and CTL1 reveals that vesicle trafficking and lipid homeostasis are tightly coupled during salt stress. Evidence indicates that VAMP714 requires CTL1-dependent lipid environments for selective cargo trafficking, particularly of PIN1, whereas PIN2 trafficking appears less dependent. This cargo-specific selectivity adds nuance to the canonical view of SNARE–lipid interactions (Dettmer et al., 2014).

The reciprocal regulation between VAMP714 and CTL1 further indicates the existence of a feedback loop that adjusts membrane trafficking capacity to environmental stress. From a mechanistic standpoint, this points to a coordinated module in which lipid metabolism and SNARE-mediated fusion co-regulate auxin transporter distribution. This insight extends earlier models of trafficking specificity by showing that lipid–SNARE partnerships can be stress-inducible and context-dependent.

A schematic model (Fig. 6.1) summarizes these interactions, contrasting root-specific and whole-seedling feedback between CTL1 and VAMP714, and highlighting the effects of choline and salt stress on this regulatory module.
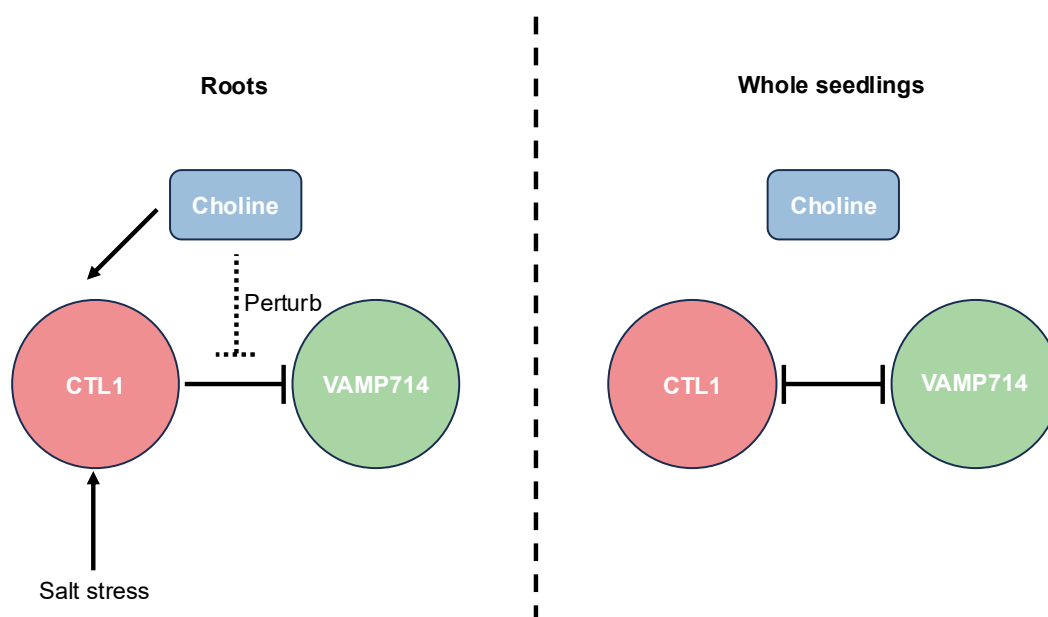
Fig. 6.1 Models of CTL1-VAMP714 interaction in roots and whole seedlings.

The left panel illustrates the root-specific model, in which CTL1 exerts a unidirectional negative regulation on *VAMP714*. This inhibitory remains effective in the presence of exogenous choline, although the response is perturbed. In addition, *CTL1* expression is responsive to both exogenous choline and salt stress. The right panel depicts the whole-seedling model, where CTL1 and VAMP714 mutually repress each other. In this context, the interaction is insensitive to exogenous choline, and CTL1 does not exhibit a detectable response to choline treatment.

6.5 VAMP714-associated ROS-pathway responses during early salt adaptation

ROS are established signals in abiotic stress (Apel and Hirt, 2004), yet the role of vesicle trafficking in their compartmentalisation has been underexplored. Evidence from this study indicates that VAMP714 deficiency leads to aberrant H_2O_2 accumulation and compensatory upregulation of detoxification pathways, aligning with observations that endomembrane systems govern ROS localisation (Leshem et al., 2006; Tang et al., 2022). These findings suggest that VAMP714 participates in shaping the spatial dynamics of ROS signalling, not merely in auxin transport. The induction of GSTF6 and catalase activity in mutants implies that trafficking defects force the plant to rely more heavily on enzymatic detoxification, underscoring that SNARE-mediated vesicle fusion is integral to redox regulation.

Beyond these general detoxification processes, transcriptome analysis identified CYP96A12 as a particularly intriguing candidate linking VAMP714 activity to redox metabolism. In WT seedlings, CYP96A12 transcripts were consistently repressed by salt stress, whereas in the *vamp714* mutant they remained unaltered. This genotype-specific divergence suggests that VAMP714 is required for salt-induced repression of CYP96A12, and thus may influence ROS balance not only through vesicular transport of H_2O_2 but also by modulating transcriptional control of metabolic enzymes. Given that CYP96A12 encodes a cytochrome P450 with roles in redox and lipid-associated metabolism (http://www.arabidopsis.org/), this connection raises the possibility that VAMP714 regulates electron-transfer and oxidative pathways in parallel with ROS detoxification. Such a model is consistent with prior suggestions that trafficking machinery can coordinate ROS distribution with metabolic adjustments (Leshem et al., 2006; Tang et al., 2022). Incorporating CYP96A12 into this framework therefore adds nuance to the conclusion: VAMP714 acts

not just as a regulator of ROS accumulation, but as an integrator of ROS-associated metabolism and detoxification during early salt adaptation.

6.6 VAMP714-associated SOS-pathway responses during early salt adaptation

While canonical SOS signalling is generally considered independent of endomembrane trafficking (Apse et al., 2003), the results presented here indicate that VAMP714 modulates the transcriptional activation of key SOS components. Interestingly, most representative genes of the SOS signalling pathway examined in this study show transcriptional trends in the WT under salt stress that are consistent with their established functions (summarized in Ali et al., 2023). However, some of them appeared to be dynamic and complex. For example, *HIS1-3* transcript level has been reported to decrease (Wu et al., 2022) or remain stable (Ascenzi and Gantt, 1997) under salt stress. These discrepancies may result from differences in detection methods, experimental conditions, reference genes, and tissue specificity, highlighting the rapid and complex nature of SOS signalling. Meanwhile, this complexity limits further mechanistic exploration of the SOS pathway in this study. Collectively, these insights position VAMP714 at the interface between vesicle trafficking and ionic signalling, offering a new perspective on how plants fine-tune salt efflux capacity.

6.7 Integration of auxin, vesicle trafficking, and ionic signalling in VAMP714

By integrating auxin transport, ROS regulation, and SOS signalling, VAMP714 emerges as a hub for early salt adaptation. Its interactions with trafficking partners such as SNAP29 and MEMB11 (key regulators of vesicle targeting and fusion) underline its centrality in stress-responsive complexes.

Ionomic analyses indicate that VAMP714 does not directly control bulk Na^+/K^+ influx but instead modulates the regulatory pathways that determine whether these fluxes can be tolerated. Auxin redistribution and YUCCA-dependent IAA biosynthesis appear particularly important for maintaining ionic balance in a VAMP714-dependent manner. These findings extend the current paradigm of salt tolerance by demonstrating that vesicle trafficking proteins can serve as integrators of hormonal and ionic signals, rather than acting solely as facilitators of membrane fusion.

6.8 Future work

Due to limitations in the methods and analyses used in this study, several limitations should be acknowledged. First, although both previous studies (Gu et al., 2021) and this study indicate that VAMP714 is highly likely to co-localise with PIN1 and PIN2, a very small possibility remains that its expression may not fully reflect its native localisation. Second, under non-salt conditions, baseline transcriptional levels of certain genes were not fully consistent between the WT and *vamp714* mutant, such as *CML37*, *PMSR1*, *GSTF6*, *SOS1*, *SOS2*, *HIS1-3*, *PLATZ2* and *AT3G06590*. While these differences do not affect the main conclusions of this study, baseline variation in SOS signalling–related genes, including *HIS1-3* and *PLATZ2*, limits the strength of detailed mechanistic interpretation based solely on transcript-level data. Third, this study focuses on the transcriptional level and lacks cross-validation at the protein level.

Building on the insights presented in this study, several avenues of future research emerge that could further refine the understanding of VAMP714 and its role in salt stress adaptation. First, while the current findings establish VAMP714 as a master regulator linking auxin distribution, ROS

compartmentalisation, and SOS activation, the molecular details of its trafficking partners remain only partially resolved. Systematic interactome analyses, for example using proximity labelling or co-immunoprecipitation combined with mass spectrometry, would allow identification of additional SNAREs, tethering factors, and lipid-modifying enzymes that cooperate with VAMP714. Such work would clarify whether the stress-specific complexes described here are unique to VAMP714 or represent a broader principle within the VAMP7 clade.

Second, the reciprocal regulation observed between VAMP714 and CTL1 highlights the importance of lipid–SNARE coordination under saline conditions. Future studies could employ lipidomics combined with live-cell imaging to dissect how changes in membrane composition influence vesicle selectivity for PIN1 versus PIN2. Addressing this question will not only advance knowledge of cargo-specific trafficking but also provide mechanistic depth to the emerging concept of stress-inducible SNARE–lipid partnerships. The use of chemical genetics, such as targeted disruption of choline or sterol metabolism, may further reveal how metabolic status tunes the CTL1–VAMP714 module in roots compared with whole seedlings.

Third, the role of VAMP714 in ROS regulation warrants detailed exploration. The identification of CYP96A12 as a putative redox-linked target suggests that VAMP714 may control transcriptional networks as well as vesicular detoxification. Future work could test whether VAMP714 influences ROS-associated transcription factors or acts upstream of NADPH oxidase activity. Advanced imaging of H_2O_2 fluxes in mutant and complemented lines would help resolve how trafficking machinery determines the spatial patterning of redox signals.

Fourth, the finding that VAMP714 is associated with the induction of SOS

signalling opens a new perspective on ionic homeostasis. Elucidating whether this control is exerted through auxin redistribution or through direct modulation of Ca^{2+}-dependent signalling remains a pressing question. Combining auxin transport inhibitors with SOS pathway reporters could reveal causal relationships, while phosphoproteomic profiling may uncover whether VAMP714 intersects with calcium-dependent protein kinases.

Finally, the translational potential of manipulating VAMP714 deserves systematic evaluation. Although constitutive overexpression proved ineffective, carefully tuned promoter-driven strategies demonstrated enhanced salt tolerance. Future work should test whether similar outcomes can be achieved in crop species, for example by tissue-specific promoters targeting vascular tissues or root meristems. Genome-editing approaches could also be employed to fine-tune regulatory regions of endogenous VAMP714 orthologues. Such applied research would not only validate the ecological relevance of the findings but also provide practical strategies for improving crop resilience in saline soils. In summary, future research should extend from mechanistic dissection of trafficking complexes and lipid interactions to integrative analyses of ROS and ionic pathways, ultimately progressing toward translational applications in agriculture. By pursuing these directions, the field will be able to determine whether VAMP714 represents a unique integrative hub or part of a more general strategy by which plants coordinate vesicle trafficking with hormonal, redox, and ionic responses to environmental stress.

6.9 Conclusion

Together, these findings establish VAMP714 as a master regulator that coordinates developmental and physiological responses to salt stress. Unlike other SNAREs, VAMP714 integrates auxin distribution, ROS compartmentalisation, and SOS activation into a coherent adaptive programme.

This highlights a new mechanistic principle: vesicle trafficking does not merely support signalling but actively shapes how plants perceive and respond to environmental challenges.

By linking hormonal, redox, and ionic pathways through a single trafficking protein, VAMP714 provides a versatile platform for early stress adaptation. This study expands the conceptual framework of SNARE biology and suggests that similar integrative modules may operate in other stress contexts. Future work could investigate how VAMP714 interacts with additional trafficking components, and whether manipulating its regulation offers a viable strategy for engineering salt-tolerant crops.

To illustrate this integrative role, a schematic model (Fig. 6.2) has been prepared. The diagram summarizes how VAMP714 links auxin transport, ROS dynamics, and SOS signalling into a unified stress-responsive network, and shows how these processes converge to facilitate salt adaptation.
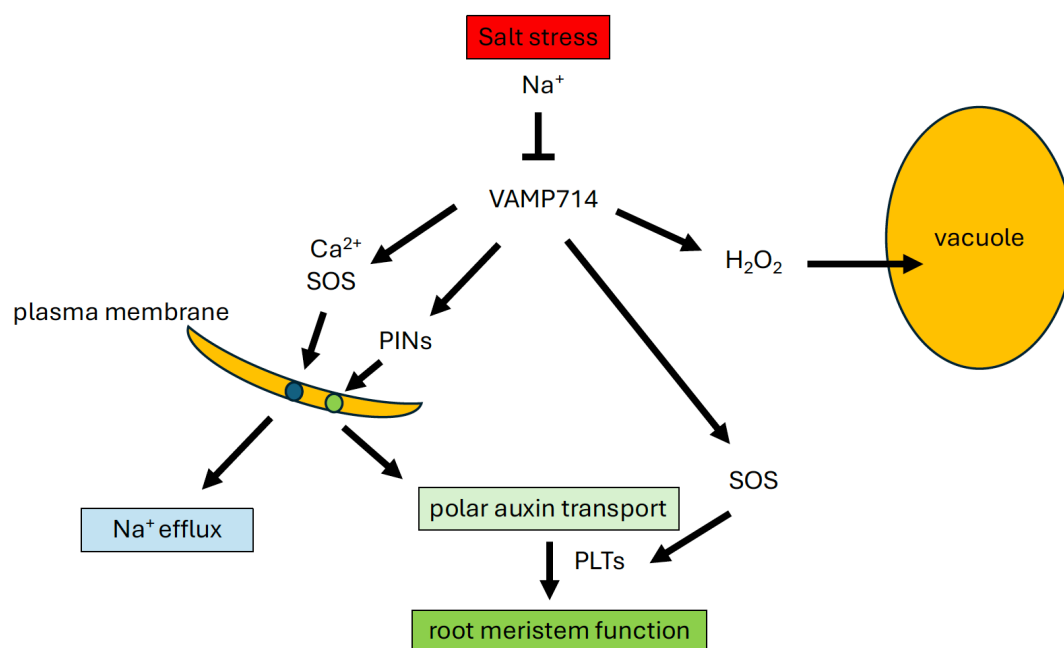
Fig. 6.2 Network of VAMP714-dependent interactions during salt stress.

VAMP714 is an integrator of polar auxin transport, ROS signalling and ion homeostasis via the

SOS pathway. Under salt stress, VAMP714 protein localisation and function is reduced, associated with 1) defective PIN protein localisation and auxin responses, 2) reduced SOS pathway activity and 3) increased cytosolic ROS accumulation. These changes lead to defective root growth.

Appendices

Appendix I Primers used in this study

Primers for homozygosis examination	
LP_SALK_020516	GTCACTCCAGATGCAGAGCTC
RP_SALK_020516	CTTCAGGAAGCAATCTAAGCG
LB_SALK	ATTTTGCCGATTTCGGAAC
LP_GABI_844B05	CTGTTGTAGCGAGAGGTACCG
RP_GABI_844B05	AAGCATGTCAACAAGACCCTG
LB_GABI	ATATTGACCATCATACTCATTGC
Primers for *vamp714DN* mutant construction	
Dom-Neg FOR	GGGGACAAGTTTGTACAAAAAAGCAGGCTTCGTTGTAGCGAGAGGTACCGTG
Dom-Neg REV	GGGGACCACTTTGTACAAGAAAGCTGGGTCCTATTAGCATTTTTCATCCAAAG
Primers for quantitative RT-PCR	
ACTIN 2 (AT3G18780) F	GGATCGGTGGTTCCATTCTTGC
ACTIN 2 (AT3G18780) R	AGAGTTTGTCACACACAAGTGCA
AT1G07400 F	AACAGCATCTTCGACCCGTT
AT1G07400 R	CCACACGTGCGTTCGTTATC
AT3G06590 F	AGCAACAGATCGAGAAAACGGAGAG
AT3G06590 R	CGGTACGGATTGTTTACCGCAAC
AUX1 (AT2G38120) F	GACGCACTTCTCGACCACTC
AUX1 (AT2G38120) R	CCCAATCACTTTCTCCCACA

CAT1 (AT1G20630) F	GCCCCTAAATGTGCTCACC
CAT1 (AT1G20630) R	AAGCACTTCTCACGATTTCCA
CBL10 (AT4G33000) F	TTAGTAAGGATGAATGGAATGTC
CBL10 (AT4G33000) R	AGTCTTCAACCTCAGTGTT
CML37 (AT5G42380) F	GGTGGAGGAAGTGGTGAAGA
CML37 (AT5G42380) R	GTAAACTCGCCGCCGTAATA
EDL3 (AT3G63060) F	AGAGTTCTTCGTGTGCGTGAAC
EDL3 (AT3G63060) R	CCTCCGATGAAAGCGGAAT
GDPD2 (AT5G41080) F	TGCGGGAAACGAGATTCACA
GDPD2 (AT5G41080) R	TAATGGCTGCTGGGTTCCTG
GSTF6 (AT1G02930) F	TCATCCTTCGCAACCCC
GSTF6 (AT1G02930) R	GCTATGATCGCCATGTCCTT
GSTF7 (AT1G02920) F	ACCAAAAGGGTTGCGGAAGA
GSTF7 (AT1G02920) R	AGTTTTCGGTCACCCAGCTT
HIS1-3 (AT2G18050) F	AACCACCACTCATCCTCCATAC
HIS1-3 (AT2G18050) R	GCTGTAGAGAAAGTGTTTACGGAC
HKT1 (AT4G10310) F	GAAAGGCAAAATCTACAACGTG
HKT1 (AT4G10310) R	CCTGCAAACCCATAACTCG
IAA1 (AT4G14560) F	CGGTTAGATCTCACTGGAGGCCAT
IAA1 (AT4G14560) R	ACTTGCTCCTCCTCCTGCAAAAC
IAA2 (AT3G23030) F	AGGAAGAGTCTAGAGCAGGAGC
IAA2 (AT3G23030) R	ACTGGATGTTGGTTGGTGATG
IRT1 (AT4G19690) F	AAGCTTTGATCACGGTTGG
IRT1 (AT4G19690) R	TTAGGTCCCATGAACTCCG

MPK4 (AT4G01370) F	CTCCTCTTCGTCCTATCGGT
MPK4 (AT4G01370) R	CCTTTACAGCAATCACATTTTCA
MSD1 (AT3G10920) F	GAACCTTGCTCCTTCCAGTG
MSD1 (AT3G10920) R	TCTTCAGTTCTTTGTCTAGTCCG
MYB42 (AT4G12350) F	ATGGAAATCGATCCTTCGAC
MYB42 (AT4G12350) R	TGTCCCATCGATCTCTACGA
NHX1 (AT5G27150) F	GTGCTGTATCTATGGCTCTTGC
NHX1 (AT5G27150) R	GGTAGCTTATGAGTGGTTTGGTC
NIT2 (AT3G44300) F	CCGTTTAATGGCGTTGCCTC
NIT2 (AT3G44300) R	TGCTTGCAGCCTCCACAATA
PIN1 (AT1G73590) F	CTTACGCCATGAACCTCCGT
PIN1 (AT1G73590) R	GGTCGCCGGAGAAATTACCA
PIN2 (AT5G57090) F	TCAACAAATCTCACGGCGGA
PIN2 (AT5G57090) R	CTTGGAGCTTTGCTTGCGTT
PLATZ2 (AT1G76590) F	CGTCTGATGAGTGGTCTT
PLATZ2 (AT1G76590) R	CCCTTCCGTCTACTTGAA
PLT1 (AT3G20840) F	TCGCCGGAAACAAAGAC
PLT1 (AT3G20840) R	CCGATGGGAAGAGTGCTAC
PLT2 (AT1G51190) F	ACATTCAGCACGGAGGAAG
PLT2 (AT1G51190) R	GTGTGTTGCTCTCCAGGATG
PMSR1 (AT5G61640) F	GCACCAGCAACAAGTTGACA
PMSR1 (AT5G61640) R	CGTTGCAGCCTTTTTCCGTT
RBOHD (AT5G47910) F	GTACACCCACCATTTGTTCATC
RBOHD (AT5G47910) R	AAAGCACGGAGCAGCCT

RBOHF (AT1G64060) F	GACACGCCAAGACGAAAGA
RBOHF (AT1G64060) R	ACACCCCGTTGGTCAAGTT
RSA1 (AT2G03150) F	GAAGTTCAGTGAGTGGTGGCGCAGAAGGAG
RSA1 (AT2G03150) R	GGTGAATCAGGTAAAGTAGGGACATATC
SCR (AT3G54220) F	TCTTCAGGCTACAGGGAAACGTCT
SCR (AT3G54220) R	GTGTGTGCATCAGAGCCAGTGACA
SHR (AT4G37650) F	GGCAAACGGAGCAATCTTGG
SHR (AT4G37650) R	AGGCGTGTCGTCTGATCTTG
SOS1 (AT2G01980) F	CTGGGAAGCCATATCTGTGC
SOS1 (AT2G01980) R	GGACGCAAGAGTTTGAGAAGA
SOS2 (AT5G35410) F	CAGTTAGCTGTTGTGATAGAG
SOS2 (AT5G35410) R	CTTCTGTTGCCCTCCATA
SOS3 (AT5G24270) F	TCTTCACGAATCCGAACT
SOS3 (AT5G24270) R	TTCTTGATGAGCGATGGA
UBC1 (AT1G14400) F	GTGCTCCACAGGACAACAAC
UBC1 (AT1G14400) R	AGGATGAAACATCCGTGACA
UBC2 (AT2G02760) F	CCAGCGAGGAAGAGATTGAT
UBC2 (AT2G02760) R	TGAAAGTACCTCCATCCCAAG
UBQ5 (AT3G62250) F	CGTGGTGGTGCTAAGAAGAGG
UBQ5 (AT3G62250) R	GAAAGTCCCAGCTCCACAGGT
VAMP711 (AT4G32150) F	GGTGGAGAAACTGCAAGCTC
VAMP711 (AT4G32150) R	ACACACTTCGCAAAGCAATG
VAMP712 (AT2G25340) F	AACGTACTGATGGCCTCACC

VAMP712 (AT2G25340) R	ATGTTCGCGGTTTTATCGAC
VAMP713 (AT5G11150) F	TTGTGAAAACATATGGCCGA
VAMP713 (AT5G11150) R	CTAGCAACTCCAAACGCTCC
VAMP714 (AT5G22360) F	GAGATTCGATCGGTCATGGT
VAMP714 (AT5G22360) R	GGTAAAGTGATTCCTCCG
VAMP714 DN F	TTGTAGCGAGAGGTACCGTG
VAMP714 DN R	GGAACCCTCCTTCCAAAGGT
WRKY1 (AT2G04880) F	AGGCAGCCCATATCCAAGGAGC
WRKY1 (AT2G04880) R	TCGTGGTCGTGTTTTCCCTCGT
ZF14 (AT1G58340) F	GCCAAGTTTTCTGGAGGGCT
ZF14 (AT1G58340) R	TCCGGCTAACTCAAGCTCAC

Appendix II Related sequences

AtVAMP714/AT5G22360 full length Genomic DNA

taaaccgatgcatcagggtttaaaatgtaacaaaataatattttaggtgacaattaaaaacgtaacaataaa
acaaggggttatattcgaaacgtttgcacctaaccttataacttcgcatttttatactctgttctgatcgcagcaa
agccgacgttgaactttctcgccgccggagcgcgtgatctccactctctgtcatcgaatcactctaattgaaga
ttctccgATGGCGATTGTCTATGCTGTTGTAGCGAGAGGTACCGTGGTATTA
GCTGAATTCAGCGCCGTTACGGGAAACACAGGCGCCGTGGTGCGACGG
ATCCTCGAGAAGCTTTCACCGGAAATCTCCGATGAAAGACTTTGTTTCTC
TCAAGATCGTTATATCTTCCATATTCTTAGATCTGATGGTCTTACCTTTCT
CTGTATGGCCAATGATACCTTTGGAAgtaagtattttttcactttctccgaatcgtaatctctctta
agaagatttagtctttgtaattgattctgagtttatgttttgatgtgttggtgattggattttcagGGAGGGTTC
CATTTTCGTATTTGGAAGAGATTCATATGAGATTCATGAAAAACTATGGCA
AAGTGGCTCATAATGCTCCAGCTTATGCAATGAATGATGAATTCTCAAGG
GTTTTGCATCAGCAGATGGAGTTCTTCTCTAGTAATCCTAGTGTTGATAC
TCTCAATCGTGTTAGAGGAGAAGTCAGTGAGgtataattgtttcttcgtatgatctctagat
attactcagctatatccattgaaaaggttgaattttatgagttattacgccttcttggctcacacaggcttctttaa
atctgtcttgggtgaaagatgaagtttgttatctcattgttgtgttatcgtgtttacagATTCGATCGGTCA
TGGTAGA(GABI_844b05_T-DNA)GAACATTGAGAAGATAATGGAAAGAGG
TGATAGGATTGAGCTTCTTGTTGATAAAACAGCAACAATGCAAGATAGCT
CGTTTCACTTCAGGAAGCAATCTAAGCGCCTTCGCCGAGCTCTTTGGAT
GAAAAATGCTAAGCTCCTgtaaggatctctctcacttctagattctcttcattccttttctttgctaacta
agagatacgctcttctacattctaggtgtttcaactcgcctttgcagcatagtttattgatatgtttcttaaactaga
gatacagtagttctaagattcaacattattttcgattttgggaaattctcctcgacaaaatatctaatttttggctga
taggaactacactgccttgattccacctctgcttaaagaaatttcattattgttttgttttgatgcttgagttccagat
cacttttattaatcaacaaaactgcttttcttgtttgtgttcggcagGGTCTTGTTGACATGCTTGAT
AGTTTTCTTGCTGTACATAATAATCGCATCTTTCTGCGGA(SALK_020516_
T-DNA)GGAATCACTTTACCATCATGCAGATCTTAAaatctggcggccttatctaaggt
atactgaaacggaccactgttttgtaaatcaactcagtcgcatcatttcgatttgaagccttggttttgtcatgaa
aatgactgtgagtttgaagttacatgtcatggtcctccttgcttatgtaactcttgtaaatgtcaaaatcaaaatg

atacagaggttcattgaactcttgccttgtcttttagatttagtcacgtgagtgagtttgttctctgtatttccaaaact
ttatccgctgtgtctttataattttttgcatttgcaatgtacatcacatattcgttatttttgttgttaaaattacttcagttttc
atctttgtttaataacatttctgattcacaaata

AtVAMP714/AT5G22360 full length cDNA (DN)

TAAACCGATGCATCAGGGTTTAAAATGTAACAAAATAATATTTTAGGTGACA
ATTAAAAACGTAACAATAAAACAAGGGGTTATATTCGAAACGTTTGCACCTA
ACCTTATAACTTCGCATTTTTATACTCTGTTCTGATCGCAGCAAAGCCGAC
GTTGAACTTTCTCGCCGCCGGAGCGCGTGATCTCCACTCTCTGTCATCG
AATCACTCTAATTGAAGATTCTCCGATGGCGATTGTCTATGCTGTTGTAGC
GAGAGGTACCGTGGTATTAGCTGAATTCAGCGCCGTTACGGGAAACACA
GGCGCCGTGGTGCGACGGATCCTCGAGAAGCTTTCACCGGAAATCTCC
GATGAAAGACTTTGTTTCTCTCAAGATCGTTATATCTTCCATATTCTTAGAT
CTGATGGTCTTACCTTTCTCTGTATGGCCAATGATACCTTTGGAAGGAGG
GTTCCATTTTCGTATTTGGAAGAGATTCATATGAGATTCATGAAAAACTATG
GCAAAGTGGCTCATAATGCTCCAGCTTATGCAATGAATGATGAATTCTCAA
GGGTTTTGCATCAGCAGATGGAGTTCTTCTCTAGTAATCCTAGTGTTGATA
CTCTCAATCGTGTTAGAGGAGAAGTCAGTGAGATTCGATCGGTCATGGTA
GAGAACATTGAGAAGATAATGGAAAGAGGTGATAGGATTGAGCTTCTTGT
TGATAAAACAGCAACAATGCAAGATAGCTCGTTTCACTTCAGGAAGCAATC
TAAGCGCCTTCGCCGAGCTCTTTGGATGAAAAATGCTAAGCTCCTGGTCT
TGTTGACATGCTTGATAGTTTTCTTGCTGTACATAATAATCGCATCTTTCTG
CGGAGGAATCACTTTACCATCATGCAGATCTTAAAATCTGGCGGCCTTATC
TAAGGTATACTGAAACGGACCACTGTTTTTGTAAATCAACTCAGTCGCATC
ATTTCGATTTGAAGCCTTGGTTTTGTCATGAAAATGACTGTGAGTTTGAAG
TTACATGTCATGGTCCTCCTTGCTTATGTAACTCTTGTAAATGTCAAAATCA
AAATGATACAGAGGTTCATTGAACTCTTGCCTTGTCTTTTAGATTTAGTCAC
GTGAGTGAGTTTGTTCTCTGTATTTCCAAAACTTTATCCGCTGTGTCTTTAT
AATTTTTGCATTTGCAATGTACATCACATATTCGTTATTTTTGTTGTTAAAATT
ACTTCAGTTTTCATCTTTGTTTAATAACATTTCTGATTCACAAATA

T for Longin Domain

T for SNARE Domain

T for Trans-membrane Domain

Appendix III Related analysis software and thresholds for RNA-seq

Analysis	Software	Version	Parameter	Remarks
Mapping	hisat2	2.0.5	Default	Mapping to a reference
Assembly	Stringtie	1.3.3b	Default	
Quantification	featureCounts	1.5.0-p3	Default	
Differential Analysis	DESeq2	1.20.0	|log2(FoldChange)| >= 1 & padj <= 0.05	For sample with bio-replicate
Enrichment Analysis	clusterProfiler	3.8.1	padj < 0.05	For GO, KEGG enrichment analysis

Appendix IV Differential gene volcano map
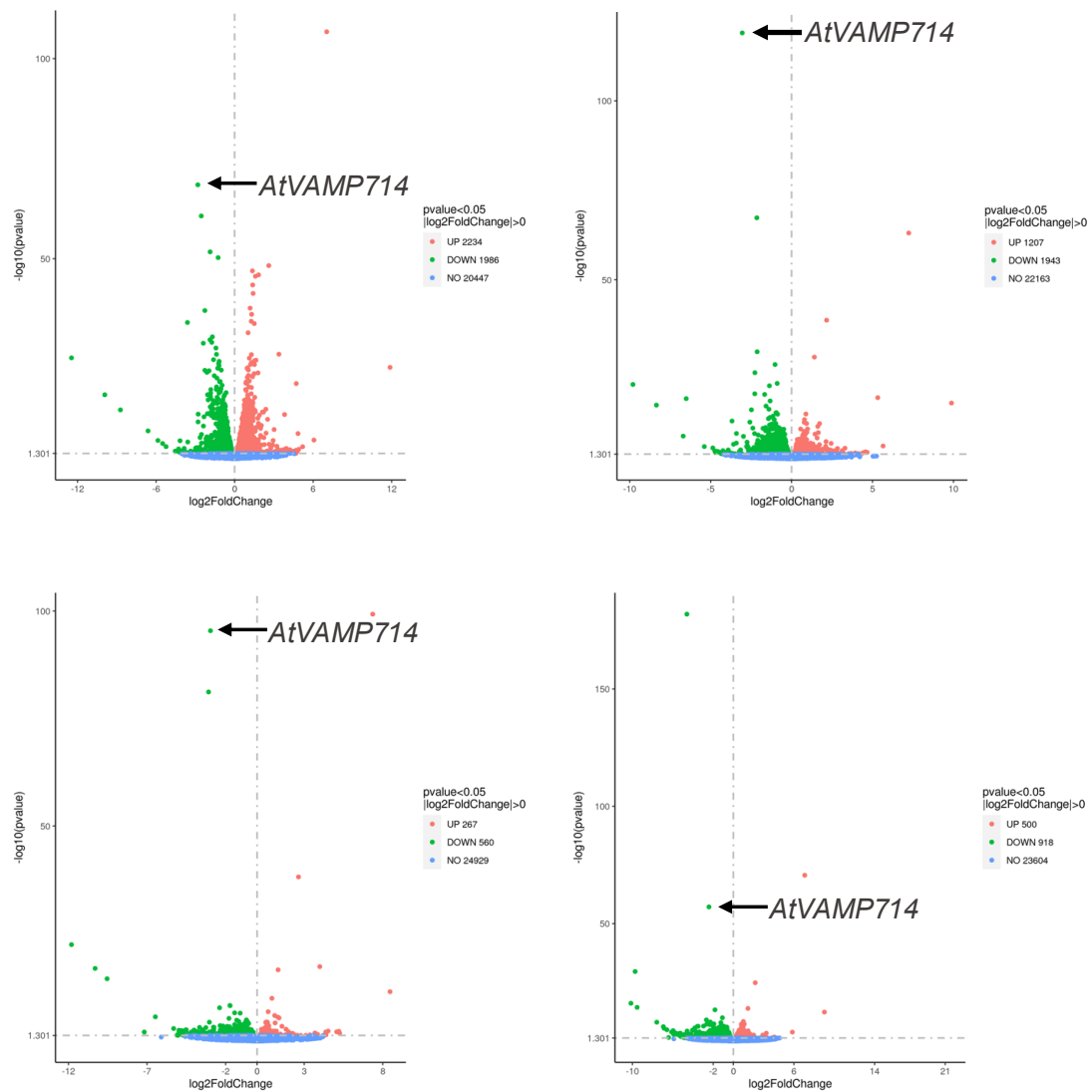
GABI = *vamp714* mutant, Mock = wild type (Col-0). From left to right, they are the results of GABI 0 h vs *Col-0* (Mock) 0 h, GABI 3 h vs Mock 3 h, GABI 9 h vs Mock 9 h, and GABI 24 h vs Mock 24 h. The abscissa in the figure is log2FoldChange, and the ordinate is -log10padj or -log10pvalue, the dashed line indicates the threshold line for differential gene screening criteria.

Appendix V List of differential genes

Gene_id	Gene_name	Test	Gene function
832297	**VAMP714**	Y	AT5G22360, protein localization involved in auxin polar transport, vesicle-mediated transport, vesicle-mediated transport to the plasma membrane
843750	**SOT16**		AT1G74100, sulfation
822807	**QQS**		AT3G30720
3771313	**AT5G35935**		AT5G35935, pseudogene
827713	**IRT1**	Y	AT4G19690, zinc ion transmembrane transport
28718910	**AT3G06355**		AT3G06355, lncRNA
829324	**CYP82C4**		AT4G31940, response to alkaline pH
836289	**AT5G61670**		AT5G61670, response to light stimulus
28717429	**AT1G75945**		AT1G75945
28719965	**AT4G08093**		AT4G08093, pseudogene
836294	**AT5G61720**		AT5G61720
28719368	**AT3G44006**		AT3G44006
3769769	**AT3G62455**		AT3G62455, pseudogene
844028	**EXT4**		AT1G76930, plant-type cell wall organization
838122	ABCG40		AT1G15520, abscisic acid transport, abscisic acid-activated signaling pathway, cellular response to water deprivation, defense response to oomycetes, import across plasma membrane…
5008282	**AT5G38005**		AT5G38005, ncRNA
834672	**AT5G46295**		AT5G46295

3768988	**AT3G29120**		AT3G29120, pseudogene
837252	**AT1G07400**	Y	AT1G07400, protein complex oligomerization, protein folding, response to heat, response to hydrogen peroxide, response to salt stress
836281	**ERF104**		AT5G61600
829588	AT4G34380		AT4G34380
28718015	**AT2G08735**		AT2G08735, lncRNA
838314	**LOX3**		AT1G17420, lipid oxidation, response to high light intensity, response to jasmonic acid, response to wounding
825163	**AT3G59930**		AT3G59930, stress response to metal ion
842944	BGLU21		AT1G66270, cellular response to phosphate starvation, glucosinolate catabolic process, response to salt stress
832695	AT5G26260		AT5G26260
3766690	AT1G10160		AT1G10160, pseudogene
823555	**NIT2**	Y	AT3G44300, detoxification of nitrogen compound
827113	**GLP9**		AT4G14630
824571	**AT3G54040**		AT3G54040
839295	**GSTF7**	Y	AT1G02920, glutathione metabolic process
834466	AT5G44400		AT5G44400
825420	**AT3G62460**		AT3G62460, regulation of gene expression
825481	**EDL3**	Y	AT3G63060

834996	**BXL1**		AT5G49360, arabinan catabolic process, plant-type cell wall biogenesis, xylan catabolic process
829955	ELI3-2		AT4G37990, lignin biosynthetic process
836286	**PMSR1**	Y	AT5G61640, cellular response to oxidative stress
818914	AT2G43120		AT2G43120
829140	AT4G30170		AT4G30170, response to oxidative stress
833779	AT5G38000		AT5G38000, response to oxidative stress
28717757	**AT2G06995**		AT2G06995, lncRNA
827226	PPDK		AT4G15530, pyruvate metabolic process
834244	**CML37**	Y	AT5G42380, response to water deprivation
834110	**GDPD2**	Y	AT5G41080, cellular response to hpoxia
839748	GRX480		AT1G28480
834301	**COR27**		AT5G42900, negative regulation of DNA-templated transcription, regulation of circadian rhythm, regulation of photoperiodism, flowering, response to abscisic acid, response to absence of light...
842203	**ZF14**	Y	AT1G58340, response to abscisic acid, absence of light, heat, osmotic stress, root morphogenesis, and xenobiotic detoxification by transmembrane export across the plasma membrane

840228	AT1G33340		AT1G33340, clathrin-dependent endocytosis, vesicle budding from membrane
830105	CYP96A12		AT4G39510, biological_process
28718416	**AT3G00680**		AT3G00680, misc_RNA
818183	CASP1		AT2G36100, cell wall modification, cell-cell junction assembly
816830	**SNG1**		AT2G22990, secondary metabolic process
28721044	AT5G09020		AT5G09020, snoRNA
818961	**AT2G43590**		AT2G43590, cell wall macromolecule catabolic process
840127	AOX1D		AT1G32350, alternative respiration
825083	ABCC10		AT3G59140, transmembrane transport
831375	GASA4		AT5G15230
838824	AT1G22190		AT1G22190, negative regulation of seed germination, positive regulation of abscisic acid biosynthetic process, regulation of DNA-templated transcription
819250	AT2G46420		AT2G46420
834385	BHLH92		AT5G43650
824168	MYB77		AT3G50060, positive regulation of auxin mediated signaling pathway, regulation of DNA-templated transcription
829721	AT4G35690		AT4G35690, root development, shoot system development
10723131	**AT2G01422**		AT2G01422, ncRNA
831134	AT5G12940		AT5G12940

830859	**PROPEP4**		AT5G09980, innate immune response
831935	GDH1		AT5G18170, glutamate catabolic process
28718878	AT3G05955		AT3G05955, lncRNA
815247	XTH4		AT2G06850, cell wall biogenesis, xyloglucan metabolic process
841784	**HEI10**		AT1G53490, chiasma assembly, protein ubiquitination, reciprocal meiotic recombination
824623	AT3G54580		AT3G54580, plant-type cell wall organization

Gene_id represents the National Centre for Biotechnology Information (NCBI) (https://www.ncbi.nlm.nih.gov/) gene number. Gene function represents the GO Biological Process keyword with omitting more than five keywords from TAIR (https://www.arabidopsis.org/). The bold 41 differential genes are from GABI 0h vs *Col-0* (Mock) 0h, GABI 3h vs Mock 3h, GABI 9h vs Mock 9h, and GABI 24h vs Mock 24h, with the mark 'Y' were used for subsequent study. The other 29 differential genes are from GABI 3h vs Mock 3h, GABI 9h vs Mock 9h, and GABI 24h vs Mock 24h.

Appendix VI Analysis of salt-specific differential genes

Gene_name	Mock 0h vs Mock 3h	Mock 0h vs Mock 9h	Mock 0h vs Mock 24h	GABI 0h vs GABI 3h	GABI 0h vs GABI 9h	GABI 0h vs GABI 24h
ABCG40	0.00040	0.00578	0.03695	0.00075	0.01411	0.00007
AT4G34380	0.00040	0.00034	0.01038	0.00026	0.00043	0.00063
BGLU21	0.00026	0.00014	0.00775	0.00035	0.00012	0.00035
AT5G26260	0.00001	0.00001	0.00887	0.00004	0.00001	0.00003
AT1G10160	0.00000	0.06668	0.00519	0.02691	0.22752	0.20189
AT5G44400	0.12999	0.06600	0.01183	0.17651	0.01085	0.04960
ELI3-2	0.00004	0.00168	0.04363	0.00000	0.02568	0.05252
AT2G43120	0.00008	0.02214	0.01164	0.01778	0.19088	0.20674
AT4G30170	0.00001	0.00001	0.00234	0.00008	0.00005	0.00006
AT5G38000	0.35301	0.04151	0.00185	0.08083	0.01636	0.00010
PPDK	0.39013	0.00204	0.00464	0.00904	0.00236	0.00090
GRX480	0.05436	0.08135	0.89551	0.21346	0.48657	0.15981
AT1G33340	0.01765	0.00002	0.39275	0.10700	0.11533	0.07604
CYP96A12	0.00880	0.00096	0.00223	0.93077	0.05437	0.21645
CASP1	0.00154	0.00002	0.00005	0.14505	0.00016	0.00027
AT5G09020	0.03638	0.02513	0.00370	/	/	/
ABCC10	0.00012	0.00014	0.00020	0.00004	0.00001	0.00001
GASA4	0.92795	0.40809	0.67272	0.08704	0.46828	0.00106
AT1G22190	0.00046	0.00513	0.00014	0.00055	0.00012	0.00223
AT2G46420	0.00016	0.00002	0.00218	0.00045	0.00000	0.00000
BHLH92	0.09935	0.26649	0.02447	0.04154	0.06609	0.15430
MYB77	0.06930	0.01146	0.97345	0.03413	0.54946	0.00417
AT4G35690	0.00010	0.00342	0.00037	0.00008	0.00008	0.00146

AT5G12940	0.00016	0.00258	0.03217	0.00006	0.00014	0.00016
GDH1	0.00002	0.00016	0.00014	0.00000	0.00000	0.00002
AT3G05955	0.00100	0.01554	0.36630	0.04667	0.06802	0.06915
XTH4	0.00001	0.00007	0.00362	0.00007	0.00000	0.00000
AT3G54580	0.00037	0.00007	0.01667	0.02040	0.01369	0.01258
AOX1D	0.66145	0.00989	0.13762	0.46130	0.15537	0.22601

The *p* value in the orange box represents a significant increase, meanwhile, in the blue box represent a significant decrease, and no fill represents no significant change. $p < 0.05$, Student's *t*-test.

References

Agneessens, J., 2024. *A study of the vesicle trafficking pathways regulating polar auxin transport and root development* (Doctoral dissertation, Durham University).

Ahmad, P., Jaleel, C.A., Salem, M.A., Nabi, G. and Sharma, S., 2010. Roles of enzymatic and nonenzymatic antioxidants in plants during abiotic stress. *Critical reviews in biotechnology*, *30*(3), pp.161-175.

Aida, M., Beis, D., Heidstra, R., Willemsen, V., Blilou, I., Galinha, C., Nussaume, L., Noh, Y.S., Amasino, R. and Scheres, B., 2004. The PLETHORA genes mediate patterning of the Arabidopsis root stem cell niche. *Cell*, *119*(1), pp.109-120.

Ali, A., Petrov, V., Yun, D.J. and Gechev, T., 2023. Revisiting plant salt tolerance: novel components of the SOS pathway. *Trends in Plant Science*, *28*(9), pp.1060-1069.

Alonso, J.M., Stepanova, A.N., Leisse, T.J., Kim, C.J., Chen, H., Shinn, P., Stevenson, D.K., Zimmerman, J., Barajas, P., Cheuk, R. and Gadrinab, C., 2003. Genome-wide insertional mutagenesis of Arabidopsis thaliana. *Science*, *301*(5633), pp.653-657.

Amack, S.C. and Antunes, M.S., 2020. CaMV35S promoter–A plant biology and biotechnology workhorse in the era of synthetic biology. *Current Plant Biology*, *24*, p.100179.

Apel, K. and Hirt, H., 2004. Reactive oxygen species: metabolism, oxidative stress, and signal transduction. *Annu. Rev. Plant Biol.*, *55*(1), pp.373-399.

Apse, M.P., Sottosanto, J.B. and Blumwald, E., 2003. Vacuolar cation/H+ exchange, ion homeostasis, and leaf development are altered in a T-DNA insertional mutant of AtNHX1, the Arabidopsis vacuolar Na+/H+ antiporter. *The plant journal*, *36*(2), pp.229-239.

Arabidopsis Genome Initiative genome analysis, 2000. Analysis of the genome

sequence of the flowering plant Arabidopsis thaliana. *nature*, *408*(6814), pp.796-815.

Arto, I. and Dietzenbacher, E., 2014. Drivers of the growth in global greenhouse gas emissions. *Environmental science & technology*, *48*(10), pp.5388-5394.

Ascenzi, R. and Gantt, J.S., 1997. A drought-stress-inducible histone gene in Arabidopsis thaliana is a member of a distinct class of plant linker histone variants. *Plant molecular biology*, *34*(4), pp.629-641.

Ashburner, M., Ball, C.A., Blake, J.A., Botstein, D., Butler, H., Cherry, J.M., Davis, A.P., Dolinski, K., Dwight, S.S., Eppig, J.T. and Harris, M.A., 2000. Gene ontology: tool for the unification of biology. *Nature genetics*, *25*(1), pp.25-29.

Asseng, S., Ewert, F., Martre, P., Rötter, R.P., Lobell, D.B., Cammarano, D., Kimball, B.A., Ottman, M.J., Wall, G.W., White, J.W. and Reynolds, M.P., 2015. Rising temperatures reduce global wheat production. *Nature climate change*, *5*(2), pp.143-147.

Band, L.R., Wells, D.M., Fozard, J.A., Ghetiu, T., French, A.P., Pound, M.P., Wilson, M.H., Yu, L., Li, W., Hijazi, H.I. and Oh, J., 2014. Systems analysis of auxin transport in the Arabidopsis root apex. *The Plant Cell*, *26*(3), pp.862-875.

Barba-Espín, G., Clemente-Moreno, M.J., Alvarez, S., García-Legaz, M.F., Hernández, J.A. and Díaz-Vivancos, P., 2011. Salicylic acid negatively affects the response to salt stress in pea plants. *Plant Biology*, *13*(6), pp.909-917.

Barlowe, C., Orci, L., Yeung, T., Hosobuchi, M., Hamamoto, S., Salama, N., Rexach, M.F., Ravazzola, M., Amherdt, M. and Schekman, R., 1994. COPII: a membrane coat formed by Sec proteins that drive vesicle budding from the endoplasmic reticulum. *Cell*, *77*(6), pp.895-907.

Bartel, B., 1997. Auxin biosynthesis. *Annual review of plant biology*, *48*(1), pp.51-66.

Bassham, D.C. and Blatt, M.R., 2008. SNAREs: cogs and coordinators in signaling and development. *Plant Physiology*, *147*(4), pp.1504-1515.

Baster, P., Robert, S., Kleine-Vehn, J., Vanneste, S., Kania, U., Grunewald, W., De Rybel, B., Beeckman, T. and Friml, J., 2013. SCFTIR1/AFB-auxin signalling regulates PIN vacuolar trafficking and auxin fluxes during root gravitropism. *The EMBO journal*, *32*(2), pp.260-274.

Ben Mariem, S., Soba, D., Zhou, B., Loladze, I., Morales, F. and Aranjuelo, I., 2021. Climate change, crop yields, and grain quality of C3 cereals: A meta-analysis of [CO2], temperature, and drought effects. *Plants*, *10*(6), p.1052.

Benjamins, R., Malenica, N. and Luschnig, C., 2005. Regulating the regulator: the control of auxin transport. *Bioessays*, *27*(12), pp.1246-1255.

Bennett, M.J., Marchant, A., Green, H.G., May, S.T., Ward, S.P., Millner, P.A., Walker, A.R., Schulz, B. and Feldmann, K.A., 1996. Arabidopsis AUX1 gene: a permease-like regulator of root gravitropism. *Science*, *273*(5277), pp.948-950.

Blilou, I., Xu, J., Wildwater, M., Willemsen, V., Paponov, I., Friml, J., Heidstra, R., Aida, M., Palme, K. and Scheres, B., 2005. The PIN auxin efflux facilitator network controls growth and patterning in Arabidopsis roots. *Nature*, *433*(7021), pp.39-44.

Bonifacino, J.S. and Glick, B.S., 2004. The mechanisms of vesicle budding and fusion. *cell*, *116*(2), pp.153-166.

Bonifacino, J.S. and Lippincott-Schwartz, J., 2003. Coat proteins: shaping membrane transport. *Nature reviews Molecular cell biology*, *4*(5), pp.409-414.

Bray, N.L., Pimentel, H., Melsted, P. and Pachter, L., 2016. Near-optimal probabilistic RNA-seq quantification. *Nature biotechnology*, *34*(5), pp.525-527.

Cackett, L., Cannistraci, C.V., Meier, S., Ferrandi, P., Pěnčík, A., Gehring, C., Novák, O., Ingle, R.A. and Donaldson, L., 2022. Salt-specific gene expression reveals elevated auxin levels in Arabidopsis thaliana plants

grown under saline conditions. *Frontiers in plant science*, *13*, p.804716.

Cai, H., Reinisch, K. and Ferro-Novick, S., 2007. Coats, tethers, Rabs, and SNAREs work together to mediate the intracellular destination of a transport vesicle. *Developmental cell*, *12*(5), pp.671-682.

Calderón Villalobos, L.I.A., Lee, S., De Oliveira, C., Ivetac, A., Brandt, W., Armitage, L., Sheard, L.B., Tan, X.U., Parry, G., Mao, H. and Zheng, N., 2012. A combinatorial TIR1/AFB–Aux/IAA co-receptor system for differential sensing of auxin. *Nature chemical biology*, *8*(5), pp.477-485.

Cao, W.H., Liu, J., Zhou, Q.Y., Cao, Y.R., Zheng, S.F., Du, B.X., Zhang, J.S. and Chen, S.Y., 2006. Expression of tobacco ethylene receptor NTHK1 alters plant responses to salt stress. *Plant, Cell & Environment*, *29*(7), pp.1210-1219.

Cao, X., Yang, H., Shang, C., Ma, S., Liu, L. and Cheng, J., 2019. The roles of auxin biosynthesis YUCCA gene family in plants. *International journal of molecular sciences*, *20*(24), p.6343.

Carrier, D.J., Bakar, N.T.A., Swarup, R., Callaghan, R., Napier, R.M., Bennett, M.J. and Kerr, I.D., 2008. The binding of auxin to the Arabidopsis auxin influx transporter AUX1. *Plant physiology*, *148*(1), pp.529-535.

Chalfun-Junior, A., Mes, J.J., Mlynárová, L., Aarts, M.G. and Angenent, G.C., 2003. Low frequency of T-DNA based activation tagging in Arabidopsis is correlated with methylation of CaMV 35S enhancer sequences. *FEBS letters*, *555*(3), pp.459-463.

Challinor, A.J., Watson, J., Lobell, D.B., Howden, S.M., Smith, D.R. and Chhetri, N., 2014. A meta-analysis of crop yield under climate change and adaptation. *Nature climate change*, *4*(4), pp.287-291.

Chen, R., Hilson, P., Sedbrook, J., Rosen, E., Caspar, T. and Masson, P.H., 1998. The Arabidopsis thaliana AGRAVITROPIC 1 gene encodes a component of the polar-auxin-transport efflux carrier. *Proceedings of the National Academy of Sciences*, *95*(25), pp.15112-15117.

Chen, T.H. and Murata, N., 2008. Glycinebetaine: an effective protectant

against abiotic stress in plants. *Trends in plant science*, *13*(9), pp.499-505.

Chen, Y.A. and Scheller, R.H., 2001. SNARE-mediated membrane fusion. *Nature reviews Molecular cell biology*, *2*(2), pp.98-106.

Chinnusamy, V., Jagendorf, A. and Zhu, J.K., 2005. Understanding and improving salt tolerance in plants. *Crop science*, *45*(2), pp.437-448.

Cho, M. and Cho, H., 2013. The function of ABCB transporters in auxin transport. *Plant signaling & behavior*, *8*(2), pp.642-54.

Chung, Y., Kwon, S.I. and Choe, S., 2014. Antagonistic regulation of Arabidopsis growth by brassinosteroids and abiotic stresses. *Molecules and cells*, *37*(11), pp.795-803.

Clark, N.M., Fisher, A.P., Berckmans, B., Van den Broeck, L., Nelson, E.C., Nguyen, T.T., Bustillo-Avendaño, E., Zebell, S.G., Moreno-Risueno, M.A., Simon, R. and Gallagher, K.L., 2020. Protein complex stoichiometry and expression dynamics of transcription factors modulate stem cell division. *Proceedings of the National Academy of Sciences*, *117*(26), pp.15332-15342.

Clough, S.J. and Bent, A.F., 1998. Floral dip: a simplified method for Agrobacterium-mediated transformation of Arabidopsis thaliana. *The plant journal*, *16*(6), pp.735-743.

Clowes, F.A.L., 1953. The cytogenerative centre in roots with broad columellas. *The New Phytologist*, *52*(1), pp.48-57.

Clowes, F.A.L., 1954. The promeristem and the minimal constructional centre in grass root apices. *The New Phytologist*, *53*(1), pp.108-116.

Clowes, F.A.L., 1958. Development of quiescent centres in root meristems. *New Phytologist*, *57*(1), pp.85-88.

Cui, H., Levesque, M.P., Vernoux, T., Jung, J.W., Paquette, A.J., Gallagher, K.L., Wang, J.Y., Blilou, I., Scheres, B. and Benfey, P.N., 2007. An evolutionarily conserved mechanism delimiting SHR movement defines a single layer of endodermis in plants. *Science*, *316*(5823), pp.421-425.

Curtin, T.R.C., 2009. Climate change and food production. *Energy &*

environment, *20*(7), pp.1099-1116.

Das, K. and Roychoudhury, A., 2014. Reactive oxygen species (ROS) and response of antioxidants as ROS-scavengers during environmental stress in plants. *Frontiers in environmental science*, *2*, p.53.

Das, S., Weijers, D. and Borst, J.W., 2021. Auxin response by the numbers. *Trends in Plant Science*, *26*(5), pp.442-451.

Della Rovere, F., Fattorini, L., Ronzan, M., Falasca, G. and Altamura, M.M., 2016. The quiescent center and the stem cell niche in the adventitious roots of Arabidopsis thaliana. *Plant signaling & behavior*, *11*(5), p.e1176660.

Demidchik, V. and Tester, M., 2002. Sodium fluxes through nonselective cation channels in the plasma membrane of protoplasts from Arabidopsis roots. *Plant physiology*, *128*(2), pp.379-387.

Dettmer, J., Ursache, R., Campilho, A., Miyashima, S., Belevich, I., O'Regan, S., Mullendore, D.L., Yadav, S.R., Lanz, C., Beverina, L. and Papagni, A., 2014. CHOLINE TRANSPORTER-LIKE1 is required for sieve plate development to mediate long-distance cell-to-cell communication. *Nature communications*, *5*(1), p.4276.

Dey, N., Sarkar, S., Acharya, S. and Maiti, I.B., 2015. Synthetic promoters in planta. *Planta*, *242*(5), pp.1077-1094.

Dhonukshe, P., Aniento, F., Hwang, I., Robinson, D.G., Mravec, J., Stierhof, Y.D. and Friml, J., 2007. Clathrin-mediated constitutive endocytosis of PIN auxin efflux carriers in Arabidopsis. *Current Biology*, *17*(6), pp.520-527.

Di, D.W., Zhang, C., Luo, P., An, C.W. and Guo, G.Q., 2016. The biosynthesis of auxin: how many paths truly lead to IAA?. *Plant growth regulation*, *78*(3), pp.275-285.

Diffenbaugh, N.S., Singh, D., Mankin, J.S., Horton, D.E., Swain, D.L., Touma, D., Charland, A., Liu, Y., Haugen, M., Tsiang, M. and Rajaratnam, B., 2017. Quantifying the influence of global warming on unprecedented extreme climate events. *Proceedings of the National Academy of*

Sciences, *114*(19), pp.4881-4886.

Ding, Z. and Friml, J., 2010. Auxin regulates distal stem cell differentiation in Arabidopsis roots. *Proceedings of the National Academy of Sciences*, *107*(26), pp.12046-12051.

Ding, Z., Galván-Ampudia, C.S., Demarsy, E., Łangowski, Ł., Kleine-Vehn, J., Fan, Y., Morita, M.T., Tasaka, M., Fankhauser, C., Offringa, R. and Friml, J., 2011. Light-mediated polarization of the PIN3 auxin transporter for the phototropic response in Arabidopsis. *Nature cell biology*, *13*(4), pp.447-452.

Ding, Z., Wang, B., Moreno, I., Dupláková, N., Simon, S., Carraro, N., Reemmer, J., Pěnčík, A., Chen, X., Tejos, R. and Skůpa, P., 2012. ER-localized auxin transporter PIN8 regulates auxin homeostasis and male gametophyte development in Arabidopsis. *Nature communications*, *3*(1), p.941.

Dinneny, J.R., 2019. Developmental responses to water and salinity in root systems. *Annual Review of Cell and Developmental Biology*, *35*(1), pp.239-257.

Duan, L., Sebastian, J. and Dinneny, J.R., 2014. Salt-stress regulation of root system growth and architecture in Arabidopsis seedlings. *Plant Cell Expansion: Methods and Protocols*, pp.105-122.

Dubey, R.S., 1999. Protein synthesis by plants under stressful conditions. *Handbook of plant and crop stress*, *2*, pp.365-397.

Dubrovsky, J.G. and Barlow, P.W., 2015. The origins of the quiescent centre concept. *New Phytologist*, *206*(2), pp.493-496.

Dubrovsky, J.G. and Ivanov, V.B., 2021. The quiescent centre of the root apical meristem: conceptual developments from Clowes to modern times. *Journal of Experimental Botany*, *72*(19), pp.6687-6707.

El Kasmi, F., Krause, C., Hiller, U., Stierhof, Y.D., Mayer, U., Conner, L., Kong, L., Reichardt, I., Sanderfoot, A.A. and Jürgens, G., 2013. SNARE complexes of different composition jointly mediate membrane fusion in Arabidopsis cytokinesis. *Molecular biology of the cell*, *24*(10), pp.1593-

1601.

Ellouzi, H., Ben Hamed, K., Cela, J., Munné-Bosch, S. and Abdelly, C., 2011. Early effects of salt stress on the physiological and oxidative status of Cakile maritima (halophyte) and Arabidopsis thaliana (glycophyte). *Physiologia Plantarum*, *142*(2), pp.128-143.

Fang, Q., Wang, Q., Mao, H., Xu, J., Wang, Y., Hu, H., He, S., Tu, J., Cheng, C., Tian, G. and Wang, X., 2018. AtDIV2, an RR-type MYB transcription factor of Arabidopsis, negatively regulates salt stress by modulating ABA signaling. *Plant Cell Reports*, *37*(11), pp.1499-1511.

Farooq, M., Hussain, M., Wahid, A. and Siddique, K.H.M., 2012. Drought stress in plants: an overview. *Plant responses to drought stress: From morphological to molecular features*, pp.1-33.

Fasshauer, D., Sutton, R.B., Brunger, A.T. and Jahn, R., 1998. Conserved structural features of the synaptic fusion complex: SNARE proteins reclassified as Q-and R-SNAREs. *Proceedings of the national academy of sciences*, *95*(26), pp.15781-15786.

Ferguson, J.N., 2019. Climate change and abiotic stress mechanisms in plants. *Emerging Topics in Life Sciences*, *3*(2), pp.165-181.

Foyer, C.H. and Noctor, G., 2005. Redox homeostasis and antioxidant signaling: a metabolic interface between stress perception and physiological responses. *The plant cell*, *17*(7), pp.1866-1875.

Friml, J., 2010. Subcellular trafficking of PIN auxin efflux carriers in auxin transport. *European journal of cell biology*, *89*(2-3), pp.231-235.

Friml, J., Benková, E., Blilou, I., Wisniewska, J., Hamann, T., Ljung, K., Woody, S., Sandberg, G., Scheres, B., Jürgens, G. and Palme, K., 2002a. AtPIN4 mediates sink-driven auxin gradients and root patterning in Arabidopsis. *Cell*, *108*(5), pp.661-673.

Friml, J., Benková, E., Mayer, U., Palme, K. and Muster, G., 2003a. Automated whole mount localisation techniques for plant seedlings. *The Plant Journal*, *34*(1), pp.115-124.

Friml, J., Vieten, A., Sauer, M., Weijers, D., Schwarz, H., Hamann, T., Offringa, R. and Jürgens, G., 2003b. Efflux-dependent auxin gradients establish the apical–basal axis of Arabidopsis. *Nature, 426*(6963), pp.147-153.

Friml, J., Wiśniewska, J., Benková, E., Mendgen, K. and Palme, K., 2002b. Lateral relocation of auxin efflux regulator PIN3 mediates tropism in Arabidopsis. *Nature, 415*(6873), pp.806-809.

Fu, X. and Harberd, N.P., 2003. Auxin promotes Arabidopsis root growth by modulating gibberellin response. *Nature, 421*(6924), pp.740-743.

Fu, Y., Yang, Y., Chen, S., Ning, N. and Hu, H., 2019. Arabidopsis IAR4 modulates primary root growth under salt stress through ROS-mediated modulation of auxin distribution. *Frontiers in Plant Science, 10*, p.522.

Galbiati, M., Moreno, M.A., Nadzan, G., Zourelidou, M. and Dellaporta, S.L., 2000. Large-scale T-DNA mutagenesis in Arabidopsis for functional genomic analysis. *Functional & integrative genomics, 1*(1), pp.25-34.

Galinha, C., Hofhuis, H., Luijten, M., Willemsen, V., Blilou, I., Heidstra, R. and Scheres, B., 2007. PLETHORA proteins as dose-dependent master regulators of Arabidopsis root development. *Nature, 449*(7165), pp.1053-1057.

Galvan-Ampudia, C.S. and Testerink, C., 2011. Salt stress signals shape the plant root. *Current opinion in plant biology, 14*(3), pp.296-302.

Galweiler, L., Guan, C., Müller, A., Wisman, E., Mendgen, K., Yephremov, A. and Palme, K., 1998. Regulation of polar auxin transport by AtPIN1 in Arabidopsis vascular tissue. *Science, 282*(5397), pp.2226-2230.

Gao, Y. and Zhao, Y., 2013. Epigenetic suppression of T-DNA insertion mutants in Arabidopsis. *Molecular Plant, 6*(2), pp.539-545.

Gao, Y.Q., Chen, J.G., Chen, Z.R., An, D., Lv, Q.Y., Han, M.L., Wang, Y.L., Salt, D.E. and Chao, D.Y., 2017. A new vesicle trafficking regulator CTL1 plays a crucial role in ion homeostasis. *PLoS Biology, 15*(12), p.e2002978.

Geldner, N., Friml, J., Stierhof, Y.D., Jürgens, G. and Palme, K., 2001. Auxin transport inhibitors block PIN1 cycling and vesicle

trafficking. *Nature*, *413*(6854), pp.425-428.

Geng, Y., Wu, R., Wee, C.W., Xie, F., Wei, X., Chan, P.M.Y., Tham, C., Duan, L. and Dinneny, J.R., 2013. A spatio-temporal understanding of growth regulation during the salt stress response in Arabidopsis. *The Plant Cell*, *25*(6), pp.2132-2154.

Gerasimavicius, L., Livesey, B.J. and Marsh, J.A., 2022. Loss-of-function, gain-of-function and dominant-negative mutations have profoundly different effects on protein structure. *Nature communications*, *13*(1), p.3895.

Goldsmith, M.H.M., 1977. The polar transport of auxin. *Annual Review of Plant Physiology*, *28*(1), pp.439-478.

Gomes, G.L.B. and Scortecci, K.C., 2021. Auxin and its role in plant development: structure, signalling, regulation and response mechanisms. *Plant Biology*, *23*(6), pp.894-904.

Gong, D., Guo, Y., Schumaker, K.S. and Zhu, J.K., 2004. The SOS3 family of calcium sensors and SOS2 family of protein kinases in Arabidopsis. *Plant physiology*, *134*(3), pp.919-926.

Gong, Z., Xiong, L., Shi, H., Yang, S., Herrera-Estrella, L.R., Xu, G., Chao, D.Y., Li, J., Wang, P.Y., Qin, F. and Li, J., 2020. Plant abiotic stress response and nutrient use efficiency. *Science China Life Sciences*, *63*(5), pp.635-674.

Gregory, P.J., Ingram, J.S. and Brklacich, M., 2005. Climate change and food security. *Philosophical Transactions of the Royal Society B: Biological Sciences*, *360*(1463), pp.2139-2148.

Gu, X., Fonseka, K., Agneessens, J., Casson, S.A., Smertenko, A., Guo, G., Topping, J.F., Hussey, P.J. and Lindsey, K., 2021. The Arabidopsis R-SNARE VAMP714 is essential for polarisation of PIN proteins and auxin responses. *New Phytologist*, *230*(2), pp.550-566.

Guan, Q., Wu, J., Yue, X., Zhang, Y. and Zhu, J., 2013. A nuclear calcium-sensing pathway is critical for gene regulation and salt stress tolerance in Arabidopsis. *PLoS Genetics*, *9*(8), p.e1003755.

Gueta-Dahan, Y., Yaniv, Z., Zilinskas, B.A. and Ben-Hayyim, G., 1997. Salt and oxidative stress: similar and specific responses and their relation to salt tolerance in citrus. *Planta*, *203*(4), pp.460-469.

Guo, D., Kong, S., Chu, X., Li, X. and Pan, H., 2019. De novo biosynthesis of indole-3-acetic acid in engineered Escherichia coli. *Journal of Agricultural and Food Chemistry*, *67*(29), pp.8186-8190.

Halfter, U., Ishitani, M. and Zhu, J.K., 2000. The Arabidopsis SOS2 protein kinase physically interacts with and is activated by the calcium-binding protein SOS3. *Proceedings of the National Academy of Sciences*, *97*(7), pp.3735-3740.

Halliwell, B., 2006. Reactive species and antioxidants. Redox biology is a fundamental theme of aerobic life. *Plant physiology*, *141*(2), pp.312-322.

Hameed, A., Ahmed, M.Z., Hussain, T., Aziz, I., Ahmad, N., Gul, B. and Nielsen, B.L., 2021. Effects of salinity stress on chloroplast structure and function. *Cells*, *10*(8), p.2023.

Hammer III, J.A. and Wu, X.S., 2002. Rabs grab motors: defining the connections between Rab GTPases and motor proteins. *Current opinion in cell biology*, *14*(1), pp.69-75.

Han, H., Adamowski, M., Qi, L., Alotaibi, S.S. and Friml, J., 2021. PIN-mediated polar auxin transport regulations in plant tropic responses. *New Phytologist*, *232*(2), pp.510-522.

Han, J., Pluhackova, K. and Böckmann, R.A., 2017. The multifaceted role of SNARE proteins in membrane fusion. *Frontiers in physiology*, *8*, p.5.

Hanson, P.I., Roth, R., Morisaki, H., Jahn, R. and Heuser, J.E., 1997. Structure and conformational changes in NSF and its membrane receptor complexes visualized by quick-freeze/deep-etch electron microscopy. *Cell*, *90*(3), pp.523-535.

Hao, R., Zhou, W., Li, J., Luo, M., Scheres, B. and Guo, Y., 2023. On salt stress, PLETHORA signaling maintains root meristems. *Developmental Cell*, *58*(18), pp.1657-1669.

Haro, R., Bañuelos, M.A., Senn, M.E., Barrero-Gil, J. and Rodríguez-Navarro, A., 2005. HKT1 mediates sodium uniport in roots. Pitfalls in the expression of HKT1 in yeast. *Plant Physiology*, *139*(3), pp.1495-1506.

Harrison, S.J., Mott, E.K., Parsley, K., Aspinall, S., Gray, J.C. and Cottage, A., 2006. A rapid and robust method of identifying transformed Arabidopsis thaliana seedlings following floral dip transformation. *Plant methods*, *2*(1), p.19.

Hasanuzzaman, M., Raihan, M.R.H., Masud, A.A.C., Rahman, K., Nowroz, F., Rahman, M., Nahar, K. and Fujita, M., 2021. Regulation of reactive oxygen species and antioxidant defense in plants under salinity. *International Journal of Molecular Sciences*, *22*(17), p.9326.

Hasegawa, P.M., Bressan, R.A., Zhu, J.K. and Bohnert, H.J., 2000. Plant cellular and molecular responses to high salinity. *Annual review of plant biology*, *51*(1), pp.463-499.

Hayat, S., Hayat, Q., Alyemeni, M.N., Wani, A.S., Pichtel, J. and Ahmad, A., 2012. Role of proline under changing environments: a review. *Plant signaling & behavior*, *7*(11), pp.1456-1466.

He, W., Brumos, J., Li, H., Ji, Y., Ke, M., Gong, X., Zeng, Q., Li, W., Zhang, X., An, F. and Wen, X., 2011. A small-molecule screen identifies L-kynurenine as a competitive inhibitor of TAA1/TAR activity in ethylene-directed auxin biosynthesis and root growth in Arabidopsis. *The Plant Cell*, *23*(11), pp.3944-3960.

He, X.J., Mu, R.L., Cao, W.H., Zhang, Z.G., Zhang, J.S. and Chen, S.Y., 2005. AtNAC2, a transcription factor downstream of ethylene and auxin signaling pathways, is involved in salt stress response and lateral root development. *The Plant Journal*, *44*(6), pp.903-916.

Hegerl, G.C., Brönnimann, S., Cowan, T., Friedman, A.R., Hawkins, E., Iles, C., Müller, W., Schurer, A. and Undorf, S., 2019. Causes of climate change over the historical record. *Environmental Research Letters*, *14*(12), p.123006.

Hirsch, R.E., Lewis, B.D., Spalding, E.P. and Sussman, M.R., 1998. A role for the AKT1 potassium channel in plant nutrition. *Science*, *280*(5365), pp.918-921.

Hoagland, D. and Arnon, D.I., 1950. The water culture method for growing plants without soil. *Calif. Agric. Exp. Stn. Circ*, *347*(32), p.1.

Holtorf, S., Apel, K. and Bohlmann, H., 1995. Comparison of different constitutive and inducible promoters for the overexpression of transgenes in Arabidopsis thaliana. *Plant molecular biology*, *29*(4), pp.637-646.

Hootsmans, M.J. and Wiegman, F., 1998. Four helophyte species growing under salt stress: their salt of life?. *Aquatic botany*, *62*(2), pp.81-94.

Howden, S.M., Soussana, J.F., Tubiello, F.N., Chhetri, N., Dunlop, M. and Meinke, H., 2007. Adapting agriculture to climate change. *Proceedings of the national academy of sciences*, *104*(50), pp.19691-19696.

Hull, R., Covey, S.N. and Dale, P., 2000. Genetically modified plants and the 35S promoter: assessing the risks and enhancing the debate. *Microbial Ecology in Health and Disease*, *12*(1), pp.1-5.

Ikeya, S., Aoyanagi, T., Ishizuka, I., Takeuchi, A. and Kozaki, A., 2020. Nitrate promotes germination under inhibition by NaCl or high concentration of glucose. *Plants*, *9*(6), p.707.

Isayenkov, S.V. and Maathuis, F.J., 2019. Plant salinity stress: many unanswered questions remain. *Frontiers in plant science*, *10*, p.80.

Ishitani, M., Liu, J., Halfter, U., Kim, C.S., Shi, W. and Zhu, J.K., 2000. SOS3 function in plant salt tolerance requires N-myristoylation and calcium binding. *The Plant Cell*, *12*(9), pp.1667-1677.

Jahn, R. and Scheller, R.H., 2006. SNAREs—engines for membrane fusion. *Nature reviews Molecular cell biology*, *7*(9), pp.631-643.

Jahn, R., Cafiso, D.C. and Tamm, L.K., 2024. Mechanisms of SNARE proteins in membrane fusion. *Nature Reviews Molecular Cell Biology*, *25*(2), pp.101-118.

Jedličková, V., Ebrahimi Naghani, S. and Robert, H.S., 2022. On the trail of

auxin: reporters and sensors. *The Plant Cell*, *34*(9), pp.3200-3213.

Jentsch, A., Kreyling, J. and Beierkuhnlein, C., 2007. A new generation of climate-change experiments: events, not trends. *Frontiers in Ecology and the Environment*, *5*(7), pp.365-374.

Ji, H., Pardo, J.M., Batelli, G., Van Oosten, M.J., Bressan, R.A. and Li, X., 2013. The salt overly sensitive (SOS) pathway: established and emerging roles. *Molecular plant*, *6*(2), pp.275-286.

Jiang, K., Moe-Lange, J., Hennet, L. and Feldman, L.J., 2016. Salt stress affects the redox status of Arabidopsis root meristems. *Frontiers in Plant Science*, *7*, p.81.

Jiang, Y. and Deyholos, M.K., 2009. Functional characterization of Arabidopsis NaCl-inducible WRKY25 and WRKY33 transcription factors in abiotic stresses. *Plant molecular biology*, *69*(1), pp.91-105.

Jin, J., Li, K., Qin, J., Yan, L., Wang, S., Zhang, G., Wang, X. and Bi, Y., 2021. The response mechanism to salt stress in Arabidopsis transgenic lines over-expressing of GmG6PD. *Plant Physiology and Biochemistry*, *162*, pp.74-85.

Julkowska, M.M., Hoefsloot, H.C., Mol, S., Feron, R., de Boer, G.J., Haring, M.A. and Testerink, C., 2014. Capturing Arabidopsis root architecture dynamics with ROOT-FIT reveals diversity in responses to salinity. *Plant Physiology*, *166*(3), pp.1387-1402.

Jupe, F., Rivkin, A.C., Michael, T.P., Zander, M., Motley, S.T., Sandoval, J.P., Slotkin, R.K., Chen, H., Castanon, R., Nery, J.R. and Ecker, J.R., 2019. The complex architecture and epigenomic impact of plant T-DNA insertions. *PLoS genetics*, *15*(1), p.e1007819.

Kakei, Y., Yamazaki, C., Suzuki, M., Nakamura, A., Sato, A., Ishida, Y., Kikuchi, R., Higashi, S., Kokudo, Y., Ishii, T. and Soeno, K., 2015. Small-molecule auxin inhibitors that target YUCCA are powerful tools for studying auxin function. *The Plant Journal*, *84*(4), pp.827-837.

Kanehisa, M. and Goto, S., 2000. KEGG: kyoto encyclopedia of genes and

genomes. *Nucleic acids research*, *28*(1), pp.27-30.

Kaneyasu, T., Kobayashi, A., Nakayama, M., Fujii, N., Takahashi, H. and Miyazawa, Y., 2007. Auxin response, but not its polar transport, plays a role in hydrotropism of Arabidopsis roots. *Journal of experimental botany*, *58*(5), pp.1143-1150.

Ke, Q., Kim, H.S., Wang, Z., Ji, C.Y., Jeong, J.C., Lee, H.S., Choi, Y.I., Xu, B., Deng, X., Yun, D.J. and Kwak, S.S., 2017. Down-regulation of GIGANTEA-like genes increases plant growth and salt stress tolerance in poplar. *Plant Biotechnology Journal*, *15*(3), pp.331-343.

Kienle, N., Kloepper, T.H. and Fasshauer, D., 2009. Phylogeny of the SNARE vesicle fusion machinery yields insights into the conservation of the secretory pathway in fungi. *BMC evolutionary biology*, *9*(1), p.19.

Kim, W.Y., Ali, Z., Park, H.J., Park, S.J., Cha, J.Y., Perez-Hormaeche, J., Quintero, F.J., Shin, G., Kim, M.R., Qiang, Z. and Ning, L., 2013. Release of SOS2 kinase from sequestration with GIGANTEA determines salt tolerance in Arabidopsis. *Nature communications*, *4*(1), p.1352.

Kleine-Vehn, J., Dhonukshe, P., Sauer, M., Brewer, P.B., Wiśniewska, J., Paciorek, T., Benková, E. and Friml, J., 2008. ARF GEF-dependent transcytosis and polar delivery of PIN auxin carriers in Arabidopsis. *Current biology*, *18*(7), pp.526-531.

Kleine-Vehn, J., Ding, Z., Jones, A.R., Tasaka, M., Morita, M.T. and Friml, J., 2010. Gravity-induced PIN transcytosis for polarization of auxin fluxes in gravity-sensing root cells. *Proceedings of the National Academy of Sciences*, *107*(51), pp.22344-22349.

Kloepper, T.H., Kienle, C.N. and Fasshauer, D., 2007. An elaborate classification of SNARE proteins sheds light on the conservation of the eukaryotic endomembrane system. *Molecular biology of the cell*, *18*(9), pp.3463-3471.

Koepfli, J.B., Thimann, K.V. and Went, F.W., 1938. Phytohormones: structure and physiological activity.

Koevoets, I.T., Venema, J.H., Elzenga, J.T.M. and Testerink, C., 2016. Roots withstanding their environment: exploiting root system architecture responses to abiotic stress to improve crop tolerance. *Frontiers in plant science*, *7*, p.1335.

Koike, I., Watanabe, S., Okazaki, K., Hayashi, K.I., Kasahara, H., Shimomura, K. and Umehara, M., 2020. Endogenous auxin determines the pattern of adventitious shoot formation on internodal segments of ipecac. *Planta*, *251*(3), p.73.

Koike, S. and Jahn, R., 2022. SNARE proteins: zip codes in vesicle targeting?. *Biochemical Journal*, *479*(3), pp.273-288.

Koizumi, K., Hayashi, T. and Gallagher, K.L., 2012. SCARECROW reinforces SHORT-ROOT signaling and inhibits periclinal cell divisions in the ground tissue by maintaining SHR at high levels in the endodermis. *Plant signaling & behavior*, *7*(12), pp.1573-1577.

Krämer, U., 2015. Planting molecular functions in an ecological context with Arabidopsis thaliana. *Elife*, *4*, p.e06100.

Kraner, M.E., Müller, C. and Sonnewald, U., 2017. Comparative proteomic profiling of the choline transporter-like1 (CHER 1) mutant provides insights into plasmodesmata composition of fully developed Arabidopsis thaliana leaves. *The Plant Journal*, *92*(4), pp.696-709.

Křeček, P., Skůpa, P., Libus, J., Naramoto, S., Tejos, R., Friml, J. and Zažímalová, E., 2009. The PIN-FORMED (PIN) protein family of auxin transporters. *Genome biology*, *10*(12), p.249.

Ladeiro, B., 2012. Saline agriculture in the 21st century: using salt contaminated resources to cope food requirements. *Journal of Botany*, *2012*(1), p.310705.

Lamb, W.F., Wiedmann, T., Pongratz, J., Andrew, R., Crippa, M., Olivier, J.G., Wiedenhofer, D., Mattioli, G., Al Khourdajie, A., House, J. and Pachauri, S., 2021. A review of trends and drivers of greenhouse gas emissions by sector from 1990 to 2018. *Environmental research letters*, *16*(7), p.073005.

Laplaze, L., Benkova, E., Casimiro, I., Maes, L., Vanneste, S., Swarup, R., Weijers, D., Calvo, V., Parizot, B., Herrera-Rodriguez, M.B. and Offringa, R., 2007. Cytokinins act directly on lateral root founder cells to inhibit root initiation. *The Plant Cell*, *19*(12), pp.3889-3900.

Lavenus, J., Goh, T., Roberts, I., Guyomarc'h, S., Lucas, M., De Smet, I., Fukaki, H., Beeckman, T., Bennett, M. and Laplaze, L., 2013. Lateral root development in Arabidopsis: fifty shades of auxin. *Trends in plant science*, *18*(8), pp.450-458.

Lee, H.J., Kim, H.S., Park, J.M., Cho, H.S. and Jeon, J.H., 2020. PIN-mediated polar auxin transport facilitates root− obstacle avoidance. *New Phytologist*, *225*(3), pp.1285-1296.

Leshem, Y., Golani, Y., Kaye, Y. and Levine, A., 2010. Reduced expression of the v-SNAREs AtVAMP71/AtVAMP7C gene family in Arabidopsis reduces drought tolerance by suppression of abscisic acid-dependent stomatal closure. *Journal of experimental botany*, *61*(10), pp.2615-2622.

Leshem, Y., Melamed-Book, N., Cagnac, O., Ronen, G., Nishri, Y., Solomon, M., Cohen, G. and Levine, A., 2006. Suppression of Arabidopsis vesicle-SNARE expression inhibited fusion of H2O2-containing vesicles with tonoplast and increased salt tolerance. *Proceedings of the National Academy of Sciences*, *103*(47), pp.18008-18013.

Leshem, Y., Seri, L. and Levine, A., 2007. Induction of phosphatidylinositol 3-kinase-mediated endocytosis by salt stress leads to intracellular production of reactive oxygen species and salt tolerance. *The Plant Journal*, *51*(2), pp.185-197.

Lewis, D.R., Negi, S., Sukumar, P. and Muday, G.K., 2011. Ethylene inhibits lateral root development, increases IAA transport and expression of PIN3 and PIN7 auxin efflux carriers. *Development*, *138*(16), pp.3485-3495.

Li, J., Zhou, H., Zhang, Y., Li, Z., Yang, Y. and Guo, Y., 2020. The GSK3-like kinase BIN2 is a molecular switch between the salt stress response and growth recovery in Arabidopsis thaliana. *Developmental Cell*, *55*(3),

pp.367-380.

Li, M., Guo, S., Xu, Y., Meng, Q., Li, G. and Yang, X., 2014a. Glycine betaine-mediated potentiation of HSP gene expression involves calcium signaling pathways in tobacco exposed to NaCl stress. *Physiologia plantarum*, *150*(1), pp.63-75.

Li, S., Li, F., Wang, J., Zhang, W.E.N., Meng, Q., Chen, T.H., Murata, N. and Yang, X., 2011. Glycinebetaine enhances the tolerance of tomato plants to high temperature during germination of seeds and growth of seedlings. *Plant, cell & environment*, *34*(11), pp.1931-1943.

Li, X., Chang, S.X. and Salifu, K.F., 2014b. Soil texture and layering effects on water and salt dynamics in the presence of a water table: a review. *Environmental reviews*, *22*(1), pp.41-50.

Li, X., Li, C., Shi, L., Lv, G., Li, X., Liu, Y., Jia, X., Liu, J., Chen, Y., Zhu, L. and Fu, Y., 2024. Jasmonate signaling pathway confers salt tolerance through a NUCLEAR FACTOR-Y trimeric transcription factor complex in Arabidopsis. *Cell reports*, *43*(3).

Liang, W., Ma, X., Wan, P. and Liu, L., 2018. Plant salt-tolerance mechanism: A review. *Biochemical and biophysical research communications*, *495*(1), pp.286-291.

Limón-Pacheco, J. and Gonsebatt, M.E., 2009. The role of antioxidants and antioxidant-related enzymes in protective responses to environmentally induced oxidative stress. *Mutation Research/Genetic Toxicology and Environmental Mutagenesis*, *674*(1-2), pp.137-147.

Lin, C.C. and Kao, C.H., 1996. Proline accumulation is associated with inhibition of rice seedling root growth caused by NaCl. *Plant Science*, *114*(2), pp.121-128.

Lipka, V., Kwon, C. and Panstruga, R., 2007. SNARE-ware: the role of SNARE-domain proteins in plant biology. *Annu. Rev. Cell Dev. Biol.*, *23*(1), pp.147-174.

Liu, J. and Zhu, J.K., 1998. A calcium sensor homolog required for plant salt

tolerance. *Science*, *280*(5371), pp.1943-1945.

Liu, J., Ishitani, M., Halfter, U., Kim, C.S. and Zhu, J.K., 2000. The Arabidopsis thaliana SOS2 gene encodes a protein kinase that is required for salt tolerance. *Proceedings of the national academy of sciences*, *97*(7), pp.3730-3734.

Liu, M., Yu, H., Ouyang, B., Shi, C., Demidchik, V., Hao, Z., Yu, M. and Shabala, S., 2020a. NADPH oxidases and the evolution of plant salinity tolerance. *Plant, Cell & Environment*, *43*(12), pp.2957-2968.

Liu, S., Yang, R., Liu, M., Zhang, S., Yan, K., Yang, G., Huang, J., Zheng, C. and Wu, C., 2020b. PLATZ2 negatively regulates salt tolerance in Arabidopsis seedlings by directly suppressing the expression of the CBL4/SOS3 and CBL10/SCaBP8 genes. *Journal of experimental botany*, *71*(18), pp.5589-5602.

Liu, W., Li, R.J., Han, T.T., Cai, W., Fu, Z.W. and Lu, Y.T., 2015. Salt stress reduces root meristem size by nitric oxide-mediated modulation of auxin accumulation and signaling in Arabidopsis. *Plant physiology*, *168*(1), pp.343-356.

Lombardi, M., Bellucci, M., Cimini, S., Locato, V., Loreto, F. and De Gara, L., 2024. Exploring natural variations in Arabidopsis thaliana: Plant adaptability to salt stress. *Plants*, *13*(8), p.1069.

Luo, X., Dai, Y., Zheng, C., Yang, Y., Chen, W., Wang, Q., Chandrasekaran, U., Du, J., Liu, W. and Shu, K., 2021. The ABI4-RbohD/VTC2 regulatory module promotes reactive oxygen species (ROS) accumulation to decrease seed germination under salinity stress. *New Phytologist*, *229*(2), pp.950-962.

Ma, L., Ye, J., Yang, Y., Lin, H., Yue, L., Luo, J., Long, Y.U., Fu, H., Liu, X., Zhang, Y. and Wang, Y., 2019. The SOS2-SCaBP8 complex generates and fine-tunes an AtANN4-dependent calcium signature under salt stress. *Developmental cell*, *48*(5), pp.697-709.

Ma, L., Zhang, H., Sun, L., Jiao, Y., Zhang, G., Miao, C. and Hao, F., 2012.

NADPH oxidase AtrbohD and AtrbohF function in ROS-dependent regulation of Na+/K+ homeostasis in Arabidopsis under salt stress. *Journal of Experimental Botany*, *63*(1), pp.305-317.

Mahajan, S. and Tuteja, N., 2005. Cold, salinity and drought stresses: an overview. *Archives of biochemistry and biophysics*, *444*(2), pp.139-158.

Mahajan, S., Pandey, G.K. and Tuteja, N., 2008. Calcium-and salt-stress signaling in plants: shedding light on SOS pathway. *Archives of biochemistry and biophysics*, *471*(2), pp.146-158.

Malik, A., Lan, J. and Lenzen, M., 2016. Trends in global greenhouse gas emissions from 1990 to 2010. *Environmental science & technology*, *50*(9), pp.4722-4730.

Manishankar, P., Wang, N., Köster, P., Alatar, A.A. and Kudla, J., 2018. Calcium signaling during salt stress and in the regulation of ion homeostasis. *Journal of experimental botany*, *69*(17), pp.4215-4226.

Marhava, P., 2022. Recent developments in the understanding of PIN polarity. *New Phytologist*, *233*(2), pp.624-630.

Marhavý, P., Bielach, A., Abas, L., Abuzeineh, A., Duclercq, J., Tanaka, H., Pařezová, M., Petrášek, J., Friml, J., Kleine-Vehn, J. and Benková, E., 2011. Cytokinin modulates endocytic trafficking of PIN1 auxin efflux carrier to control plant organogenesis. *Developmental cell*, *21*(4), pp.796-804.

Marzi, D., Brunetti, P., Saini, S.S., Yadav, G., Puglia, G.D. and Dello Ioio, R., 2024. Role of transcriptional regulation in auxin-mediated response to abiotic stresses. *Frontiers in Genetics*, *15*, p.1394091.

Mason, M.G., Jha, D., Salt, D.E., Tester, M., Hill, K., Kieber, J.J. and Eric Schaller, G., 2010. Type-B response regulators ARR1 and ARR12 regulate expression of AtHKT1; 1 and accumulation of sodium in Arabidopsis shoots. *The Plant Journal*, *64*(5), pp.753-763.

Matanis, T., Akhmanova, A., Wulf, P., Del Nery, E., Weide, T., Stepanova, T., Galjart, N., Grosveld, F., Goud, B., De Zeeuw, C.I. and Barnekow, A., 2002. Bicaudal-D regulates COPI-independent Golgi–ER transport by recruiting

the dynein–dynactin motor complex. *Nature cell biology*, *4*(12), pp.986-992.

Mayer, A., 2002. Membrane fusion in eukaryotic cells. *Annual review of cell and developmental biology*, *18*(1), pp.289-314.

Michniewicz, M., Brewer, P.B. and Friml, J., 2007. Polar auxin transport and asymmetric auxin distribution. *The Arabidopsis Book/American Society of Plant Biologists*, *5*, p.e0108.

Millar, C.I. and Woolfenden, W.B., 1999. The role of climate change in interpreting historical variability. *Ecological Applications*, *9*(4), pp.1207-1216.

Miller, G., Shulaev, V. and Mittler, R., 2008. Reactive oxygen signaling and abiotic stress. *Physiologia plantarum*, *133*(3), pp.481-489.

Mittler, R., 2002. Oxidative stress, antioxidants and stress tolerance. *Trends in plant science*, *7*(9), pp.405-410.

Mittler, R., 2017. ROS are good. *Trends in plant science*, *22*(1), pp.11-19.

Mittler, R., Vanderauwera, S., Gollery, M. and Van Breusegem, F., 2004. Reactive oxygen gene network of plants. *Trends in plant science*, *9*(10), pp.490-498.

Mlotshwa, S., Pruss, G.J., Gao, Z., Mgutshini, N.L., Li, J., Chen, X., Bowman, L.H. and Vance, V., 2010. Transcriptional silencing induced by Arabidopsis T-DNA mutants is associated with 35S promoter siRNAs and requires genes involved in siRNA-mediated chromatin silencing. *The Plant Journal*, *64*(4), pp.699-704.

Møller, I.M., 2001. Plant mitochondria and oxidative stress: electron transport, NADPH turnover, and metabolism of reactive oxygen species. *Annual review of plant biology*, *52*(1), pp.561-591.

Morohashi, K., Okamoto, M., Yamazaki, C., Fujii, N., Miyazawa, Y., Kamada, M., Kasahara, H., Osada, I., Shimazu, T., Fusejima, Y. and Higashibata, A., 2017. Gravitropism interferes with hydrotropism via counteracting auxin dynamics in cucumber roots: clinorotation and spaceflight experiments. *New Phytologist*, *215*(4), pp.1476-1489.

Morris, D.A., 2000. Transmembrane auxin carrier systems–dynamic regulators of polar auxin transport. *Plant Growth Regulation*, *32*(2), pp.161-172.

Mortazavi, A., Williams, B.A., McCue, K., Schaeffer, L. and Wold, B., 2008. Mapping and quantifying mammalian transcriptomes by RNA-Seq. *Nature methods*, *5*(7), pp.621-628.

Moser, S.C. and Hart, J.A.F., 2015. The long arm of climate change: societal teleconnections and the future of climate change impacts studies. *Climatic Change*, *129*(1), pp.13-26.

Mravec, J., Skůpa, P., Bailly, A., Hoyerová, K., Křeček, P., Bielach, A., Petrášek, J., Zhang, J., Gaykova, V., Stierhof, Y.D. and Dobrev, P.I., 2009. Subcellular homeostasis of phytohormone auxin is mediated by the ER-localized PIN5 transporter. *Nature*, *459*(7250), pp.1136-1140.

Müller, A., Guan, C., Gälweiler, L., Tänzler, P., Huijser, P., Marchant, A., Parry, G., Bennett, M., Wisman, E. and Palme, K., 1998. AtPIN2 defines a locus of Arabidopsis for root gravitropism control. *The EMBO journal*.

Munns, R. and Tester, M., 2008. Mechanisms of salinity tolerance. *Annu. Rev. Plant Biol.*, *59*(1), pp.651-681.

Murashige, T. and Skoog, F., 1962. A revised medium for rapid growth and bio assays with tobacco tissue cultures. *Physiologia plantarum*, *15*(3).

Nabi, R.B.S., Tayade, R., Deshmukh, R., Hussain, A., Shahid, M., Adhikari, A., AbuQamar, S.F. and Yun, B.W., 2025. The stress-induced gene AtDUF569 positively regulates salt stress responses in Arabidopsis thaliana. *BMC Plant Biology*, *25*(1), p.585.

Nakajima, K., Sena, G., Nawy, T. and Benfey, P.N., 2001. Intercellular movement of the putative transcription factor SHR in root patterning. *Nature*, *413*(6853), pp.307-311.

Nakamura, T., Fujiwara, R., Ishiguro, N., Oyabu, M., Nakanishi, T., Shirasaka, Y., Maeda, T. and Tamai, I., 2010. Involvement of choline transporter-like proteins, CTL1 and CTL2, in glucocorticoid-induced acceleration of phosphatidylcholine synthesis via increased choline uptake. *Biological and*

Pharmaceutical Bulletin, *33*(4), pp.691-696.

Naorem, A., Jayaraman, S., Dang, Y.P., Dalal, R.C., Sinha, N.K., Rao, C.S. and Patra, A.K., 2023. Soil constraints in an arid environment—challenges, prospects, and implications. *Agronomy*, *13*(1), p.220.

Osabe, K., Harukawa, Y., Miura, S. and Saze, H., 2017. Epigenetic regulation of intronic transgenes in Arabidopsis. *Scientific reports*, *7*(1), p.45166.

Paciorek, T., Zažímalová, E., Ruthardt, N., Petrášek, J., Stierhof, Y.D., Kleine-Vehn, J., Morris, D.A., Emans, N., Jürgens, G., Geldner, N. and Friml, J., 2005. Auxin inhibits endocytosis and promotes its own efflux from cells. *Nature*, *435*(7046), pp.1251-1256.

Park, S.J., Kwak, K.J., Oh, T.R., Kim, Y.O. and Kang, H., 2009. Cold shock domain proteins affect seed germination and growth of Arabidopsis thaliana under abiotic stress conditions. *Plant and Cell Physiology*, *50*(4), pp.869-878.

Parmesan, C. and Hanley, M.E., 2015. Plants and climate change: complexities and surprises. *Annals of botany*, *116*(6), pp.849-864.

Parry, G., Provart, N.J., Brady, S.M., Uzilday, B., Multinational Arabidopsis Steering Committee, Adams, K., Araújo, W., Aubourg, S., Baginsky, S., Bakker, E. and Bärenfaller, K., 2020. Current status of the multinational Arabidopsis community. *Plant Direct*, *4*(7), p.e00248.

Pasternak, T., Groot, E.P., Kazantsev, F.V., Teale, W., Omelyanchuk, N., Kovrizhnykh, V., Palme, K. and Mironova, V.V., 2019. Salicylic acid affects root meristem patterning via auxin distribution in a concentration-dependent manner. *Plant physiology*, *180*(3), pp.1725-1739.

Peer, W.A., Blakeslee, J.J., Yang, H. and Murphy, A.S., 2011. Seven things we think we know about auxin transport. *Molecular plant*, *4*(3), pp.487-504.

Peleg, Z. and Blumwald, E., 2011. Hormone balance and abiotic stress tolerance in crop plants. *Current opinion in plant biology*, *14*(3), pp.290-295.

Peng, J., Li, Z., Wen, X., Li, W., Shi, H., Yang, L., Zhu, H. and Guo, H., 2014.

Salt-induced stabilization of EIN3/EIL1 confers salinity tolerance by deterring ROS accumulation in Arabidopsis. *PLoS Genetics*, *10*(10), p.e1004664.

Péret, B., Swarup, K., Ferguson, A., Seth, M., Yang, Y., Dhondt, S., James, N., Casimiro, I., Perry, P., Syed, A. and Yang, H., 2012. AUX/LAX genes encode a family of auxin influx transporters that perform distinct functions during Arabidopsis development. *The Plant Cell*, *24*(7), pp.2874-2885.

Perrot-Rechenmann, C. and Napier, R.M., 2005. Auxins. *Vitamins & Hormones*, *72*, pp.203-233.

Petersson, S.V., Johansson, A.I., Kowalczyk, M., Makoveychuk, A., Wang, J.Y., Moritz, T., Grebe, M., Benfey, P.N., Sandberg, G. and Ljung, K., 2009. An auxin gradient and maximum in the Arabidopsis root apex shown by high-resolution cell-specific analysis of IAA distribution and synthesis. *The Plant Cell*, *21*(6), pp.1659-1668.

Petrášek, J. and Friml, J., 2009. Auxin transport routes in plant development.

Pi, L., Aichinger, E., van der Graaff, E., Llavata-Peris, C.I., Weijers, D., Hennig, L., Groot, E. and Laux, T., 2015. Organizer-derived WOX5 signal maintains root columella stem cells through chromatin-mediated repression of CDF4 expression. *Developmental cell*, *33*(5), pp.576-588.

Pitzschke, A. and Hirt, H., 2009. Disentangling the complexity of mitogen-activated protein kinases and reactive oxygen species signaling. *Plant physiology*, *149*(2), pp.606-615.

Platten, J.D., Cotsaftis, O., Berthomieu, P., Bohnert, H., Davenport, R.J., Fairbairn, D.J., Horie, T., Leigh, R.A., Lin, H.X., Luan, S. and Mäser, P., 2006. Nomenclature for HKT transporters, key determinants of plant salinity tolerance. *Trends in plant science*, *11*(8), pp.372-374.

Porter, W.L. and Thimann, K.V., 1965. Molecular requirements for auxin action—I.: Halogenated indoles and indoleacetic acid. *Phytochemistry*, *4*(2), pp.229-243.

Provart, N.J., Alonso, J., Assmann, S.M., Bergmann, D., Brady, S.M., Brkljacic,

J., Browse, J., Chapple, C., Colot, V., Cutler, S. and Dangl, J., 2016. 50 years of Arabidopsis research: highlights and future directions. *New Phytologist*, *209*(3), pp.921-944.

Qi, Z. and Spalding, E.P., 2004. Protection of plasma membrane K+ transport by the salt overly sensitive1 Na+-H+ antiporter during salinity stress. *Plant Physiology*, *136*(1), pp.2548-2555.

Quint, M. and Gray, W.M., 2006. Auxin signaling. *Current opinion in plant biology*, *9*(5), pp.448-453.

Raabe, K., Sun, L., Schindfessel, C., Honys, D. and Geelen, D., 2024. A word of caution: T-DNA-associated mutagenesis in plant reproduction research. *Journal of Experimental Botany*, *75*(11), pp.3248-3258.

Radhamony, R.N., Mohan Prasad, A. and Srinivasan, R., 2005. T-DNA insertional mutagenesis in Arabidopsis: a tool for functional genomics. *Electronic Journal of Biotechnology*, *8*(1), pp.82-106.

Rahman, A., Bannigan, A., Sulaman, W., Pechter, P., Blancaflor, E.B. and Baskin, T.I., 2007. Auxin, actin and growth of the Arabidopsis thaliana primary root. *The Plant Journal*, *50*(3), pp.514-528.

Raihan, A., 2023. A review of the global climate change impacts, adaptation strategies, and mitigation options in the socio-economic and environmental sectors. *Journal of Environmental Science and Economics*, *2*(3), pp.36-58.

Raja, V., Majeed, U., Kang, H., Andrabi, K.I. and John, R., 2017. Abiotic stress: Interplay between ROS, hormones and MAPKs. *Environmental and Experimental Botany*, *137*, pp.142-157.

Rakusová, H., Gallego-Bartolomé, J., Vanstraelen, M., Robert, H.S., Alabadí, D., Blázquez, M.A., Benková, E. and Friml, J., 2011. Polarization of PIN3-dependent auxin transport for hypocotyl gravitropic response in Arabidopsis thaliana. *The Plant Journal*, *67*(5), pp.817-826.

Rashotte, A.M., Brady, S.R., Reed, R.C., Ante, S.J. and Muday, G.K., 2000. Basipetal auxin transport is required for gravitropism in roots of Arabidopsis. *Plant physiology*, *122*(2), pp.481-490.

Ratnakumar, P., Khan, M.I.R., Minhas, P.S., Farooq, M.A., Sultana, R., Per, T.S., Deokate, P.P., Khan, N.A., Singh, Y. and Rane, J., 2016. Can plant bio-regulators minimize crop productivity losses caused by drought, salinity and heat stress? An integrated review. *J. Appl. Bot. Food Qual*, *89*, pp.113-125.

Raupach, M.R., Marland, G., Ciais, P., Le Quéré, C., Canadell, J.G., Klepper, G. and Field, C.B., 2007. Global and regional drivers of accelerating CO2 emissions. *Proceedings of the National Academy of Sciences*, *104*(24), pp.10288-10293.

Raven, J.A., 1975. Transport of indoleacetic acid in plant cells in relation to pH and electrical potential gradients, and its significance for polar IAA transport. *New Phytologist*, *74*(2), pp.163-172.

Raza, A., Razzaq, A., Mehmood, S.S., Zou, X., Zhang, X., Lv, Y. and Xu, J., 2019. Impact of climate change on crops adaptation and strategies to tackle its outcome: A review. *Plants*, *8*(2), p.34.

Rehman, R.U. and Di Sansebastiano, G.P., 2013. SNARE proteins as signaling elements. In *Plant signaling: Understanding the molecular crosstalk* (pp. 39-49). New Delhi: Springer India.

Rengasamy, P., Chittleborough, D. and Helyar, K., 2003. Root-zone constraints and plant-based solutions for dryland salinity. *Plant and Soil*, *257*(2), pp.249-260.

Ribba, T., Garrido-Vargas, F. and O'Brien, J.A., 2020. Auxin-mediated responses under salt stress: From developmental regulation to biotechnological applications. *Journal of Experimental Botany*, *71*(13), pp.3843-3853.

Rivero, R.M., Mittler, R., Blumwald, E. and Zandalinas, S.I., 2022. Developing climate-resilient crops: improving plant tolerance to stress combination. *The Plant Journal*, *109*(2), pp.373-389.

Rodriguez, H.G., Roberts, J.K., Jordan, W.R. and Drew, M.C., 1997. Growth, water relations, and accumulation of organic and inorganic solutes in roots

of maize seedlings during salt stress. *Plant physiology*, *113*(3), pp.881-893.

Rosenzweig, C., Iglesius, A., Yang, X.B., Epstein, P.R. and Chivian, E., 2001. Climate change and extreme weather events-Implications for food production, plant diseases, and pests.

Rosenzweig, C., Tubiello, F.N., Goldberg, R., Mills, E. and Bloomfield, J., 2002. Increased crop damage in the US from excess precipitation under climate change. *Global Environmental Change*, *12*(3), pp.197-202.

Rothman, J.E., 1994. Mechanisms of intracellular protein transport. *Nature*, *372*(6501), pp.55-63.

Rowe, J.H., Topping, J.F., Liu, J. and Lindsey, K., 2016. Abscisic acid regulates root growth under osmotic stress conditions via an interacting hormonal network with cytokinin, ethylene and auxin. *New Phytologist*, *211*(1), pp.225-239.

Růžička, K., Šimášková, M., Duclercq, J., Petrášek, J., Zažímalová, E., Simon, S., Friml, J., Van Montagu, M.C. and Benková, E., 2009. Cytokinin regulates root meristem activity via modulation of the polar auxin transport. *Proceedings of the National Academy of Sciences*, *106*(11), pp.4284-4289.

Sabatini, S., Heidstra, R., Wildwater, M. and Scheres, B., 2003. SCARECROW is involved in positioning the stem cell niche in the Arabidopsis root meristem. *Genes & development*, *17*(3), pp.354-358.

Saed-Moucheshi, A., Shekoofa, A. and Pessarakli, M., 2014. Reactive oxygen species (ROS) generation and detoxifying in plants. *Journal of Plant Nutrition*, *37*(10), pp.1573-1585.

Safdar, H., Amin, A., Shafiq, Y., Ali, A., Yasin, R., Shoukat, A., Hussan, M.U. and Sarwar, M.I., 2019. A review: Impact of salinity on plant growth. *Nat. Sci*, *17*(1), pp.34-40.

Sanderfoot, A., 2007. Increases in the number of SNARE genes parallels the rise of multicellularity among the green plants. *Plant physiology*, *144*(1), pp.6-17.

Sarkar, A.K., Luijten, M., Miyashima, S., Lenhard, M., Hashimoto, T., Nakajima, K., Scheres, B., Heidstra, R. and Laux, T., 2007. Conserved factors regulate signalling in Arabidopsis thaliana shoot and root stem cell organizers. *Nature*, *446*(7137), pp.811-814.

Sasidharan, R., Schippers, J.H. and Schmidt, R.R., 2021. Redox and low-oxygen stress: signal integration and interplay. *Plant Physiology*, *186*(1), pp.66-78.

Schindelin, J., Arganda-Carreras, I., Frise, E., Kaynig, V., Longair, M., Pietzsch, T., Preibisch, S., Rueden, C., Saalfeld, S., Schmid, B. and Tinevez, J.Y., 2012. Fiji: an open-source platform for biological-image analysis. *Nature methods*, *9*(7), pp.676-682.

Schmidhuber, J. and Tubiello, F.N., 2007. Global food security under climate change. *Proceedings of the national academy of sciences*, *104*(50), pp.19703-19708.

Seok, H.Y., Tran, H.T., Lee, S.Y. and Moon, Y.H., 2022. AtERF71/HRE2, an Arabidopsis AP2/ERF transcription factor gene, contains both positive and negative cis-regulatory elements in its promoter region involved in hypoxia and salt stress responses. *International Journal of Molecular Sciences*, *23*(10), p.5310.

Shan, C., Mei, Z., Duan, J., Chen, H., Feng, H. and Cai, W., 2014. OsGA2ox5, a gibberellin metabolism enzyme, is involved in plant growth, the root gravity response and salt stress. *PloS one*, *9*(1), p.e87110.

Sheppard, D., 1994. Dominant negative mutants: tools for the study of protein function in vitro and in vivo. *American journal of respiratory cell and molecular biology*, *11*(1), pp.1-6.

Shi, H., Ishitani, M., Kim, C. and Zhu, J.K., 2000. The Arabidopsis thaliana salt tolerance gene SOS1 encodes a putative Na+/H+ antiporter. *Proceedings of the national academy of sciences*, *97*(12), pp.6896-6901.

Shu, K., Qi, Y., Chen, F., Meng, Y., Luo, X., Shuai, H., Zhou, W., Ding, J., Du, J., Liu, J. and Yang, F., 2017. Salt stress represses soybean seed

germination by negatively regulating GA biosynthesis while positively mediating ABA biosynthesis. *Frontiers in plant science*, *8*, p.1372.

Simon, S. and Petrášek, J., 2011. Why plants need more than one type of auxin. *Plant Science*, *180*(3), pp.454-460.

Simon, S., Skůpa, P., Viaene, T., Zwiewka, M., Tejos, R., Klíma, P., Čarná, M., Rolčík, J., De Rycke, R., Moreno, I. and Dobrev, P.I., 2016. PIN6 auxin transporter at endoplasmic reticulum and plasma membrane mediates auxin homeostasis and organogenesis in Arabidopsis. *New Phytologist*, *211*(1), pp.65-74.

Smith, P. and Gregory, P.J., 2013. Climate change and sustainable food production. *Proceedings of the nutrition society*, *72*(1), pp.21-28.

Smolko, A., Bauer, N., Pavlović, I., Pěnčík, A., Novák, O. and Salopek-Sondi, B., 2021. Altered root growth, auxin metabolism and distribution in Arabidopsis thaliana exposed to salt and osmotic stress. *International Journal of Molecular Sciences*, *22*(15), p.7993.

Söllner, T., Whiteheart, S.W., Brunner, M., Erdjument-Bromage, H., Geromanos, S., Tempst, P. and Rothman, J.E., 1993. SNAP receptors implicated in vesicle targeting and fusion. *Nature*, *362*(6418), pp.318-324.

Sozzani, R., Cui, H., Moreno-Risueno, M.A., Busch, W., Van Norman, J.M., Vernoux, T., Brady, S.M., Dewitte, W., Murray, J.A.H. and Benfey, P.N., 2010. Spatiotemporal regulation of cell-cycle genes by SHORTROOT links patterning and growth. *Nature*, *466*(7302), pp.128-132.

Spadaro, D., Yun, B.W., Spoel, S.H., Chu, C., Wang, Y.Q. and Loake, G.J., 2010. The redox switch: dynamic regulation of protein function by cysteine modifications. *Physiologia plantarum*, *138*(4), pp.360-371.

Steinmann, T., Geldner, N., Grebe, M., Mangold, S., Jackson, C.L., Paris, S., Gälweiler, L., Palme, K. and Jurgens, G., 1999. Coordinated polar localization of auxin efflux carrier PIN1 by GNOM ARF GEF. *Science*, *286*(5438), pp.316-318.

Stokes, T.L., Kunkel, B.N. and Richards, E.J., 2002. Epigenetic variation in

Arabidopsis disease resistance. *Genes & development*, *16*(2), pp.171-182.

Strotmann, V.I. and Stahl, Y., 2021. At the root of quiescence: function and regulation of the quiescent center. *Journal of experimental botany*, *72*(19), pp.6716-6726.

Sun, Y., Zhao, J., Li, X. and Li, Y., 2020. E2 conjugases UBC1 and UBC2 regulate MYB42-mediated SOS pathway in response to salt stress in Arabidopsis. *New Phytologist*, *227*(2), pp.455-472.

Surpin, M., Zheng, H., Morita, M.T., Saito, C., Avila, E., Blakeslee, J.J., Bandyopadhyay, A., Kovaleva, V., Carter, D., Murphy, A. and Tasaka, M., 2003. The VTI family of SNARE proteins is necessary for plant viability and mediates different protein transport pathways. *The Plant Cell*, *15*(12), pp.2885-2899.

Swarup, R. and Bhosale, R., 2019. Developmental roles of AUX1/LAX auxin influx carriers in plants. *Frontiers in plant science*, *10*, p.1306.

Swarup, R. and Péret, B., 2012. AUX/LAX family of auxin influx carriers—an overview. *Frontiers in plant science*, *3*, p.225.

Swarup, R., Kramer, E.M., Perry, P., Knox, K., Leyser, H.O., Haseloff, J., Beemster, G.T., Bhalerao, R. and Bennett, M.J., 2005. Root gravitropism requires lateral root cap and epidermal cells for transport and response to a mobile auxin signal. *Nature cell biology*, *7*(11), pp.1057-1065.

Sztul, E. and Lupashin, V., 2006. Role of tethering factors in secretory membrane traffic. *American Journal of Physiology-Cell Physiology*, *290*(1), pp.C11-C26.

Tan, X., Calderon-Villalobos, L.I.A., Sharon, M., Zheng, C., Robinson, C.V., Estelle, M. and Zheng, N., 2007. Mechanism of auxin perception by the TIR1 ubiquitin ligase. *Nature*, *446*(7136), pp.640-645.

Tang, W.S., Zhong, L., Ding, Q.Q., Dou, Y.N., Li, W.W., Xu, Z.S., Zhou, Y.B., Chen, J., Chen, M. and Ma, Y.Z., 2022. Histone deacetylase AtSRT2 regulates salt tolerance during seed germination via repression of vesicle-associated membrane protein 714 (VAMP714) in Arabidopsis. *New*

Phytologist, *234*(4), pp.1278-1293.

Tester, M. and Davenport, R., 2003. Na+ tolerance and Na+ transport in higher plants. *Annals of botany*, *91*(5), pp.503-527.

Trapnell, C., Williams, B.A., Pertea, G., Mortazavi, A., Kwan, G., Van Baren, M.J., Salzberg, S.L., Wold, B.J. and Pachter, L., 2010. Transcript assembly and quantification by RNA-Seq reveals unannotated transcripts and isoform switching during cell differentiation. *Nature biotechnology*, *28*(5), pp.511-515.

Uemura, T. and Ueda, T., 2014. Plant vacuolar trafficking driven by RAB and SNARE proteins. *Current opinion in plant biology*, *22*, pp.116-121.

Uemura, T., Sato, M.H. and Takeyasu, K., 2005. The longin domain regulates subcellular targeting of VAMP7 in Arabidopsis thaliana. *Febs Letters*, *579*(13), pp.2842-2846.

Uemura, T., Ueda, T., Ohniwa, R.L., Nakano, A., Takeyasu, K. and Sato, M.H., 2004. Systematic analysis of SNARE molecules in Arabidopsis: dissection of the post-Golgi network in plant cells. *Cell structure and function*, *29*(2), pp.49-65.

Ulmasov, T., Murfett, J., Hagen, G. and Guilfoyle, T.J., 1997. Aux/IAA proteins repress expression of reporter genes containing natural and highly active synthetic auxin response elements. *The Plant Cell*, *9*(11), pp.1963-1971.

Upadhyay, R.K., 2020. Markers for global climate change and its impact on social, biological and ecological systems: A review. *American Journal of Climate Change*.

Vanstraelen, M. and Benková, E., 2012. Hormonal interactions in the regulation of plant development. *Annual review of cell and developmental biology*, *28*, pp.463-487.

Vaughan, M.M., Block, A., Christensen, S.A., Allen, L.H. and Schmelz, E.A., 2018. The effects of climate change associated abiotic stresses on maize phytochemical defenses. *Phytochemistry Reviews*, *17*(1), pp.37-49.

Veitia, R.A., 2007. Exploring the molecular etiology of dominant-negative

mutations. *The plant cell*, *19*(12), pp.3843-3851.

Verbelen, J.P., Cnodder, T.D., Le, J., Vissenberg, K. and Baluška, F., 2006. The root apex of Arabidopsis thaliana consists of four distinct zones of growth activities: meristematic zone, transition zone, fast elongation zone and growth terminating zone. *Plant signaling & behavior*, *1*(6), pp.296-304.

Vieten, A., Sauer, M., Brewer, P.B. and Friml, J., 2007. Molecular and cellular aspects of auxin-transport-mediated development. *Trends in plant science*, *12*(4), pp.160-168.

Wang, H., Inukai, Y. and Yamauchi, A., 2006. Root development and nutrient uptake. *Critical reviews in plant sciences*, *25*(3), pp.279-301.

Wang, P., Wang, C.M., Gao, L., Cui, Y.N., Yang, H.L., de Silva, N.D., Ma, Q., Bao, A.K., Flowers, T.J., Rowland, O. and Wang, S.M., 2020. Aliphatic suberin confers salt tolerance to Arabidopsis by limiting Na+ influx, K+ efflux and water backflow. *Plant and Soil*, *448*(1), pp.603-620.

Wang, W., Vinocur, B. and Altman, A., 2003. Plant responses to drought, salinity and extreme temperatures: towards genetic engineering for stress tolerance. *Planta*, *218*(1), pp.1-14.

Wang, Y., Li, K. and Li, X., 2009. Auxin redistribution modulates plastic development of root system architecture under salt stress in Arabidopsis thaliana. *Journal of plant physiology*, *166*(15), pp.1637-1645.

Wang, Y., Yang, L., Tang, Y., Tang, R., Jing, Y., Zhang, C., Zhang, B., Li, X., Cui, Y., Zhang, C. and Shi, J., 2017. Arabidopsis choline transporter-like 1 (CTL1) regulates secretory trafficking of auxin transporters to control seedling growth. *PLoS Biology*, *15*(12), p.e2004310.

Wang, Y.H., 2008. How effective is T-DNA insertional mutagenesis in Arabidopsis?. *Journal of Biochemical Technology*, *1*(1), pp.11-20.

Wei, L.X., Lv, B.S., Wang, M.M., Ma, H.Y., Yang, H.Y., Liu, X.L., Jiang, C.J. and Liang, Z.W., 2015. Priming effect of abscisic acid on alkaline stress tolerance in rice (Oryza sativa L.) seedlings. *Plant Physiology and Biochemistry*, *90*, pp.50-57.

Weigel, D., 2012. Natural variation in Arabidopsis: from molecular genetics to ecological genomics. *Plant physiology*, *158*(1), pp.2-22.

Weinhold, A., Kallenbach, M. and Baldwin, I.T., 2013. Progressive 35S promoter methylation increases rapidly during vegetative development in transgenic Nicotiana attenuata plants. *BMC plant biology*, *13*(1), p.99.

Wheeler, T. and Von Braun, J., 2013. Climate change impacts on global food security. *Science*, *341*(6145), pp.508-513.

Whyte, J.R. and Munro, S., 2002. Vesicle tethering complexes in membrane traffic. *Journal of cell science*, *115*(13), pp.2627-2637.

World Health Organization, 2020. *The state of food security and nutrition in the world 2020: transforming food systems for affordable healthy diets* (Vol. 2020). Food & Agriculture Org..

Worley, C.K., Zenser, N., Ramos, J., Rouse, D., Leyser, O., Theologis, A. and Callis, J., 2000. Degradation of Aux/IAA proteins is essential for normal auxin signalling. *The Plant Journal*, *21*(6), pp.553-562.

Wu, S.J., Ding, L. and Zhu, J.K., 1996. SOS1, a genetic locus essential for salt tolerance and potassium acquisition. *The Plant Cell*, *8*(4), pp.617-627.

Wu, X., Xu, J., Meng, X., Fang, X., Xia, M., Zhang, J., Cao, S. and Fan, T., 2022. Linker histone variant HIS1-3 and WRKY1 oppositely regulate salt stress tolerance in Arabidopsis. *Plant Physiology*, *189*(3), pp.1833-1847.

Xiao, X., Li, X., Chen, C. and Guo, W., 2020. DR5 is a suitable system for studying the auxin response in the Poncirus trifoliata-Xanthomonas axonopodis pv. citri Interaction. *Horticultural Plant Journal*, *6*(5), pp.277-283.

Xie, Q., Essemine, J., Pang, X., Chen, H., Jin, J. and Cai, W., 2021. Abscisic acid regulates the root growth trajectory by reducing auxin transporter PIN2 protein levels in Arabidopsis thaliana. *Frontiers in Plant Science*, *12*, p.632676.

Xu, Z., Wang, C., Xue, F., Zhang, H. and Ji, W., 2015. Wheat NAC transcription factor TaNAC29 is involved in response to salt stress. *Plant Physiology*

and Biochemistry, *96*, pp.356-363.

Xue, Y., Yang, Y., Yang, Z., Wang, X. and Guo, Y., 2018. VAMP711 is required for abscisic acid-mediated inhibition of plasma membrane H+-ATPase activity. *Plant Physiology*, *178*(3), pp.1332-1343.

Yadav, D., Hacisuleyman, A., Dergai, M., Khalifeh, D., Abriata, L.A., Peraro, M.D. and Fasshauer, D., 2024. A look beyond the QR code of SNARE proteins. Protein Science, 33(9), p.e5158.

Yadav, S., Irfan, M., Ahmad, A. and Hayat, S., 2011. Causes of salinity and plant manifestations to salt stress: a review. *Journal of environmental biology*, *32*(5), p.667.

Yamaguchi, T., Fukada-Tanaka, S., Inagaki, Y., Saito, N., Yonekura-Sakakibara, K., Tanaka, Y., Kusumi, T. and Iida, S., 2001. Genes encoding the vacuolar Na+/H+ exchanger and flower coloration. *Plant and Cell Physiology*, *42*(5), pp.451-461.

Yang, H. and Murphy, A.S., 2009. Functional expression and characterization of Arabidopsis ABCB, AUX 1 and PIN auxin transporters in Schizosaccharomyces pombe. *The Plant Journal*, *59*(1), pp.179-191.

Yang, Y., Hammes, U.Z., Taylor, C.G., Schachtman, D.P. and Nielsen, E., 2006. High-affinity auxin transport by the AUX1 influx carrier protein. *Current Biology*, *16*(11), pp.1123-1127.

Yoon, E.K., Dhar, S., Lee, M.H., Song, J.H., Lee, S.A., Kim, G., Jang, S., Choi, J.W., Choe, J.E., Kim, J.H. and Lee, M.M., 2016. Conservation and diversification of the SHR-SCR-SCL23 regulatory network in the development of the functional endodermis in Arabidopsis shoots. *Molecular Plant*, *9*(8), pp.1197-1209.

Yu, Y., Li, Y., Yan, Z. and Duan, X., 2022. The role of cytokinins in plant under salt stress. *Journal of Plant Growth Regulation*, *41*(6), pp.2279-2291.

Yu, Z., Duan, X., Luo, L., Dai, S., Ding, Z. and Xia, G., 2020. How plant hormones mediate salt stress responses. *Trends in plant science*, *25*(11), pp.1117-1130.

Yuan, T.T., Xu, H.H., Zhang, K.X., Guo, T.T. and Lu, Y.T., 2014. Glucose inhibits root meristem growth via ABA INSENSITIVE 5, which represses PIN1 accumulation and auxin activity in A rabidopsis. *Plant, Cell & Environment*, *37*(6), pp.1338-1350.

Yun, H.S., Kwaaitaal, M., Kato, N., Yi, C., Park, S., Sato, M.H., Schulze-Lefert, P. and Kwon, C., 2013. Requirement of vesicle-associated membrane protein 721 and 722 for sustained growth during immune responses in Arabidopsis. *Molecules and Cells*, *35*(6), pp.481-488.

Zažímalová, E., Murphy, A.S., Yang, H., Hoyerová, K. and Hošek, P., 2010. Auxin transporters—why so many?. *Cold Spring Harbor perspectives in biology*, *2*(3), p.a001552.

Zhang, J.S., Xie, C., Shen, Y.G. and Chen, S.Y., 2001. A two-component gene (NTHK1) encoding a putative ethylene-receptor homolog is both developmentally and stress regulated in tobacco. *Theoretical and Applied Genetics*, *102*(6), pp.815-824.

Zhang, J.Z., 2003. Overexpression analysis of plant transcription factors. *Current opinion in plant biology*, *6*(5), pp.430-440.

Zhang, L., Zhang, H., Liu, P., Hao, H., Jin, J.B. and Lin, J., 2011. Arabidopsis R-SNARE proteins VAMP721 and VAMP722 are required for cell plate formation. *PLoS one*, *6*(10), p.e26129.

Zhang, S. and Klessig, D.F., 2001. MAPK cascades in plant defense signaling. *Trends in plant science*, *6*(11), pp.520-527.

Zhang, Y. and Friml, J., 2019. Auxin guides roots to avoid obstacles during gravitropic growth. *The New Phytologist*, *225*(3), p.1049.

Zhao, C., Liu, B., Piao, S., Wang, X., Lobell, D.B., Huang, Y., Huang, M., Yao, Y., Bassu, S., Ciais, P. and Durand, J.L., 2017. Temperature increase reduces global yields of major crops in four independent estimates. *Proceedings of the National Academy of sciences*, *114*(35), pp.9326-9331.

Zhao, X.C. and Schaller, G.E., 2004. Effect of salt and osmotic stress upon

expression of the ethylene receptor ETR1 in Arabidopsis thaliana. *Febs Letters*, *562*(1-3), pp.189-192.

Zhao, Y., Wang, T., Zhang, W. and Li, X., 2011. SOS3 mediates lateral root development under low salt stress through regulation of auxin redistribution and maxima in Arabidopsis. *New Phytologist*, *189*(4), pp.1122-1134.

Zhao, Y., Yang, Z., Ding, Y., Liu, L., Han, X., Zhan, J., Wei, X., Diao, Y., Qin, W., Wang, P. and Liu, P., 2019. Over-expression of an R2R3 MYB Gene, GhMYB73, increases tolerance to salt stress in transgenic Arabidopsis. *Plant science*, *286*, pp.28-36.

Zhong, H. and Läuchli, A., 1993. Spatial and temporal aspects of growth in the primary root of cotton seedlings: effects of NaCl and CaCl2. *Journal of experimental botany*, *44*(4), pp.763-771.

Zhou, H., Shi, H., Yang, Y., Feng, X., Chen, X., Xiao, F., Lin, H. and Guo, Y., 2024. Insights into plant salt stress signaling and tolerance. *Journal of Genetics and Genomics*, *51*(1), pp.16-34.

Zhou, H.L., Cao, W.H., Cao, Y.R., Liu, J., Hao, Y.J., Zhang, J.S. and Chen, S.Y., 2006. Roles of ethylene receptor NTHK1 domains in plant growth, stress response and protein phosphorylation. *FEBS letters*, *580*(5), pp.1239-1250.

Zhu, J.K., 2001. Plant salt tolerance. *Trends in plant science*, *6*(2), pp.66-71.

Zia-ur-Rehman, M., Murtaza, G., Qayyum, M.F., Saifullah, Rizwan, M., Ali, S., Akmal, F. and Khalid, H., 2016. Degraded soils: origin, types and management. In *Soil science: Agricultural and environmental prospectives* (pp. 23-65). Cham: Springer International Publishing.

Zimmerman, P.W. and Wilcoxon, F., 1935. Several chemical growth substances which cause initiation of roots and other responses in plants.

Zolla, G., Heimer, Y.M. and Barak, S., 2010. Mild salinity stimulates a stress-induced morphogenic response in Arabidopsis thaliana roots. *Journal of experimental botany*, *61*(1), pp.211-224.